UNIVERSITY OF CALIFORNIA, SAN DIEGO

Investigating the roles of protein-protein interactions and conformational changes in nitrogenase catalysis

A dissertation submitted in partial satisfaction of the requirements for the degree of Doctor of Philosophy

in

Chemistry

by

Faith Erin Heffernan Katz

Committee in charge:

Professor F. Akif Tezcan, Chair
Professor Lihini Aluwihare
Professor Simpson Joseph
Professor Judy Kim
Professor Francesco Paesani

2018

This Dissertation of Faith Erin Heffernan Katz is approved, and it is acceptable in quality and form for publication on microfilm and electronically:

Chair

University of California, San Diego

2018

DEDICATION

To my husband, mother, and father, my fierce advocates and relentless supporters.

EPIGRAPH

“It was always me versus the world
Until I found it's me versus me”

- 2018 Pulitzer Prize winner Kendrick Lamar

TABLE OF CONTENTS

LIST OF ABBREVIATIONS

ADP	Adenosine diphosphate
AMPPCP	Non-hydrolyzable ATP-analog adenylylmethylenediphosphonate
ATP	Adenosine triphosphate
ATP	Adenosine triphosphate
BME	β-mercaptoethanol
Cys	Cysteine
DCM	Dichloromethane
DEAE	Diethylaminoethanol
DG	Docking geometry
DI	Deionized
DMSO	Dimethyl sulfoxide
DNA	Deoxyribonucleic acid
DT	Dithionite
EF-G	Elongation factor G
ENDOR	Electron nuclear double resonance
EPR	Electron paramagnetic resonance
ESI-MS	Electrospray ionization mass spectrometry
Fe protein	Iron protein
FeMoco	Iron Molybdenum Cofactor
FID	Flame induction detector
FPLC	Fast protein liquid chromatography
FRET	Förster resonance energy transfer
GC	Gas chromatography
GdHCl	Guanidine hydrochloride
Glu	Glutamic acid
Glu	Glutamic acid
GTP	Guanidine triphosphate
HEPES	2-[4-(2-hydroxyethyl)piperazin-1-yl]ethanesulfonic acid
HisZiFiT	Zn-chelating molecule: 2,7-bis(pyridyl-2-sulfonamido)-4,5-dimethylfluorescein
HPLC	High-performance liquid chromatography
IAEDANS	5-naphthalene-1-sulfonic acid
IC_{50}	Half maximal inhibitory concentration
ICP-MS	Inductively coupled plasma-mass spectrometry
ICP-OES	Inductively coupled plasma-optical emission spectroscopy
IDS	Indigo disulfonate
K_d	Dissociation constant
kDa	Kilodalton
K_M	Michaelis constant
Lys	Lysine
MoFe protein	Molybdenum-Iron protein
MOPS	3-(N-morpholino)propanesulfonic acid
MPD	2-methyl-2,4-pentadiol
nif	Nitrogen fixation genes
OPA	*o*-phthalaldehyde
OPC	Organic phosphate compounds

PCR	Polymerase chain reaction
PDB	Protein Data Bank
PhenIA	Iodoacetamido-1,10-phenanthroline
P_i	Inorganic phosphate
PPI	Protein-protein interactions
RP-HPLC	Reverse-phase high-performance liquid chromatography
Ru-PhenIA	Ru(2,2'-bipyridine)2(5-iodoacetamido-1,10-phenanthroline)
SDS-PAGE	Sodium dodecyl sulfate-polyacrylamide gel electrophoresis
SEC	Size exclusion chromatography
Ser	Serine
SOP	Standard operating procedure
T-L	Thorneley-Lowe
T&L	Thorneley and Lowe
TCD	Thermal conductivity detector
TLC	thin-layer chromatography
Tris	tris(hydroxymethyl)aminomethane
UV-Vis	Ultraviolet-visible spectroscopy
V_{max}	Maximum velocity

LIST OF FIGURES

LIST OF TABLES

ACKNOWLEDGEMENTS

First and foremost, I would like to thank my research advisor, Professor Akif Tezcan, for knowing how to push me harder than I could push myself and making me the scientist I am today. I am also extremely grateful for the opportunities he gave me in the lab to run with crazy ideas and try a little bit of just about every kind of chemistry.

I couldn't have asked for a better lab mates, mentors, and friends than those I found in Team Nitro – Dr. Cedric Owens, Cole Carter, Hannah Rutledge, Alkane Xu, and Laura Williamson. The enthusiasm, creativity, and perseverance in this group are contagious. I would also like to thank the other members of the Tezcan Lab, past and present, for making lab a fun, intellectually stimulating place to work.

Many other members of the UCSD community have made this research possible, including Professor Joseph and members of his lab, Dr. Krista Trappl and Dr. Xinying Shi. They graciously allowed me to use their equipment, taught me how to purify ribosomes, and gladly collaborated on the work discussed in Chapter 7. While I was a TA for 100A, Professor Pomeroy and George Anderson helped me think about how to apply methods from oceanography in enzyme biochemistry. I am grateful to both of them for discussions about phosphate and ammonia measurements in seawater analysis. Finally, I am indebted to Dr. Richard Cochran, who, while he was the director of the Environmental and Complex Analysis Laboratory, taught me so much about ICP-MS and offered invaluable insight about the inner workings of GCs.

In addition to the UCSD community, I also received assistance from the nitrogenase community, in particular, Professor Dennis Dean and his Senior Lab Specialist Valerie Cash. I would not have been able to make any site-directed nitrogenase mutants without the deletion strains and expert advice Valerie provided.

Finally, I would like to thank my family and friends who have supported me along my academic journey, especially my parents, who have been my teachers and cheerleaders from the beginning. I also had the privilege of marrying my best friend, Skyler, during my time in graduate school. I am thankful not only for the support I received from Skyler but also his family as well, who has become my family, too.

Chapter 2 was reproduced in part, with permission, from Owens, C. P.; Katz, F. E. H.; Carter, C. H.; Luca, M. A.; Tezcan, F. A. “Evidence for functionally relevant encounter complexes in nitrogenase catalysis.” *J. Am. Chem. Soc.* **2015**, *137*, 12704–12712. Copyright 2015, American Chemical Society. The dissertation author is a contributing author. Chapter 2 also includes unpublished work in which the dissertation author is the primary author.

Chapter 3 was reproduced in part, with permission, from Owens, C. P.; Katz, F. E. H.; Carter, C. H.; Oswald, V. F.; Tezcan, F. A. “Tyrosine-coordinated P-cluster in *G. diazotrophicus* nitrogenase: evidence for the importance of O-based ligands in conformationally gated electron transfer.” *J. Am. Chem. Soc.* **2016**, *138*, 10124–10127. Copyright 2016, American Chemical Society. The dissertation author is a contributing author. Chapter 3 also includes unpublished work in which the dissertation author is the primary author.

Chapter 4 is unpublished work in which the dissertation author is the primary author.

Chapter 5 was reproduced in part, with permission, from Katz, F. E. H.; Shi, X.; Owens, C. P.; Joseph, S.; Tezcan, F. A. “Determination of nucleoside triphosphatase activities from measurement of true inorganic phosphate in the presence of labile phosphate compounds.” *Anal. Biochem.* **2017**, *520*, 62–67. Copyright 2017, Elsevier. The dissertation author is the primary author. Chapter 5 includes unpublished work in which the dissertation author is the primary author.

This dissertation was funded by an NIH grant (GM099813) and a Frasch Foundation Award (735-HF12) to Professor Akif Tezcan.

VITA

Education

2013 B.A., Chemistry, Scripps College

2015 M.S., Chemistry, University of California, San Diego

2018 Ph.D., Chemistry, University of California, San Diego

Awards and Honors

2013 ACS Undergraduate Award in Inorganic Chemistry

2016 Teddy Traylor Award

2018 Summer Graduate Teaching Scholar

Publications

1. "Determination of nucleoside triphosphatase activities from measurement of true inorganic phosphate in the presence of labile phosphate compounds" Katz, F. E. H.; Shi, X., Owens, C. P.; Joseph, S.; Tezcan, F. A. *Anal. Biochem*. **2017**, 520, 62-67.

2. "Electron transfer reactions in biological nitrogen fixation" Katz, F. E. H.; Owens, C. P.; Tezcan, F. A. *Isr. J. Chem.,* **2016**, 56, 682-692.

3. "Tyrosine-coordinated P-cluster in *G. diazotrophicus* nitrogenase: evidence for the importance of O-based ligands in conformationally gated electron transfer" Owens, C. P.; Katz, F. E. H.; Carter, C. H.; Oswald, V. F.; Tezcan, F. A. *J. Am. Chem. Soc.,* **2016**, *138*(32), 10124-10127.

4. "Evidence for functionally relevant encounter complexes in nitrogenase catalysis" Owens, C. P.; Katz, F. E. H.; Carter, C. H.; Luca, M. A.; Tezcan, F. A. *J. Am. Chem. Soc.*, **2015**, *137*(39), 12704-12712.

Fields of Study

Major Field: Biochemistry

Biochemistry: Bioinorganic chemistry, Analytical Biochemistry, Molecular Biology

ABSTRACT OF THE DISSERTATION

Investigating the roles of protein-protein interactions and conformational changes in nitrogenase catalysis

by

Faith Erin Heffernan Katz

Doctor of Philosophy in Chemistry

University of California, San Diego, 2018

Professor F. Akif Tezcan, Chair

Many adverse environmental effects are associated with the industrial production of commodity chemicals like ammonia (NH_3) from atmospheric dinitrogen (N_2). Nitrogenase is the only enzyme capable of reducing N_2 gas to a bioavailable form. Remarkably, the two-component protein system nitrogenase achieves this reaction at room temperature and atmospheric pressure, using ATP as the energy source. Though biological nitrogen fixation has been studied for nearly a century, the precise mechanism by which Nature activates N_2 remains elusive. The overarching goal of this dissertation is to understand the molecular mechanism of biological nitrogen fixation, as this will lead to the development of more environmentally sustainable catalysts for industrial N_2 activation and accelerate efforts to engineer the ability to fix nitrogen into plants.

Specifically, protein-protein interactions between and conformational changes within the nitrogenase component proteins are investigated in this work to gain insight as to why biological nitrogen fixation requires a specific, ATP-dependent electron donor protein to support catalysis. Through the study of site-directed nitrogenase mutants, a negatively-charged patch on the surface of the electron donor protein and a positively-charged patch on the surface of the catalytic component protein of nitrogenase were found to associate during turnover *en route* to the formation of a complex capable of interprotein electron transfer. While changes in the abilities of these mutant proteins to reduce H^+ to H_2 and C_2H_2 to C_2H_4 were explained well by the consensus Thorneley-Lowe model for nitrogenase reactivity, the model could neither predict nor explain the behavior of either wild-type or mutant proteins under an N_2 atmosphere, performing the biologically relevant reduction of N_2 to yield NH_3 and H_2.

Finally, the possibility for the electron donor protein in nitrogenase to transduce structural changes within the catalytic protein component upon binding is evaluated, and a mechanism for conformational gating of electron transfer in nitrogenase proposed. The findings of this dissertation would not have been achieved without significant efforts to create, optimize, and improve experimental methods in molecular biology and analytical biochemistry related to the study of nitrogenase, which are the subjects of the final chapters in this dissertation.

1 Introduction to nitrogen fixation

Reduced formed of nitrogen are required for all life on earth, as nitrogen is a key element in the building blocks of proteins and DNA, yet only a small number of bacteria are capable of reducing atmospheric nitrogen to a biologically usable form. Thus, despite the abundance of nitrogen in the earth's atmosphere, reduced forms of nitrogen are often the limiting nutrient to plant growth. Most of the planet's nitrogen is stored in the form of atmospheric dinitrogen (N_2) and must be fixed before plants can utilize it. Biological nitrogen fixation is accomplished by a small group of soil-dwelling bacteria, termed diazotrophs, which carry out the reduction of N_2 to NH_3. For most of human history, biological nitrogen fixation was the only way to introduce NH_3 to plants. At the beginning of the 20th century, however, scientists discovered a way to convert N_2 to NH_3 on an industrial scale. This process revolutionized farming and made possible the global population explosion that has occurred in the last century. Unfortunately, there are many unintended consequences of the industrial production of NH_3.

1.1 Breaking the N-N triple bond

Reaction of N_2 and H_2 gases to form NH_3 is thermodynamically favorable at ambient temperature and atmospheric pressure, but kinetic considerations make reduction of N_2 to NH_3 one of the most challenging chemical transformations known. This juxtaposition is demonstrated well by a comparison of the positive enthalpy of formation of N_2H_2 from N_2 with the subsequent negative enthalpies of formation for N_2H_4 from N_2H_2 and NH_3 from N_2H_4.[1] Indeed, there is only one class of enzymes capable of carrying out N_2 reduction in Nature and one viable industrial process for

NH_3 production from N_2, as the majority of small molecules designed to reduce N_2 to NH_3 are extremely inefficient or produce exclusively H_2.[2-5]

1.2 Industrial nitrogen fixation: the Haber-Bosch process

Even before the importance of nitrogen was realized, ancient agricultures practiced a variety of strategies to increase the amount of fixed nitrogen in soil and improve crop yields, yet all of these strategies can be summarized as either recycling already fixed nitrogen or increasing the rate of biological nitrogen fixation.[6] Many agricultures, both past and present, recycle fixed nitrogen by adding animal manure to soil and rotate leguminous and cereal crops to increase the rate of biological nitrogen fixation. Neither of these strategies, however, offers a substantial increase in the total amount of fixed nitrogen available.

In 19th century Europe, the population was growing steadily, but this was made possible only by continuously increasing the amount of farmland. Toward the latter half of the 19th century, politicians, scientists, and farmers began searching frantically for a way to increase the productivity of existing farmland in order to sustain populations growth rates, because there simply wasn't any more land.[7] Since by this time, scientists had identified nitrogen as a common limiting nutrient in crop growth, a variety of techniques were employed to increase the productivity of existing farmland by adding sources of fixed nitrogen to the land. One strategy was to cover farmland with guano, a pellet form of dried bird excrement found in dry climates around Peru. Another strategy was to cover farmland with nitrate salts, which had been mined in Chile. Unfortunately, as these were both limited natural resources, neither was a long-term solution to the farming problem.

Alternatively, fixed nitrogen in the form of NH_3 could be recovered from coking plants. Coking is the process of refining coal, which contains hydrogen and carbon, to

coke, a solid carbon-only fuel, and NH_3 is one of the many by-products of this industrial process. The total amount of NH_3 that could be recovered from coking plants, though, was insignificant in comparison to the total amount of fixed nitrogen needed to fertilize Europe's farmland. Many scientists were thus engaged in efforts to synthesize sources of fixed nitrogen, either using N_2 and electricity or N_2 and extremely high temperatures.

After a thorough investigation of the temperature-dependent equilibrium of NH_3 with N_2 and H_2, German scientist Fritz Haber showed conclusively at the turn of the 20^{th} century that NH_3 could be made from its components N_2 and H_2. Shortly thereafter, Carl Bosch scaled up Haber's reaction conditions, enabling first industrial plant for nitrogen fixation to open in 1910. Though the identity of the heterogeneous catalyst for this reaction and the precise temperatures and pressures have changed over time, the fundamental reaction used today is still remarkably similar to what Haber and Bosch used, and it is summarized in Equation 1. Industrial nitrogen fixation today typically requires temperatures in excess of 400°C and pressures of at least 250 atm.

$$N_2 + 3\ H_2 \Leftrightarrow 2\ NH_3 \qquad (1)$$

In Haber and Bosch's time, the energy input required for the high temperatures and pressures driving Equation 1 came from the burning of fossil fuels, and that is still largely true today. The pure N_2 starting material is generated from distillation of air, just as it was a century ago in the first NH_3 production. One major change to industrial nitrogen fixation is in how the pure H_2 is formed. In 1929 the American company Shell reported the first production of pure H_2 gas from steam reforming of methane, which is the primarily means of pure H_2 production today, and it is summarized in Equation 2. When considering the environmental impact of the Haber-Bosch process, it is critical to account not just for the CO_2 generated from the

burning of fossil fuels to create high temperatures and pressures, but also the CO_2 produced as a by-product in the production of pure H_2 gas.

$$CH_4 + 2\ H_2O \Leftrightarrow 4\ H_2 + CO_2 \quad (2)$$

Though the global population has increased less than 10-fold in the last 100 years, global utilization of inorganic nitrogen fertilizers, generated almost exclusively through the Haber-Bosch process, has increased over 100-fold during this same time period. In addition to the environmental damages caused by the industrial synthesis of NH_3, the overuse of NH_3 in agriculture is also adversely affecting the environment. First, excess NH_3 left in the soil is quickly converted to N_2O by denitrifying bacteria. N_2O is a potent greenhouse gas, approximately 200 times more potent than CO_2, and contributes substantially to global warming. Second, excess NH_3 left in soil is carried by rain into nearby bodies of water, which can lead to eutrophication. One example of this is in the Gulf of Mexico, the world's largest "Dead Zone," a hypoxic region. Because of over fertilization in America's Corn Belt, NH_3 finds its way to the Mississippi River, and eventually enters the Gulf of Mexico. The abrupt and large increase in NH_3 in ocean water allows algae to thrive at the expense of most other marine life. As algae grow, the entire ecosystem is deprived of adequate levels of oxygen, leading to death and, in extreme cases, species extinction.

1.3 Biological nitrogen fixation: nitrogenase

1.3.1 Nitrogenase is the enzyme responsible for biological nitrogen fixation

Conversely, nitrogenase is the enzyme responsible for the biological conversion of abundant but inert N_2 into bioavailable NH_3. Nitrogenase achieves this reaction at ambient temperature and atmospheric pressure using the renewable energy source ATP. Furthermore, nitrogenase is able to utilize protons and electrons from H_2O to reduce N_2 rather than relying on a source of pure H_2.

The most well studied form of nitrogenase is the molybdenum-containing nitrogenase (Mo-nitrogenase) from *Azotobacter vinelandii*, which contains two component proteins (Figure 1.1), the electron donor Fe protein and the catalytic MoFe protein, named for the Mo and Fe it contains.[1,8,9] Fe protein is a 60 kDa γ_2 homodimer joined by a 4Fe:4S cluster, and each monomer contains one ATP binding site. MoFe protein is a 230 kDa $\alpha_2\beta_2$ heterotetramer, and Figure 1.1 shows one half of MoFe protein. Each half of MoFe protein contains one 8Fe:7S cluster, termed P-cluster, which resides at the α/β interface, and one 7Fe:1Mo:9S:1C:homocitrate cluster called FeMo-cofactor or FeMoco, which is located in the α-subunit. The crystal structure shown in Figure 1.1 was obtained in the presence of the non-hydrolyzable ATP analog AMPPCP (PDB: 4WZB).[10]

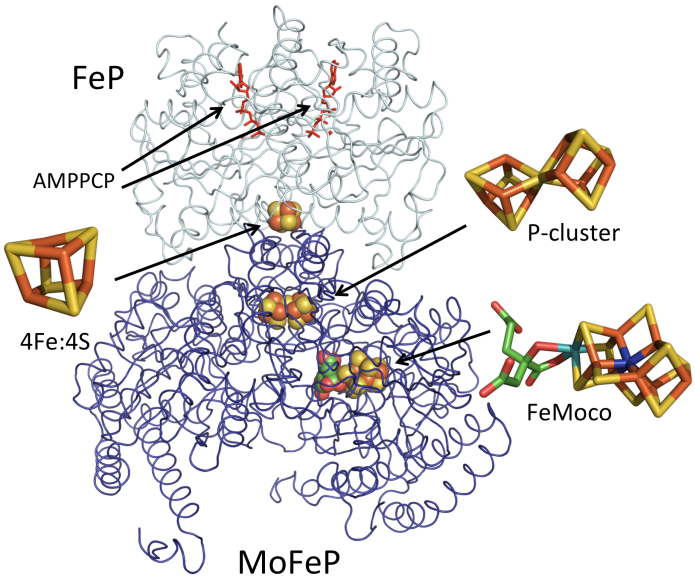

Figure 1.1 Crystal structure of the nitrogenase complex.

Electrons flow from Fe protein to FeMoco, where N_2 binds and is ultimately reduced, through the intermediary P-cluster.[11] The Fe protein cycle represented in Figure 1.2 provides a brief overview of electron flow.[12] First, ATP-bound Fe protein binds to MoFe protein. Rapid electron transfer and ATP hydrolysis take place in the

activated complex, and inorganic phosphate (P_i) is released. Then, oxidized, ADP-bound Fe protein dissociates from MoFe protein, so it can be re-reduced and its nucleotides exchanged. Recently, co-crystal structures of the nitrogenase component proteins revealed nucleotide-dependent docking geometries (DGs),[10] which have been termed *DG1*, *DG2*, and *DG3* and are pictured in Figure 1.3.[13] In *DG1*, which was crystallized in the absence of any nucleotides, Fe protein associates primarily with the β-subunit of MoFe protein, and this electrostatic interaction is boxed in Figure 1.3 A. In *DG2*, Figure 1.3 B, Fe protein associates with MoFe protein over the α/β interface of MoFe protein, and it is in this complex that the 4Fe:4S cluster of Fe protein and the P-cluster move within rapid electron transfer distance. This complex, which was crystallized in the presence of the non-hydrolyzable ATP analog AMPPCP, is typically believed to most closely represent the activated nitrogenase complex. In *DG3*, Figure 1.3 C, which was crystallized in the presence of ADP, Fe protein makes a small number of contacts with the α-subunit of MoFe protein. Taken together, these structures demonstrate that Fe protein can explore large portions of the surface of MoFe protein in a nucleotide-dependent manner.

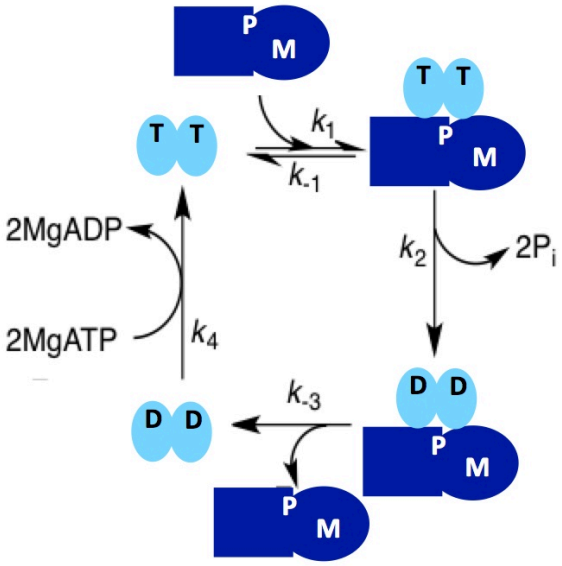

Figure 1.2 Simplified Fe protein cycle for nitrogenase reactivity, emphasizing that Fe and MoFe proteins must associate and dissociate in each cycle.

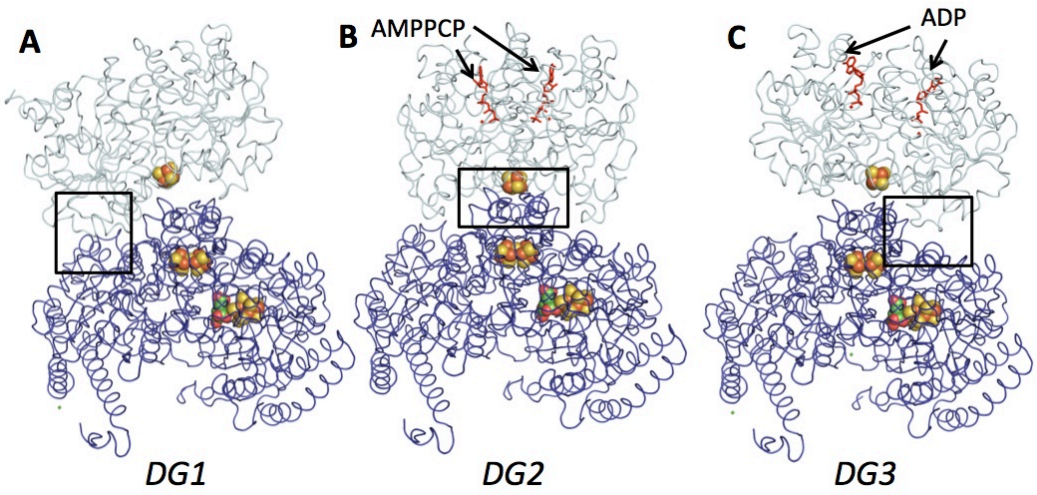

Figure 1.3 Structures of the **A** nucleotide-free (PDB: 2AFH), **B** AMPPCP- (PDB: 4WZB), and **C** ADP- bound (PDB ID: 2AFI) nitrogenase complexes, termed *DG1*, *DG2*, and *DG3*, adapted from ref *25.*

In addition to the Mo-nitrogenase, some organisms also contain a V-nitrogenase or Fe-only nitrogenase.[14-16] Genetic and biochemical analyses, as well as the recent crystal structure of the V-nitrogenase from *A. vinelandii*,[17] suggest that all three nitrogenase systems operate by the same catalytic mechanism and the

cofactors of the three systems differ only in the identity of a single atom.[18] To date, there is no known organism that contains a V- or Fe-only nitrogenase but not the well-studied Mo-nitrogenase.

Though nitrogenase is found in a variety of soil-dwelling bacteria, *A. vinelandii* is most commonly used for interrogating nitrogenase reactivity because it is not in a symbiotic relationship with any plant, making it easy to culture in a laboratory setting.[19] Additionally, *A. vinelandii* is an obligate aerobe, so cultures do not have to be grown in the absence of oxygen. Finally, *A. vinelandii* contains one of the most active Mo-nitrogenases, so it has become the focus of many researchers. Mo-nitogenases from *Klebsiella pneumoniae* and *Clostridium pasteurianum* are also somewhat commonly studied, and their MoFe proteins have been crystallized.[20,21] Based on sequence alignments, Mo-nitrogenases have been divided into four groups,[22] which will be discussed further in Chapter 3 of this dissertation. For the remainder of this dissertation, the term nitrogenase will refer to the Mo-nitrogenase unless otherwise specified.

1.3.2 Consensus model for nitrogenase reactivity

Nitrogenase catalyzes the reduction of N_2 to NH_3, with concomitant H_2 evolution assumed to be governed by the limiting stoichiometry outlined in Equation 3. The consensus equation for nitrogenase reactivity dictates that two molecules of ATP are hydrolyzed per productive electron transferred to substrate, implying that one electron is transferred from Fe protein to MoFe protein per association cycle. The equation also implies that reduction of one molecule of N_2 requires, at a minimum, the evolution of one molecule of H_2 alongside the production of two molecules of NH_3.[23] Both of these constraints are incorporated into every model of nitrogenase reactivity to date. While the Haber-Bosch process is actually a more energy-efficient process

for NH_3 production than biological nitrogen fixation by nitrogenase, the Haber-Bosch process relies on burning fossil fuels both to generate pure H_2 as a starting material and to sustain the extremely high temperatures and pressures during the reaction, while nitrogenase utilizes the renewable energy source ATP.

$$N_2 + 8\ H^+ + 8\ e^- + 16\ MgATP \rightarrow 2\ NH_3 + H_2 + 16\ MgADP + 16P_i \quad (3)$$

1.3.3 Electron transfer through nitrogenase is conformationally gated

As mentioned previously, MoFe protein contains two metal clusters, and electrons are delivered to the catalytic FeMoco from Fe protein by way of the P-cluster. Interestingly, the P-cluster can only transfer electrons to FeMoco when Fe protein is present. Despite the fact that the P-cluster can be reversibly oxidized by small molecule oxidants,[24] spectroscopic experiments confirm that electrons only arrive at FeMoco when MoFe and Fe proteins are mixed together. Furthermore, Fe protein is the obligate biological electron donor to MoFe protein. Ferredoxins, flavodoxins, or small-molecule reductants with reduction potentials similar to or even more negative than Fe protein cannot support substrate reduction at FeMoco. Thus, interactions between the two components of nitrogenase must play a crucial role in driving catalysis.

It is hypothesized that Fe protein must transduce some conformational change or changes in MoFe protein before electron transfer from the P-cluster to FeMoco occurs.[25] At first it was assumed that ATP hydrolysis was involved in affecting this conformational change, but there is now evidence that electron transfer precedes ATP hydrolysis.[26,27] Alternatively, electron transfer from Fe protein to the P-cluster could facilitate structural changes and allow electron transfer to FeMoco to proceed. However, the P-cluster in isolated MoFe protein is in the all-ferrous state, and it is

unlikely it can be reduced further by Fe protein without first transferring an electron to FeMoco.

These observations coupled with stop-flow experiments[28] support what has been termed the “backfill” or “deficit-spending” model, which states that *intramolecular* electron transfer from P-cluster to FeMoco occurs first and is only then followed by *intermolecular* electron transfer from the 4Fe:4S cluster of Fe protein to “backfill” the oxidized P-cluster.[29] To summarize, it is known that *intramolecular* electron transfer from P-cluster to FeMoco is conformationally gated, and this conformational change requires Fe protein to be present, but the conformational change is not related to either ATP hydrolysis or *intermolecular* electron transfer. Thus, this dissertation is concerned with investigating how Fe protein communicates structural changes to metal clusters buried within MoFe protein that allow for *intramolecular* electron transfer within MoFe protein.

1.4 Goals of the dissertation

The primary goal of this dissertation is to elucidate the mechanistic roles of protein-protein interactions (PPI) and protein conformational changes in biological nitrogen fixation. Investigations detailed here are concerned with how Fe protein communicates structural changes to metal clusters buried within MoFe protein that allow for electron transfer. Specifically, the functional roles of electrostatic PPI far away from metal clusters and nucleotide binding sites and redox dependent conformational changes are explored using site-directed nitrogenase mutants and nitrogenase proteins from multiple organisms. The motivations for this are two-fold. First, because nitrogenase is an extremely complex metalloenzyme, these studies can help uncover how multiple protons and electrons are shuttled to and stored at metal centers in biology, as well as how nucleotide binding and hydrolysis are used in

Nature to drive protein movement and chemical reactivity. Second, because it is imperative to develop more environmentally sustainable ways to synthesize NH_3 and deliver it to crops, a thorough understanding of the enzyme that drives this chemistry can help inspire the design of new catalysts and the genetic engineering of nitrogenase activity into plants.

2 Nitrogenase component proteins form catalytically relevant encounter complexes

2.1 Abstract

Because a specific interaction between βK400 of MoFe protein and γE112 of Fe protein has been observed in solution and in crystals, site-directed MoFe protein mutants were created at and around βK400 to probe the potential mechanistic importance of these interactions. If the close association of Fe protein and MoFe protein in this region is catalytically relevant, it was hypothesized that charge reversal point mutations should decrease the catalytic activity of MoFe protein. If the close association is instead a stable but off-pathway interaction, it was hypothesized that charge reversal mutations should have a neutral or even positive effect on MoFe protein catalytic activity. Activity assays measuring the ability of wild-type and mutant MoFe proteins to reduce H^+ and C_2H_2 provided evidence that the Fe protein – MoFe protein interaction centered around βK400 and γE112 is electrostatic in nature, catalytically relevant, and populated during turnover on the way to the formation of the electron-transfer competent complex. Measurements of the efficiency of the coupling of ATP hydrolysis by Fe protein with productive electron transfer to substrate show that mutation of βK400 does not affect either downstream process. Instead, the drop in the activity of βK400E for C_2H_2 reduction compared to that of wild-type MoFe protein can be explained by a decrease in the rate of Fe – MoFe protein component protein association during turnover.

2.2 Introduction

2.2.1 Previous observations concerning PPI in nitrogenase

Even before any crystal structures of nitrogenase proteins were solved, biochemical studies suggested PPI play a critical role in biological nitrogen fixation. The lag phase in product formation in experiments containing a very large excess of MoFe protein compared to Fe protein was interpreted to mean that Fe and MoFe proteins must associate and dissociate with each intermolecular electron transfer event.[30] Later studies showed the component proteins of nitrogenase form one specific covalent crosslink between βK400 of MoFe protein and γE112 of Fe protein when mixed with the crosslinker EDC,[31,32] and these residues were proposed to play a role in component protein complex formation.

This hypothesis was largely discarded, however, when the first crystal structures of nitrogenase were published in the 1990's.[33-35] Residue βK400 was shown to be more than 20 Å away from both the P-cluster and FeMoco, and, similarly, residue γE112 was not located anywhere near the 4Fe:4S cluster of Fe protein or either ATP binding site. Furthermore, the first co-crystal of the nitrogenase complex confirmed that the active, electron-transfer competent complex most likely involved docking of Fe protein over the α/β interface of MoFe protein,[36] as that placed the 4Fe:4S cluster and P-cluster at an appropriate distance for rapid electron transfer.

Interest was renewed in the specific interaction between βK400 and γE112 when nitrogenase component proteins crystallized in the absence of any nucleotides placed βK400 and γE112 within hydrogen-bonding distance (PDBID: 2AFH), which is highlighted in Figure 2.1.[10] It was unclear whether this could be catalytically important, since it occurred in the absence of nucleotides, which is not a physiologically relevant condition.

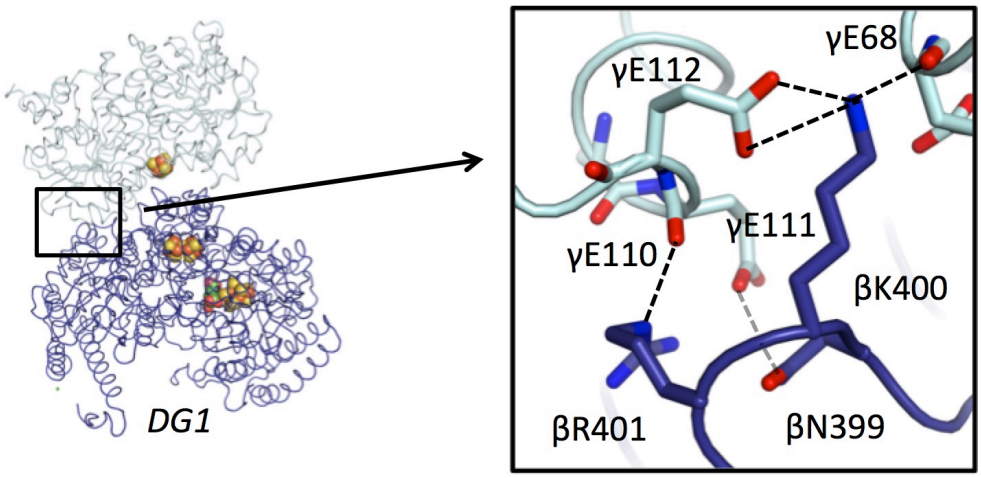

Figure 2.1 Nucleotide-free co-crystal structure of Fe and MoFe proteins, adapted from ref *22*.

2.2.2 Electrostatic interactions between the nitrogenase Fe and MoFe proteins

The nucleotide-free co-crystal structure of the nitrogenase component proteins, which placed βK400 and γE112 within hydrogen-bonding distance of one another, provided intriguing yet indirect evidence that the positively charged patch on the surface of the β-subunit of MoFe protein and the negatively charged patch on the surface of Fe protein might have mechanistic importance. Chapter 2 describes efforts to study the effects of charge neutralization and charge reversal mutations to the positively charged patch on the surface of the β-subunit of MoFe protein. βN399, βK400, and βR401 were individually and collectively mutated to Glu, and βK400→E MoFe protein, which displayed the largest drop in activity of the single mutants prepared, is the primary focus of the experiments described herein.

2.2.3 The Thorneley-Lowe model for nitrogenase reactivity

The T-L model refers to the summative efforts of R. N. F. Thorneley and D. J. Lowe in the 1980's to develop a model for nitrogenase reactivity that could accurately predict both pre-steady state and steady state behavior of nitrogenase proteins

measured experimentally for a variety of substrates.[12,37-40] Today, based largely on the doctoral work of P. Wilson while at Brigham Young University,[41] the T-L model can be mathematically simulated using Mathematica. Remarkably, the T-L model was developed before any crystal structures of nitrogenase were published. At that time, there was not even agreement as to the number or composition of the metal cofactors of MoFe protein. Nevertheless, thirty years later, after dozens of crystal structures of nitrogenase proteins in complex,[10,36,42,43] from a variety of organisms,[20,21] with altered FeMo-cofactors,[44,45] and, most recently, of the alternative V-nitrogenase VFe protein,[17,46] the T-L model endures as the consensus kinetic framework for nitrogenase. Figure 2.2 shows a simplified scheme of the T-L model, and the details of the Fe protein cycle are depicted in Figure 1.3. The T-L model is made up of two key components, the Fe protein cycle and the MoFe protein cycle.

The kinetic scheme of Figure 2.2 assumes that the two identical halves of MoFe protein function independently, and one MoFe protein can be approximated as two catalytic units. Thus, "Mε" represents one half of MoFe protein, and $M\varepsilon_0$ represents the reduction level of FeMoco in the as-isolated state, which has not yet received any electrons from Fe protein. In order to move from $M\varepsilon_0 \rightarrow M\varepsilon_1$, one Fe protein cycle must occur. In this cycle, reduced, ATP-bound Fe protein binds MoFe protein, governed by the on rate k_1 and the off rate k_{-1}. Next, an electron is transferred from Fe protein to MoFe protein, which is coupled to the hydrolysis of two ATP molecules bound to Fe protein, k_2. Finally, oxidized, ADP-bound Fe protein dissociates from reduced MoFe protein, governed by the off rate k_{-3} and the on rate k_3.

At this point, FeMoco is denoted $M\varepsilon_1$ in the scheme because it has received one electron. After a subsequent Fe protein cycle, when FeMoco receives a second electron, it is denoted $M\varepsilon_2$. Once in $M\varepsilon_2$, FeMoco can begin evolving H_2, effectively

losing two protons and two electrons. Alternatively, FeMoco can also continue receiving electrons from Fe protein and eventually bind and reduce N_2. The component protein ratio, total protein concentration, amount of reductant, amount of ATP, and pressure of N_2 all affect the rates of the pathways drawn and whether states $M\varepsilon_2$, $M\varepsilon_3$, and $M\varepsilon_4$ are more likely to evolve H_2 or continue accumulating electrons for N_2 reduction.

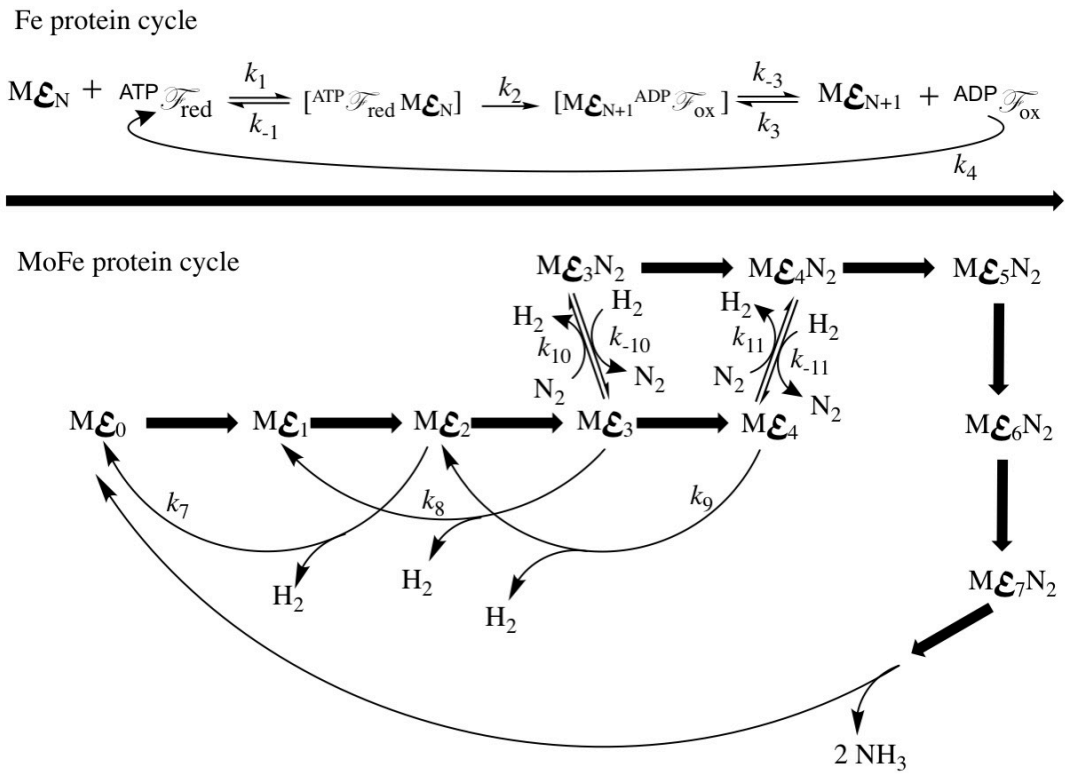

Figure 2.2 Simplified kinetic scheme for nitrogenase reactivity.

Additionally, in this model, N_2 binding is coupled to H_2 release in order to enforce the maximum efficiency limit for nitrogenase of at least one H_2 produced per N_2 reduced.[23] When FeMoco receives its eighth electron, NH_3 molecules are released, and FeMoco returns to the resting state $M\varepsilon_0$ instead of reaching "$M\varepsilon_8$." Once at E_0, the pathway begins again and every Fe protein cycle adds one electron to FeMoco.

Table 2.1 lists the rate constants used initially by T&L. At extremely low protein concentrations, the rate of nitrogenase turnover is governed by the initial rate of component protein association (k_1). At high protein concentrations, the dissociation of oxidized, ADP-bound Fe protein from MoFe protein becomes rate limiting (k_{-3}).

Table 2.1 Rate constants used in Thorneley and Lowe's original model.

Rate constant	Value
k_1	$5 \times 10^7\ M^{-1}s^{-1}$
k_{-1}	$15\ s^{-1}$
k_2	$140\ s^{-1}$
k_3	$2.3 \times 10^6\ M^{-1}s^{-1}$
k_{-3}	$14\ s^{-1}$
k_4	$3 \times 10^6\ M^{-1}s^{-1}$
k_7	$250\ s^{-1}$
k_8	$8\ s^{-1}$
k_9	$400\ s^{-1}$
k_{10}	$4 \times 10^5\ M^{-1}s^{-1}$
k_{-10}	$8 \times 10^4\ M^{-1}s^{-1}$
k_{11}	$2.2 \times 10^6\ M^{-1}s^{-1}$
k_{-11}	$3 \times 10^6\ M^{-1}s^{-1}$

2.3 Results and Discussion

2.3.1 Growth and purification of nitrogenase proteins

Site-directed MoFe protein mutants were made to study the effect electrostatic interactions in the *DG1* crystal structure might have on nitrogenase catalysis. Residues βN399, βK400, and βR401 were each individually mutated to a negatively charged Glu according to published methods. For an extended discussion of the development of procedures for site-directed mutagenesis in *A. vinelandii*, refer to Chapter 4, and implementation instructions can be found in the Appendix.

A double mutant (βN399E/R401E) and a triple mutant (βN399E/βK400E/R401E) were also constructed, but the *A. vinelandii* strains harboring these MoFe mutants grew extremely poorly, even in media containing a

source of fixed nitrogen, which was taken as preliminary evidence that changing the charge of residues at and around βK400 had an adverse effect on the catalytic ability of MoFe protein. However, since cell growth was slow and protein expression was low, these mutants were not studied as extensively as the single mutants.

All *A. vinelandii* strains harboring the single mutants, βN399E, βK400E, or βR401E, in contrast, grew well and approximately 1-2 mg of each MoFe protein mutant was routinely purified per 1 g of *A. vinelandii* cell pellet, which is comparable to purification yields for wild-type MoFe protein.

Interestingly, the *A. vinelandii* strain harboring βK400E yielded an abnormally large amount of wild-type Fe protein during purification. Typical 100 g cell pellets of *A. vinelandii* strain harboring βK400E yielded around 150 mg pure Fe protein, which is double the normal amount of pure Fe protein anticipated from a 100 g cell pellet of wild-type *A. vinelandii*. It was hypothesized but never directly tested that the *A. vinelandii* strain harboring βK400E increased its expression of nifH, the gene coding for the structural component of Fe protein, to mitigate the negative effects of an impaired MoFe protein.

2.3.2 Specific Activity of mutant MoFe proteins for reduction of C_2H_2 to C_2H_4

All three single mutants displayed a decreased catalytic ability to reduce C_2H_2 to C_2H_4 by 2 e^-. At first, however, the decreases were not reproducible over multiple days of experiments or among different researchers because an imprecise standardization method was employed. Modification of the standardization procedure greatly improved the precision of the activity measurements, and only then did it become evident that there was a significant, reproducible decrease in activity for all three single mutants compared to wild-type MoFe protein. For an extended

discussion of the switch in standardization procedure, see Chapter 5, and implementation instructions can be found in the Appendix.

βK400E MoFe protein had the most significant drop in C_2H_2 reduction activity, as shown in Figure 2.3. These experiments were carried out at a constant MoFe protein concentration of 0.2 μM and increasing concentrations of Fe protein, up to a 60-fold molar excess. Though nitrogenase cannot be fully explained by simple Michaelis-Menten kinetics, it can be useful to consider the "K_M" and "V_{max}" of these data, approximating Fe protein as a substrate. Compared to wild-type MoFe protein, which reaches half of its maximum specific activity at an Fe protein concentration of 1.5 μM (a 7.5:1 Fe:MoFe protein ratio), βK400E MoFe protein has an *increased* "K_M", as it does not reach half of its maximum specific activity until an Fe protein concentration of 3.0 μM. Additionally, βK400E MoFe protein has a *decreased* "V_{max}" or maximum specific activity of 1800 nmol C_2H_4 per minute per mg MoFe protein, while wild-type MoFe protein reaches 2500 nmol C_2H_4 per minute per mg MoFe protein under the same experimental conditions. Because βK400E MoFe protein displayed the most dramatic change in activity of the single mutants, many of the remaining experiments were carried out using only βK400E MoFe protein.

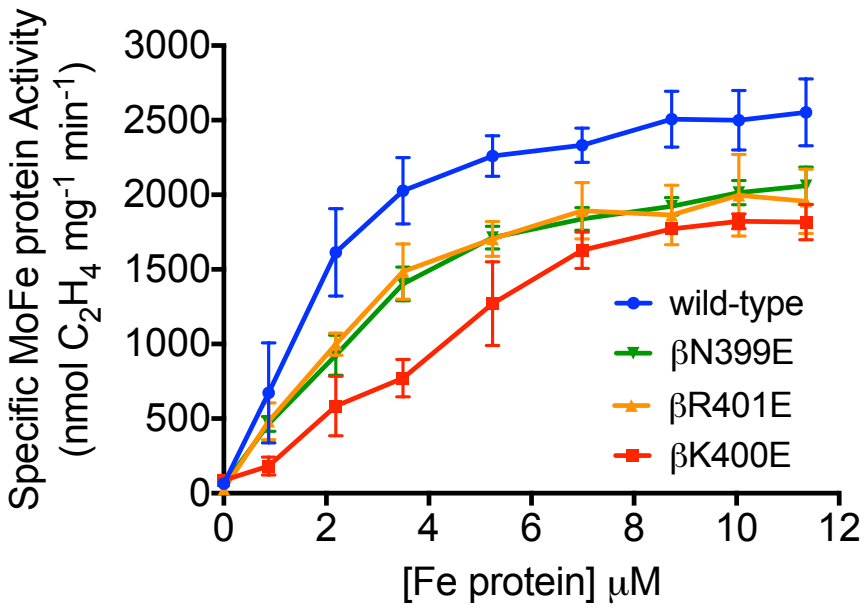

Figure 2.3 Specific activities of wild-type, βN399E, βK400E, and R401E MoFe proteins for C_2H_4 production.

2.3.3 EDC crosslinking of nitrogenase component proteins

Because nitrogenase component proteins from *A. vinelandii* form a specific crosslink in solution between βK400-γE112 when mixed with EDC, crosslinking experiments were carried out to determine whether the charge-reversal mutations made on the surface of MoFe protein altered or prevented native component-protein solution interactions. It is not surprising that βK400E MoFe protein cannot crosslink Fe protein, as is demonstrated by the lack of the high molecular weight band in Figure 2.4, since it lacks residue βK400. Unexpectedly, however, neither βN399E nor βR401E MoFe proteins were capable of crosslinking Fe protein. The approximately 90-kDa band corresponding to covalent β-γ subunit linkage is present in the far left lane of Figure 2.4, in which wild-type MoFe protein was mixed with Fe protein, but it is absent in the remaining three lanes, which from left to right represent reaction of Fe protein with βN399E, βK400E, and βR401E MoFe proteins.

One explanation for this finding is that by changing βN399→E and βR401→E, the orientation of βK400 is altered such that, even though the two proteins may associate in solution, the terminal amine group in βK400 is no longer close enough to the carboxylate of γE112 to allow for crosslinking. However, these data also point to the possibility that component protein association in this region is not just due to the specific hydrogen-bonding interaction between βK400-γE112 but also because of the large, charged patches on the surface of each protein. Fe protein has a negatively charged patch around γE112 (γE110/ γE111/ γE112) and MoFe protein has a positively charged patch around βK400 (βN399/βK400E/R401). Thus, even if βK400 is present, altering the overall charge of the βN399/βK400E/βR401 patch may still lower the likelihood of protein association or prevent it altogether.

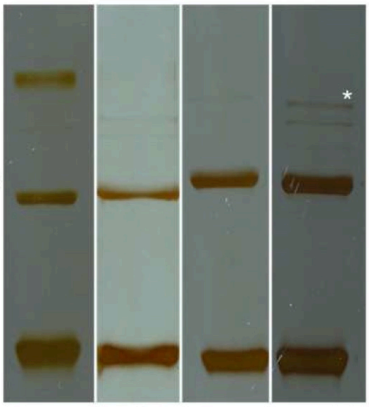

Figure 2.4 EDC crosslinking visualized by SDS-PAGE and Ag+-staining. Lanes from left to right: Fe protein was mixed with **1** wild-type, **2** βN399E, **3** βK400E, or **4** βR401E MoFe proteins.

2.3.4 Inhibition of C_2H_2 to C_2H_4 reduction activity by NaCl

To further probe the electrostatic nature of the PPI in *DG1*, the ability of MoFe proteins to reduce C_2H_2 was tested as a function of increasing concentrations of NaCl. Figure 2.5 shows a graph of normalized activity as a function of increasing NaCl, where the Fe:MoFe protein ratio and the total protein concentration were both

held constant. These data demonstrate that, while wild-type MoFe protein maintains about half of its maximum activity in the presence of 200 mM NaCl, which is in line with the results of previous researchers,[47] βK400E MoFe protein loses half of its maximum activity in just 100 mM NaCl, further highlighting the sensitivity of *DG1* interactions to this charge reversal mutation. These data were used to calculate an $IC_{50,\ NaCl}$ for wild-type MoFe protein of 250 ± 15 mM and an $IC_{50,\ NaCl}$ for βK400E MoFe protein of 130 ± 30 mM NaCl.

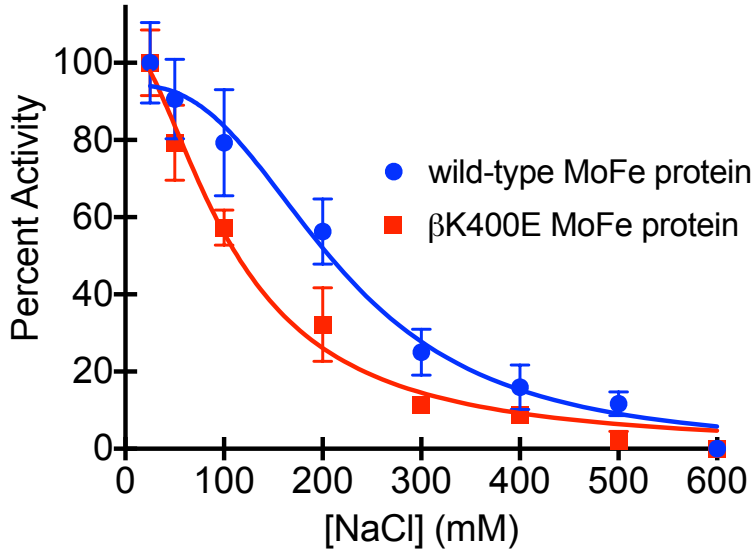

Figure 2.5 Normalized percent specific activity for C_2H_2 reduction versus increasing NaCl for wild-type and βK400E MoFe proteins.

2.3.5 Chelation of Fe from Fe protein by 2,2'-bipyridine

When Fe in Fe protein is chelated by the small molecule 2,2'-bipyridine (bipy), a pink complex ($[Fe(II)bipy_3]^{2+}$) forms, displaying a maximal absorbance at 520 nm. Typically, small amounts of denatured Fe protein are mixed with 2,2'-bipyridine to determine the concentration of Fe protein in solution, but this phenomenon can also be used to investigate the interactions between Fe protein and MoFe protein. The

rate of chelation of Fe in Fe protein increases in the presence of nucleotides but decreases in the presence of MoFe protein, since component protein association during catalysis offers a form of protection to the 4Fe:4S cluster of Fe protein, thereby slowing the rate of chelation.

An Fe chelation experiment was performed, as described previously,[48] to evaluate the ability of βK400E MoFe protein to protect Fe protein from chelation and compare it to that of wild-type MoFe protein. Figure 2.6 shows that, under turnover conditions, βK400E MoFe protein has only a minor effect on the rate of Fe chelation and is not nearly as effective in protecting Fe protein as wild-type MoFe protein. Assuming a simple first-order reaction, the apparent first-order rate constant of Fe chelation from ATP-bound Fe protein decreases from $9.9 \pm 0.1 \times 10^{-3}$ s^{-1} to $2.5 \pm 0.3 \times 10^{-3}$ s^{-1} upon addition of wild-type MoFe protein. Conversely, the addition of βK400E MoFe protein only slows the rate to $5.3 \pm 0.2 \times 10^{-3}$ s^{-1} under the same conditions. These results were interpreted to mean that the βK400→E mutation weakens the nitrogenase component protein association in a catalytically relevant way, as these experiments were conducted under turnover conditions.

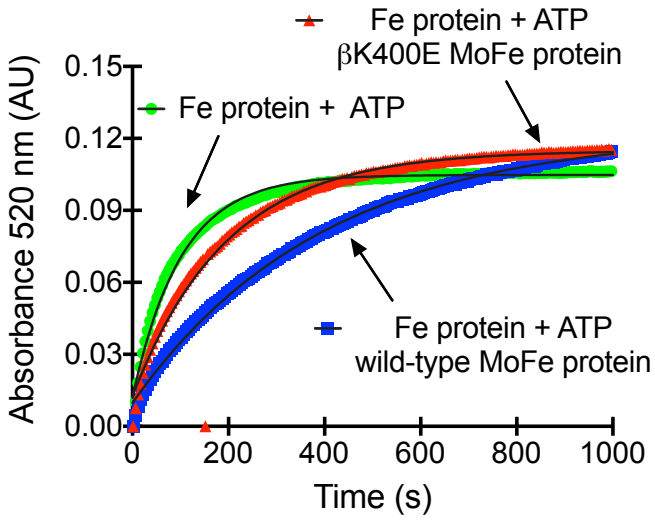

Figure 2.6 Absorbance at 520 nm versus time measures the rate of formation of $([Fe(II)bipy_3]^{2+}$ when Fe protein is mixed with ATP (green), wild-type MoFe protein and ATP (blue), and βK400E MoFe protein and ATP (red).

2.3.6 ATP/2e⁻ ratio is a measure of nitrogenase efficiency

Though the evidence gathered thus far indicates that βK400→E causes a decrease in activity because it weakens component protein association, many previously characterized mutations to the surface of nitrogenase proteins have decreased catalytic abilities because they cause an uncoupling of ATP hydrolysis and productive electron transfer to substrate. According to the Fe protein cycle depicted in Figure 1.2, as well as the nitrogen fixation reaction in Equation 3 (Chapter 1), Fe protein hydrolyzes two molecules of ATP for every electron it transfers to MoFe protein. However, mutations such as αF125A[49] and γR140Q,[50] which alter the surface of Fe and MoFe proteins, respectively, not only generate fewer products than wild-type proteins, they also hydrolyze more than two ATP molecules per electron used for substrate reduction. This finding has been interpreted to mean that these surface mutations prevent proper formation of the activated *DG2* complex, such that some Fe protein cycles involve ATP hydrolysis and component protein dissociation without any

productive electron transfer. Fe protein may be oxidized during this non-productive cycle, but substrates do not get reduced.

The extent of coupling between ATP hydrolysis and electron transfer in nitrogenase is most often evaluated by the ATP/2e$^-$ ratio because all nitrogenase substrates are reduced by multiples of 2 e$^-$. Though the theoretical ATP/2e$^-$ ratio for wild-type nitrogenase is 4 (Equation 3), ratios closer to 5 are typically measured *in vitro* when DT is utilized as the electron source and the reaction is carried out at 30°C.[51] Thus, it was critical to measure the ATP/2e$^-$ ratio for βK400E MoFe protein to rule out uncoupling of nucleotide hydrolysis with electron transfer as a cause for lowered activity. Surprisingly, measuring the ATP/2e$^-$ ratio turned out to be one of the most difficult experimental challenges in this dissertation.

Standard *in vitro* nitrogenase activity assays require the use of an ATP-regeneration system of creatine kinase and phosphocreatine, in order to maintain the large excess of ATP over ADP needed for maximal nitrogenase activity. When the ATP-regeneration system is used, ATP hydrolysis cannot be measured as ADP formed because all ADP formed is immediately reacted with phosphocreatine to regenerate ATP. Only when the regeneration system is omitted can ADP be quantified as a measure of ATP hydrolysis by nitrogenase. When the regeneration system is omitted, ATP and ADP can be separated by RP-HPLC, but in practice,[52] baseline separation of the di- and tri-nucleotides is difficult to achieve in a reasonable time frame. Additionally, nitrogenase behavior is altered when ATP is not in a large excess over ADP,[53] so quantifying ATP hydrolysis by nitrogenase in the absence of the regeneration system is not a true picture of how nitrogenase behaves under maximal activity conditions.

As an alternative to quantifying ADP, nucleotide hydrolysis is often measured by quantifying P_i released from hydrolysis. Again, the ATP-regeneration system

presents a challenge: under the acidic conditions required for colorimetric determination of P_i, phosphocreatine, ATP, and ADP, which are all essential components of the activity assay, readily release P_i through acid-catalyzed hydrolysis, causing a significant over-estimation of the true P_i created from enzymatic nucleotide hydrolysis. In order to measure the extent of ATP hydrolysis as true P_i formed from enzymatic hydrolysis under conditions of maximal activity, a procedure was developed to first separate true P_i from every other component in the activity assay matrix by precipitation with a large excess of $CaCl_2$.[54] The results of the experiments to measure ATP hydrolysis are explained below, but the development and validation of the actual method is explained in detail in Chapter 5, and step-by-step instructions for implementation of the method are provided in the Appendix.

Table 2.2 summarizes the results of efforts to measure the ATP/$2e^-$ ratio for nitrogenase proteins and includes results from work with other nitrogenase surface mutants. Activity assays were carried out in the presence of the ATP-regeneration system and stopped with the addition of 4.0 M NaCl rather than glacial acetic acid. After 50-µL aliquots of each reaction headspace were injected onto the GC to measure C_2H_4 formed, vials were opened and small aliquots of each quenched reaction solution were used to measure enzymatic ATP hydrolysis as P_i released. The nanomoles of P_i formed was divided by the nanomoles of C_2H_4 formed and multiplied by 2 to obtain the ATP/$2e^-$ ratios. As can be seen from Table 2.2, the ATP/$2e^-$ ratios for wild-type and βK400E MoFe proteins agree within one standard deviation of one another and both lie in the expected range for proteins that have fully coupled ATP hydrolysis and electron transfer processes. From these data, it can be concluded that the charge reversal βK400→E does not affect the coupling of ATP hydrolysis with productive electron transfer to substrate, so the lowered activity of this

mutant must be the result of alterations to a different step or steps in nitrogenase turnover.

Table 2.2 ATP/2e$^-$ ratios and maximum specific activity for 2-e$^-$ reductions of wild-type and mutant nitrogenase proteins.

	Location of mutation	ATP/2e$^-$	Maximum Specific activity for 2-e$^-$ reductions (nmol min^{-1}mg^{-1})
Wild-type		4.9 ± 0.3 (This work)	2500
αF125A	*DG2*	12	150
γR140Q	*DG2*	8	500
βK400E	*DG1*	4.2 ± 0.8 (This work)	1800

2.3.7 Investigating component protein interactions with fluorescence spectroscopy

Because the mutations described thus far result in a decreased catalytic ability compared to wild-type proteins, it would be advantageous to have a way to directly attribute the reduction in activity to a decrease in the association kinetics or binding affinity of the component proteins due to perturbations in this region. A method was sought to fluorescently label the Fe and MoFe proteins for interrogation of solution interactions via fluorescence polarization or Förster Resonance Energy Transfer (FRET) experiments. There is precedent for site-specific labeling of MoFe protein at amino acid αC45,[55] which is the only surface-exposed Cys residue on MoFe protein, so this work began with attempts to site-specifically label Fe protein. As MoFe protein is about four times larger than Fe protein, it was not expected that component protein binding would cause a substantial change in the fluorescence polarization of a fluorophore attached to MoFe protein. If, however, Fe protein could be fluorescently labeled, binding of the component proteins may cause a change in the fluorescence polarization of the fluorophore attached to Fe protein. Alternatively, if both component proteins could be modified with fluorophores, PPI could be monitored by FRET.

Unlike MoFe protein, there are no surface-exposed Cys residues on Fe protein, so if one were to be introduced through mutagenesis, it may be possible to site-specifically, covalent link a fluorophore to a mutated Cys residue. This strategy was not pursued, however, because Fe protein contains an extremely surface-exposed 4Fe:4S cluster. To avoid damaging the 4Fe:4S cluster with Cys-reactive chemistry, in the present work, a non-covalent strategy was employed in which a Zn^{2+}-bound fluorophore was coordinated to an N-terminal His-tag on Fe protein.

2.3.8 Expression, purification, and fluorescent labeling of His-tag Fe protein

An *A. vinelandii* strain harboring Fe protein with an N-terminal His-tag was kindly provided by Markus W. Ribbe (University of California, Irvine). Cells were capable of diazotrophic growth and had a doubling time similar to cells containing wild-type nitrogenase. His-tag Fe protein was purified following procedures reported previously to purify wild-type Fe protein[56] and achieved approximately 60% of the specific activity of wild-type Fe protein for the 2-e^- reduction of C_2H_2 to C_2H_4, shown in Figure 2.7. This figure shows the specific activity of Fe protein for the reduction of C_2H_2 to C_2H_4 in units of nmol product generated per minute of reaction per mg of Fe protein versus the molar ratio of the component proteins. In this experiment, Fe protein was held constant at 1.0 μM and MoFe protein was iteratively increased. His-tag Fe protein reached a maximum specific activity of about 60% of the maximum specific activity of wild-type Fe protein. The slight decrease in activity at high concentrations of MoFe protein is a well-documented phenomenon of Fe protein specific activity often referred to in the literature as “MoFe inhibition”.[57]

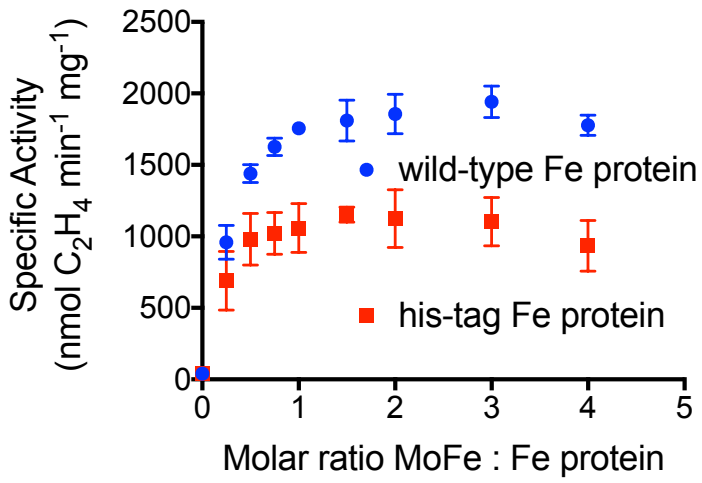

Figure 2.7 Comparison of the specific activities of wild-type and His-tag Fe proteins.

HisZiFiT is a fluorescent molecule designed to coordinate two Zn^{2+} ions, as shown in Figure 2.8.[58] HisZiFiT was synthesized according to published procedures. Coordination of HisZiFiT to His-tag Fe protein was accomplished by mixing the two components together in the presence of Zn^{2+}. After mixing, His-tag Fe protein was concentrated with a 10-kDa filter to remove excess HisZiFiT. Labeling was verified by the fact that the protein solution in the filter remained bright pink even when the flow through became clear.

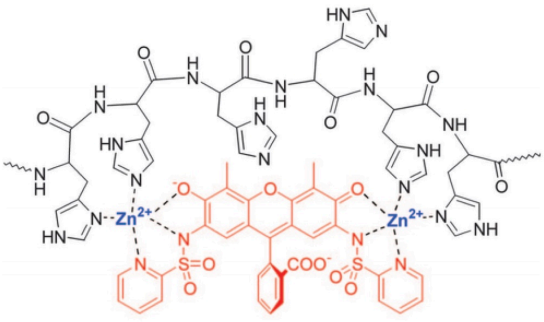

Figure 2.8 Coordination of HisZiFiT (orange) to a hexahistine polypeptide (black) via coordination of two Zn^{2+} ions, adapted from ref *58.*

2.3.9 EDC crosslinking visualized by gel electrophoresis

When no reproducible change in fluorescence intensity, wavelength of maximum emission, or polarization of emitted light was observed upon mixing HisZiFiT-labeled His-tag Fe protein with increasing concentrations of MoFe protein, chemical crosslinking experiments were carried out to assess the ability of HisZiFiT-labeled His-tag Fe protein to associate with MoFe protein in solution.

In the first experiment, His-tag Fe protein was mixed with MoFe protein, Mg^{2+}-ATP, and DT as a source of electrons, the minimum requirements for nitrogenase turnover. EDC was added to initiate the reaction, and aliquots of the reaction were removed at various times to monitor the formation of the covalent crosslink between βK400-γE112. As can be seen in the left three lanes of the reducing SDS gel in Figure 2.9, His-tag Fe protein is capable of forming the βK400-γE112 crosslink when mixed with MoFe protein. The appearance of the highest molecular weight band around 90 kDa corresponds to covalent linkage of the ~ 30 kDa γ-subunit of Fe protein to the ~ 60 kDa β-subunit of MoFe protein. The middle band corresponds to unreacted MoFe subunits, and the lowest molecular weight band corresponds to unreacted Fe protein subunits. The right three lanes of the gel in Figure 2.9 show that once His-tag Fe protein has been mixed with Zn^{2+} and HisZiFiT, it can no longer participate in the formation of the βK400-γE112 crosslink, even after a 30-minute reaction.

As a further test, this same crosslinking experiment was also performed with wild-type Fe protein and wild-type Fe protein that had been mixed with Zn^{2+} and HisZiFiT, and subsequently buffer-exchanged by repeated passage through a 10-kDa filter to remove excess Zn^{2+} and fluorophore. The results of the experiment are summarized in the SDS gel in Figure 2.10, which shows the same results as the experiments with His-tag Fe protein. Under the given experimental conditions, wild-

type Fe protein formed the specific βK400-γE112 crosslink with MoFe protein in just 5 minutes, but wild-type Fe protein that had been incubated with Zn^{2+} and fluorophore did not form any crosslink, even after 30 minutes.

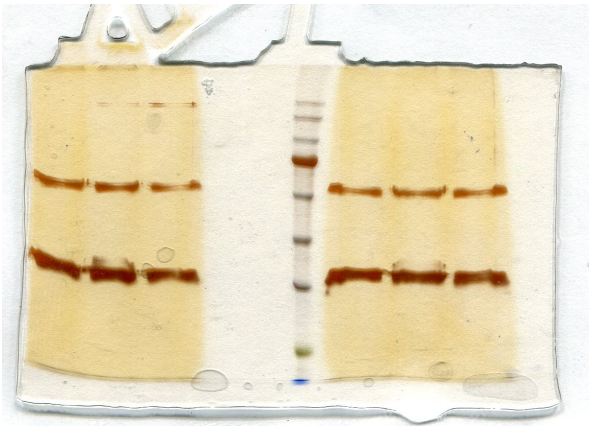

Figure 2.9 EDC crosslinking of his-tag Fe protein and HisZiFiT-labeled his-tag Fe protein with MoFe protein visualized by Ag^{+}-staining of a 10% reducing SDS gel. Lanes from left to right: his-tag Fe protein mixed with MoFe protein, Mg^{2+}-ATP, DT, and EDC at time **1** 0 min, **2** 5 min, **3** 30 min, **4** ladder, HisZiFiT-labeled his-tag Fe protein mixed with MoFe protein, Mg^{2+}-ATP, DT, and EDC at time **5** 0 min, **6** 5 min, **7** 30 min.

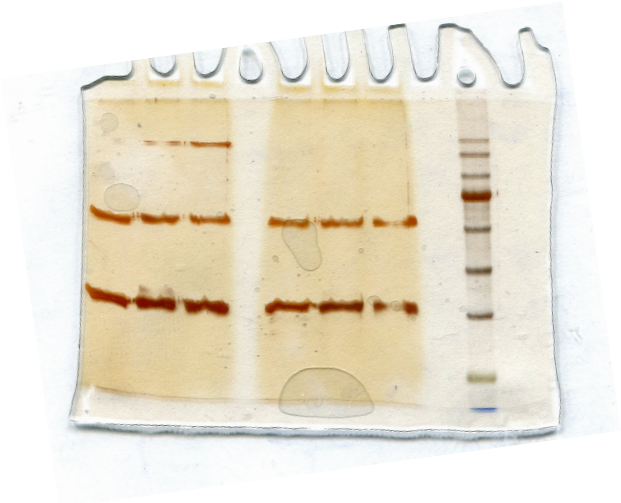

Figure 2.10 EDC crosslinking of wild-type Fe protein and HisZiFiT-labeled wild-type Fe protein with MoFe protein visualized by Ag^{+}-staining of a 10% reducing SDS gel. Lanes from left to right: wild-type Fe protein mixed with MoFe protein, Mg^{2+}-ATP, DT, and EDC at time **1** 0 min, **2** 5 min, **3** 30 min, **4** HisZiFiT-incubated Fe protein mixed with MoFe protein, Mg^{2+}-ATP, DT, and EDC at time 0 min, **5** 5 min, **6** 30 min, and **7** ladder.

2.3.10 Specific activity of Fe protein in the presence of Zn^{2+}

One interpretation of the results in Figure 2.9 is that when Zn^{2+}-HisZiFiT is bound to the N-terminal His-tag on Fe protein, Fe protein is prevented from interacting with MoFe protein in a way that brings βK400 and γE112 into close proximity with one another. The results from Figure 2.10, though, leave open the possibility that simply incubating Fe protein with Zn^{2+} and HisZiFiT can cause some irreversible conformational change that alters the surface of Fe protein, or that some Zn^{2+} binds to Fe protein so tightly that even after filtering Fe protein, Zn^{2+} remains bound in a location that prevents close association of βK400 and γE112.

To test the above hypotheses, activity assays measuring wild-type Fe protein specific activity were carried out in the presence of Zn^{2+}. Figure 2.11 shows that Fe protein activity was reduced in the presence of Zn^{2+} (green squares), as compared to activity assays conducted on the same day without Zn^{2+} (blue circles). In this experiment, Fe protein was held constant at 1.0 μM and MoFe was iteratively increased. Fe protein that had been pre-incubated with Zn^{2+} and then passed over a 10-DG column to remove Zn^{2+} before activity tests did display some activity, but this Fe protein was never as active as protein that had never been mixed with Zn^{2+}. Thus, Zn^{2+} may have some small but irreversible effect on Fe protein. Zn^{2+} may bind in an inhibitory location on the protein with high affinity and remain bound even after passage over a desalting column. Alternatively, Zn^{2+} may induce some structural rearrangement of Fe protein that persists even when Zn^{2+} is removed. Incubation of both His-tag and wild-type Fe proteins with Zn^{2+}-HisZiFiT prevents the formation the specific EDC crosslink between βK400 and γE112, suggesting solution PPI between Fe and MoFe proteins have been significantly altered. Additionally, it is unclear the extent to which Zn^{2+} irreversibly inhibits Fe protein activity even after it is removed from the solution. Taken together, these findings suggested that fluorescence labeling

of the component proteins using this strategy was not a productive way to assess the strength of PPI in *DG1*.

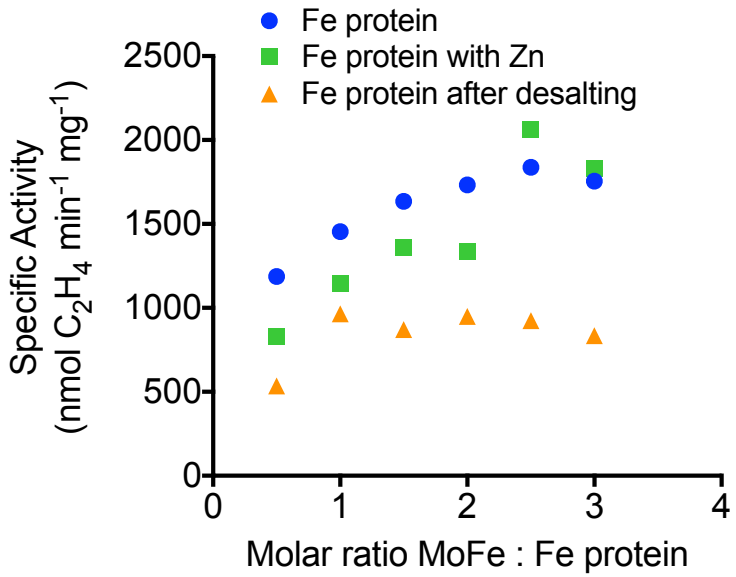

Figure 2.11 Comparison of the specific activities of Fe proteins upon various exposures to Zn^{2+}.

2.3.11 Dilution experiment and the Thorneley-Lowe model

The evidence presented thus far indirectly indicates that βK400→E weakens component protein association without affecting downstream processes that take place in the activated complex. When the fluorescence labeling efforts described above proved unsuccessful, an alternative method to measure binding affinities was devised. T-L incorporates k_1 and k_{-1} to model initial, reversible binding of Fe-MoFe protein, and this is described in Figure 2.2. T&L measured k_1 with stopped-flow experiments,[38] but k_{-1} was determined by a dilution experiment.[39] In this experiment, the Fe:MoFe protein ratio was held constant and the total protein concentration in the reaction was varied. At a low enough absolute protein concentration, k_1 becomes rate limiting in steady-state turnover experiments. At protein concentrations above the

effective K_d, the relationship between protein concentration and product formation is linear, but at protein concentrations below the effective K_d, this linear relationship disappears. Since k_1 and all other rate constants in their model had already been determined, T&L fit data from the dilution experiment to their kinetic scheme to solve for k_{-1}.[39]

In a similar way, the dilution experiment was used in this work to elucidate differences between the rate of association of wild-type and βK400E MoFe proteins with Fe protein. First, a simplified T-L kinetic model for C_2H_2 reduction to C_2H_4 was used to predict how varying the rate of component protein association would alter overall nitrogenase activity. This simplified scheme is shown in Figure 2.12; the Fe protein cycle involving k_1, k_{-1}, k_2, k_{-2}, k_3, and k_{-3} remains the same, but only 2 electrons, and thus only two Fe protein cycles, are required for the production of one molecule of product. Additionally, no transition state beyond $M\varepsilon_4$ is modeled. The values of the additional rate constants used in this scheme are listed in Table 2.3. When this kinetic model is numerically solved in Mathematica, a change in the Fe – MoFe protein association rate is predicted to have a small effect on overall activity at high Fe:MoFe ratios but a dramatic effect on overall activity at low Fe:MoFe ratios and low total protein concentrations.

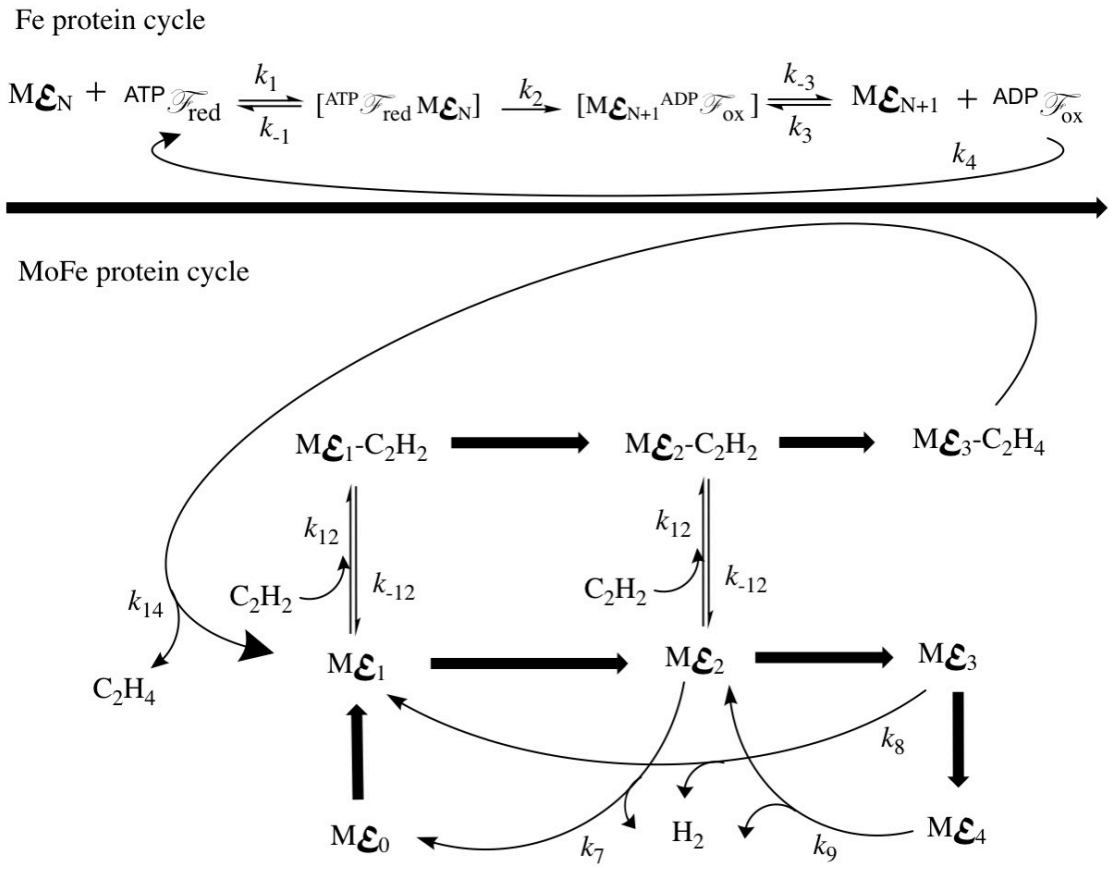

Figure 2.12 Simplified Thorneley-Lowe kinetic model for the 2-e$^-$ reduction of C_2H_2 to C_2H_4.

Table 2.3 Additional rate constants k_{12}, k_{-12}, and k_{14}, used to simulate nitrogenase reduction of C_2H_2 to C_2H_4.

Rate constant	Value
k_{12}	$4 \times 10^5\ M^{-1}s^{-1}$
k_{-12}	$8 \times 10^4\ M^{-1}s^{-1}$
k_{14}	$2.2 \times 10^6\ M^{-1}s^{-1}$

With the predictions in hand, dilution experiments were carried out for wild-type and βK400E MoFe proteins. Figure 2.13 shows experimental data obtained in a dilution experiment performed with wild-type and mutant MoFe proteins. The Fe:MoFe protein ratio was held constant at 4:1 and the total amount of protein in solution was varied. Figure 2.13 shows the total activity in units of nmol of product per

minute versus the MoFe protein concentration. The curves in Figure 2.13 are the simulations of the experimental data that were created by the T-L kinetic model in Mathematica by altering k_1 to obtain good simulations of the data. The points are the averages of at least three sets of experimental data, and the error bars represent ± one standard deviation. Wild-type dilution data were well simulated with a k_1 of 2.5 x 10^7 $M^{-1}s^{-1}$ and a k_{-1} of 15 s^{-1}. A k_{-1} of 15 s^{-1} comes from the original T-L dilution experiment using *K. pneumoniae* nitrogenase proteins. A k_1 of 5.0 x 10^7 $M^{-1}s^{-1}$ was determined by Thorneley and Lowe for *K. pneumoniae* nitrogenase, but experimental results of the dilution experiment using *A. vinelandii* nitrogenase proteins were best fit with a k_1 of 2.5 x 10^7 $M^{-1}s^{-1}$ (Figure 2.14 A).

Data from the dilution experiment for βK400E MoFe protein were well simulated when k_1 was lowered 5-fold to 0.5 x 10^7 $M^{-1}s^{-1}$ (Figure 2.14 B). All other rate constants were the same as for the wild-type simulation. Interestingly, changing k_{-1} had little effect on the simulations (Figure 2.14 C). The fact that the dilution experiment data were well simulated for βK400E simply by lowering the k_1, the rate of initial component protein association, strongly suggests that reversing the charge at position βK400 alters nitrogenase turnover by slowing the rate of component protein association but not ATP hydrolysis or electron transfer.

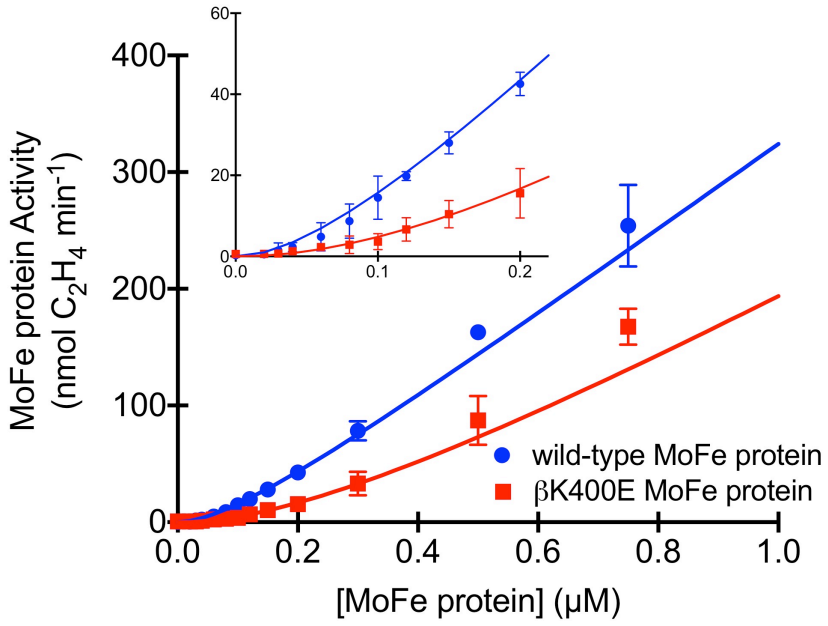

Figure 2.13 Dilution experiment measuring product formation over time versus total protein concentration.

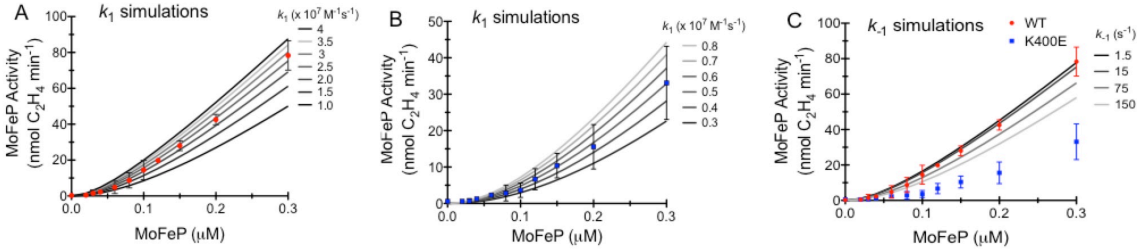

Figure 2.14 Simulations of dilution experiment data for **A** wild-type MoFe protein using multiple values for k_1, **B** βK400E MoFe protein using multiple values for k_1, and **C** wild-type MoFe protein using multiple values for k_{-1}.

2.4 Conclusions

Through investigation of the mutant βK400E MoFe protein, it was concluded that the electrostatic PPI between the positively charged patch on the surface of the β-subunit of MoFe protein and the negatively charged patch on the surface of Fe protein are catalytically relevant and involved in the pathway to the formation of the activated *DG2*-like complex. Previous work, such as the EDC crosslinking

experiments and the *DG1* crystal structure, provided indirect evidence for this hypothesis, but until this investigation it had not been explicitly evaluated. Dynamic encounter complexes have been implicated in the formation of complexes of other electron transfer partners,[59] in line with the observations about nitrogenase described here.

2.5 Future Directions

Here, the T-L model was used to rationalize the observed behavior of βK400E MoFe protein for simple 2-e^- reduction processes. There are inherent challenges associated with measuring NH_3 produced by nitrogenase, due to the complexity of the nitrogenase activity assay matrix; thus, mechanistic hypotheses concerning nitrogenase are typically evaluated by H^+ or C_2H_2 reduction alone. Recently, however, significant initial efforts were made to overcome these experimental limitations in order to measure the partitioning of electrons to H^+ and N_2 under conditions in which nitrogenase proteins are fully active but the electron flux is low, in order to evaluate whether the partitioning of electrons under N_2 differs for the mutant βK400E and wild-type MoFe proteins.

2.5.1 The ratio of N_2 reduced to H_2 produced is a measure of nitrogenase efficiency

While the ATP/2e^- ratio was previously used as a measure of nitrogenase efficiency, where the experimentally measured amount of ATP hydrolyzed per 2-e^- transferred to substrate was benchmarked against the theoretical maximum efficiency of ATP/2e^- = 4, nitrogenase efficiency can also be evaluated in terms of the NH_3:H_2 ratio. The NH_3:H_2 ratio is a way to understand the percentage of total electron flow that is actually used to reduce N_2, as compared to the percentage of total electron flow that is "wasted" as H_2 evolution. According to the consensus reaction equation, nitrogenase can never utilize more than 75% of its total electron flow for NH_3

production. For every 6-e^- used to reduce $N_2 \rightarrow NH_3$, at least 2-e^- will be diverted to H^+ reduction.

At early reaction times, low Fe:MoFe protein ratios, low total protein concentrations, limiting reductant DT, and low pN_2, nitrogenase may "waste" up to 100% of electron flow to H_2 production, but as each of these variables is altered, NH_3 production increases, until it achieves the limiting stoichiometry of 2 NH_3 produced per 1 H_2 evolved.[23,60] Surprisingly, there are no published reports of the NH_3:H_2 ratio for wild-type *A. vinelandii* nitrogenase under conditions of low electron flux in which NH_3 and H_2 are determined from the same reaction vial. When the ratio is reported, it is often an estimation based on the difference in H_2 activity of nitrogenase under Ar and N_2 atmospheres. The NH_3:H_2 formation ratio could be known much more precisely if NH_3 was actually measured and if both products of the reaction were measured from the same reaction vial.

Even before nitrogenase component proteins were ever purified, it was established from *in vivo* experiments that the system responsible for nitrogen fixation also produces H_2 and that H_2 acts as a "competitive inhibitor" of biological nitrogen fixation.[61-63] Many people simply assumed H_2 evolution by nitrogenase could be eliminated under the right experimental conditions, but this hypothesis was largely discarded in 1984 when Simpson and Burris showed that even a pressure of 50 atm N_2 could not fully suppress H_2 evolution during N_2 reduction.[23] The results of Simpson and Burris showed a maximum of about 2 NH_3 produced per H_2 evolved. To put it another way, about 1 H_2 was evolved for every N_2 reduced.

In their model, T&L ascribed mechanistic importance to this near whole number ratio. They conveniently explained both the seemingly limiting stoichiometry as well as previous observations as to the competitive nature of H_2 inhibition of N_2 reduction by coupling N_2 binding to H_2 release in their kinetic model. These dual assumptions,

that N_2 binding is coupled to H_2 release, and that nitrogenase can never produce more than 2 NH_3 per H_2, as well as the entirety T-L model itself, have gone essentially unquestioned since T&L published their model in 1984.

Intriguingly, however, though the T-L model is ubiquitous in today's scholarly work on nitrogenase, many predictions of the T-L model have never been directly tested. Specifically, while it has been established that nitrogenase produces no more than 2 NH_3 per H_2 under conditions of extremely high electron flux, that is, high Fe:MoFe protein ratios, this ratio has never been investigated at conditions of low electron flux. The T-L model was based on the experimentally observed behavior of nitrogenase at high Fe:MoFe protein ratios, but in the cell, where there are approximately equimolar amounts of each protein present, the N_2 reduction efficiency is not well understood at all.[64] Because the βK400→E mutation has the most dramatic impact of activity at low excesses of Fe protein, preliminary efforts were made to measure the product formation ratio for both wild-type and βK400E MoFe proteins under conditions of low electron flux.

2.5.2 Modified indophenol method for NH_3 detection in nitrogenase activity assays

Many procedures have been reported for the determination of NH_3 produced by nitrogenase, but in practice there are many challenges associated with each method, which are somewhat similar to the challenges encountered in measuring ATP hydrolysis by nitrogenase. Again, the ATP-regeneration system, which is necessary to study nitrogenase under conditions of maximum activity, contains components that interfere with colorimetric and fluorimetric determination of NH_3. When creatine kinase utilizes phosophocreatine to regenerate ATP, it also produces free creatine, which is a primary amine, and primary amines typically react with reagents designed to react with NH_3 for absorbance and fluorescence detection.

A first attempt to measure NH_3 production by nitrogenase was undertaken using an adaptation of the standard indophenol method for quantifying ammonia.[65] The reaction of NH_3 in basic conditions with phenol and bleach to form a colored complex is shown in Figure 2.15. The adaptation to the method involves a chromatography step prior to mixing NH_3 with phenol and bleach in order to separate the NH_3 generated by nitrogenase from the interfering substances, such as creatine, in the activity assay matrix.[66] Activity assay solutions and all NH_3 standard solutions were individually passed over small columns containing anion exchange resin in order to separate NH_3 from the interfering substances, but, unfortunately, reproducible measurements could never be obtained when the ATP-regeneration system was employed.

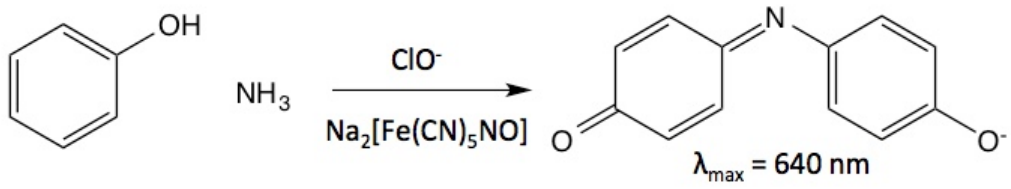

Figure 2.15 Scheme for the reaction of phenol, ammonia, and bleach with a nitroprusside catalyst to yield the colored indophenol complex.

This is most likely due to the fact that a typical analysis requires the measurement of 50 μM NH_3 in the presence of mM quantities of creatine formed from regeneration of ATP. Even if the chromatography step removes 99% of the creatine from the solution, it is feasible that as much as 20 μM creatine would remain in a solution containing 50 μM NH_3. Furthermore, if the chromatography step removes 99% of 2 mM creatine from reaction A but only 98% of 2 mM creatine from an identical reaction B, then after chromatography, reaction A would be a solution containing 50 μM NH_3 and 20 μM creatine, but reaction B, which is identical in protein added, reaction time, and all other reaction conditions, would be a solution containing

an equal amount of NH_3 but 30 μM creatine, and there would be visible difference in the color of these samples when mixed with the indophenol reagents even though they were duplicate reactions containing the same amount of NH_3. Thus, it is not at all surprising that, though this chromatography step has been suggested and implemented in the literature, it is not useful in practice.

As a result, NH_3 production by both wild-type and βK400E MoFe proteins could only be measured with the indophenol method for NH_3 determination in the absence of the ATP-regeneration system. While not a perfect parallel to behavior under maximal activity conditions, the indophenol assay constituted an initial effort to characterize the partitioning of electrons to NH_3 and H_2 by MoFe protein at a low flux (low excess of Fe protein).

Since creatine is known to be one of the largest sources of interference in the indophenol reaction, activity assays were performed to assess the specific activity of NH_3 formation by βK400E MoFe and wild-type MoFe proteins in which the ATP-regeneration system was omitted. The results of these experiments are summarized in Table 2.4. Reactions contained 0.4 μM MoFe protein, 8 μM Fe protein, 13 mM DT, 1 atm N_2, and 20 mM MgATP (20:1 Fe:MoFe protein ratio). As expected, the absolute rates of product formation are lower than what is typically reported for wild-type nitrogenase because the ATP-regeneration system was omitted. Additionally, as anticipated, the rates of NH_3 and H_2 formation by βK400E MoFe protein were lower than the rates of product formation by wild-type MoFe protein. Intriguingly, contrary to predictions using the T-L model, βK400E MoFe protein was not impaired in its ability to divert electrons to N_2 reduction and minimize loss of reducing equivalents as H_2. The range of NH_3:H_2 product formation ratios for βK400E MoFe protein overlaps with that of wild-type.

Table 2.4 Determination of the partitioning of electrons under an N_2 atmosphere using the indophenol method for ammonia detection.

	NH_3:H_2 predicted by T-L model	Experimental NH_3:H_2	nmol NH_3 min^{-1} mg $MoFe^{-1}$	nmol H_2 min^{-1} mg $MoFe^{-1}$
Maximum reported values for wild-type MoFe	1.5	≤ 2	700 – 1100	400 – 600
Wild-type MoFe without ATP-regeneration	0.5	0.8 – 1.6	400 ± 70	350 ± 60
βK400E MoFe protein without ATP-regeneration	0.1	1.0 – 2.1	270 ± 30	190 ± 50

2.5.3 Modified OPA method for NH_3 detection in nitrogenase activity assays

Because the results described thus far could only be accomplished under conditions where the nitrogenase component proteins were partially inhibited, an alternative NH_3 detection strategy was sought that would allow reliable measurement of NH_3 formation by fully active nitrogenase proteins.

Next, a well-established method for detection of NH_3 by fluorescence was implemented. When NH_3 is mixed with *o*-phthalaldehyde (OPA) and a reducing agent, such as β-mercaptoethanol (BME), a fluorescent product forms.[67,68] The reaction is shown in Figure 2.16. Like the indophenol assay, though, the OPA method also suffers from interferences due to components in the nitrogenase activity assay matrix, in particular, creatine. Thus, whenever NH_3 formed by nitrogenase is measured by fluorescence detection after reaction with OPA and BME, the procedure necessarily includes a chromatography step. Typically, aliquots of quenched nitrogenase activity assays are reacted with the OPA reagents and then separated by HPLC to quantify the amount of NH_3 in solution, in order to separate fluorescent products formed from reaction of OPA with NH_3 from fluorescent products formed from reaction of OPA with compounds containing primary amines, such as creatine.

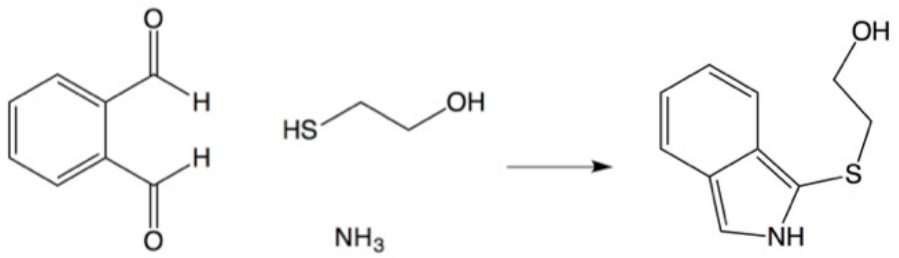

Figure 2.16 Reaction of ammonia with OPA and BME to form a fluorescent product.

Intriguingly, shortly after this OPA-HPLC method was first reported for measuring NH_3 in nitrogenase assays,[69] it was shown that replacement of BME with sulfite provides a substantial increase in the selectivity of this method for NH_3 over primary amines.[70] Indeed, when this modification was employed, the fluorescence of NH_3 standard solutions was unaffected by up to a 50-fold excess of creatine. BME was thus replaced with sulfite in order to create a simple method to measure the amount of NH_3 produced by fully active nitrogenase proteins that does not require any chromatography. A detailed explanation of the optimization and implementation of both absorbance and fluorescence NH_3 detection methods can be found in Chapter 5, and SOPs for both methods, as well as how to decide which technique is appropriate for a given experiment, can be found in the Appendix.

With the new method in hand, activity assays assessing the product formation ratio for wild-type and mutant MoFe protein were repeated under an N_2 atmosphere. This time the rates of NH_3 and H_2 formation were measured as well as the rate of ATP hydrolysis, to ensure that any changes in the product formation rates of βK400E MoFe protein were not due to an uncoupling of ATP hydrolysis with productive electron transfer. H_2 was measured by GC, and ATP hydrolysis was measured by quantifying the amount of P_i released, as reported previously.[54]

To measure NH_3, aliquots of quenched activity assays were passed through a 10-kDa filter to remove protein, and the flow-through was reacted with OPA and sulfite at pH 11 for two hours in the dark. Absolute specific activities along with the measured ATP/$2e^-$ ratios for a 15:1 Fe:MoFe protein ratio are summarized in Table 2.5. At a 15:1 Fe:MoFe protein ratio, wild-type MoFe protein displayed a specific activity of about 600 nmol min^{-1} mg^{-1} for NH_3 formation and about 470 for H_2 formation, leading to a range of NH_3:H_2 ratios between 1.0 – 1.6. In contrast, at a 15:1 Fe:MoFe ratio, βK400E MoFe protein displayed a specific activity of about 370 nmol min^{-1} mg^{-1} for NH_3 formation and about 200 for H_2 formation, leading to a range of NH_3:H_2 ratios between 1.8 – 2.1. The ATP/$2e^-$ was near 4 in all of these experiments, suggesting H_2 and NH_3 evolution rates were not substantially overestimated or underestimated.

The product formation ratio NH_3:H_2 was measured at a variety of component protein ratios over multiple days, and the results are summarized in Figure 2.17. All experiments were carried out with 0.4 μM MoFe and either a 5-, 10-, or 15-, 20-, or 30-fold molar excess of Fe protein and included the ATP-regeneration system of creatine kinase and phosphocreatine to prevent inhibition of nitrogenase by ADP. Additionally, control reactions were performed in which only one nitrogenase component protein was present, in order to confirm that no NH_3, H_2, or P_i was detected in the absence of all the requirements for turnover. The NH_3:H_2 ratio for βK400E MoFe protein when mixed with a 5-fold molar excess of Fe protein is omitted from Figure 2.17 because the H_2 produced in these reactions was below the limit of quantitation using GC-TCD detection. Figure 2.17 shows that βK400E MoFe protein, though it produces a smaller absolute quantity of NH_3 compared to wild-type MoFe protein, is more efficient in its ability to divert electrons to NH_3 and minimize H_2 formation.

Table 2.5 Repetition of the determination of the partitioning of electrons under an N_2 atmosphere using a modified OPA method for ammonia detection.

	NH_3:H_2 predicted by T-L model	Experimental NH_3:H_2	nmol NH_3 min^{-1} mg^{-1}	nmol H_2 min^{-1} mg^{-1}	ATP/$2e^-$
Reported in literature for wild-type MoFe	1.5	≤ 2	700 – 1100	400 – 600	4 – 5
Wild-type MoFe	0.5	1.0 – 1.6	460 – 710	300 – 670	3.1 – 5.5
βK400E MoFe	0.1	1.8 – 2.1	320 – 430	170 – 230	4.4 – 5.1

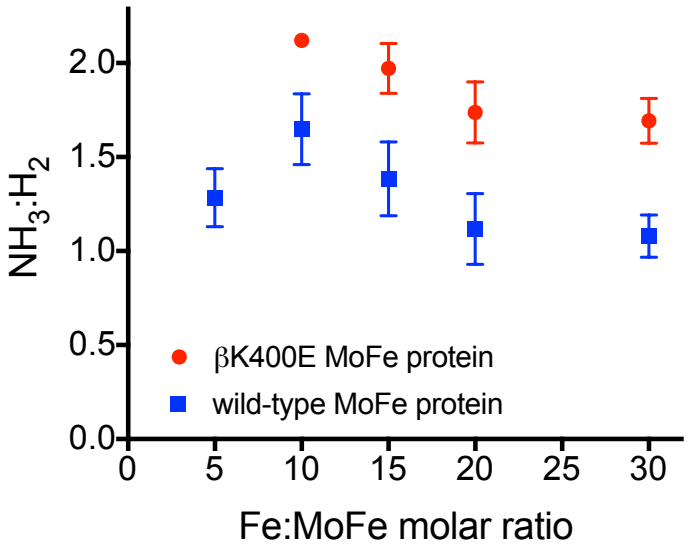

Figure 2.17 Summary of product formation ratio as a function of electron flux for wild-type and βK400E MoFe proteins. Error bars represent ± one standard deviation of at least 3 measurements, and when the error bars are not visible it is because the standard deviation is so small as to not be visible at this scale.

The T-L model predicts that by lowering the k_1 five-fold, from 2.5 x 10^7 $M^{-1}s^{-1}$ to 0.5 x 10^7 $M^{-1}s^{-1}$ for the mutant βK400E MoFe protein, not only will the total electron flow to substrate be lowered, but the efficiency of this electron flow in reducing N_2 would be impaired as well. In contrast to the T-L model, βK400E MoFe protein has a

slightly higher product formation ratio than wild-type MoFe protein, while maintaining a lower net electron flow, at all the component protein ratios tested.

Though the T-L model is able to explain the decrease in catalytic ability of βK400E MoFe protein for the 2-e^- transfer processes of H^+ and C_2H_2 reduction, the model could not simulate the experimentally measured behavior of βK400E MoFe proteins under an N_2 atmosphere. PPI, which are far away from any metal cofactors and are populated prior to the formation of the activated nitrogenase complex during turnover, affect not only net electron flow but also the distribution of those electrons to N_2 and H^+ reduction during nitrogen fixation.

According to the T-L model, at low protein concentrations, protein association is rate-limiting, and the rate of catalysis is k_1[MoFe][Fe]. At high protein concentrations, however, when protein dissociation is rate-limiting, and the rate of catalysis is k_{-3}[^{ox}Fe-MoFe]. In order to lower the overall specific activity, then, either k_1 or k_{-3} must be lowered. In the previous chapter, the behavior of βK400E MoFe protein for the 2-e^- reduction of C_2H_2 was successfully simulated by lowering k_1 5-fold relative to wild-type, while leaving k_{-3} unaffected.

A key attribute of the T-L kinetic model, though, is that only free MoFe protein, not bound to any Fe protein, can bind substrates and release products. This feature is included because T&L believed k_{-3} to be the rate-limiting step in catalysis, and the well-documented lag phase of product formation suggests two slow steps must occur before H_2 evolution, so they inferred Fe protein must dissociate before H_2 evolution, and extended this assumption to all substrates and products. Since electrons can be diverted to either H_2 evolution or N_2 reduction during biological nitrogen fixation, and H_2 can only be evolved from $M\varepsilon_2$, $M\varepsilon_3$, of $M\varepsilon_4$ when MoFe protein is not bound to Fe protein, the amount of free MoFe protein at any given time affects the overall NH_3:H_2 product formation ratio. Lowering k_1 lowers overall nitrogenase activity, but because it

increases the amount of free MoFe protein in solution, it necessarily decreases the NH_3:H_2 ratio. Lowering k_{-3} has the opposite effect – it leads to a drop in overall activity, but because it decreases the amount of free MoFe protein in solution, it necessarily increases the NH_3:H_2 ratio. No manual modulation of k_{-3} was able to simulate NH_3:H_2 product formation ratios for βK400E MoFe protein while maintaining a reasonable amount of absolute specific catalytic activity. Thus, it is not possible within the constraints of the T-L model to simulate both the small decrease in the catalytic ability of βK400E MoFe protein as well as the small increase in the NH_3:H_2 product formation ratio.

From an energetic standpoint, βK400E MoFe protein fixes nitrogen in a more energy efficient manner than wild-type MoFe protein. Since the ATP/$2e^-$ ratios are the same for both wild-type and βK400E MoFe proteins during both C_2H_2 and N_2 reduction, the formation of one molecule of NH_3 by βK400E MoFe protein is coupled to the hydrolysis of fewer molecules of ATP.

In the investigation of the charge reversal mutation βK400→E, it was discovered that the positively charged patch on the surface of the β-subunit of MoFe protein and the negatively charged patch on the surface of Fe protein found in *A. vinelandii* nitrogenase were not conserved, even among Group 1 nitrogenases. At the time, this lack of conservation could not be adequately rationalized, since these electrostatic patches seemed to be critical to maximizing nitrogen fixation by *A. vinelandii*. Now, however, these new results in hand suggest the charged patches may play a role, not just in regulating total electron flow, but also in determining where those electrons end up, whether they are used to reduce N_2 or lost as H_2. On the one hand, *A. vinelandii*, an organism with an extremely high rate of respiration, may have evolved a nitrogenase to produce NH_3 as quickly as possible, even though more ATP would be “wasted” to accomplish this. On the other hand, organisms that

cannot afford to waste any ATP may have evolved a nitrogenase with weaker PPI in the putative *DG1* region, which would result in a slower rate of product formation but a more efficient use of ATP to fix nitrogen.

Taken together, the results presented in this chapter challenge some assumptions embedded in the T-L model and underscore the need to more routinely measure the product formation ratio from the same reaction vial and under a variety of conditions, including a low component protein ratio.

In this investigation, using 0.4 μM MoFe protein, it was not possible to measure the NH_3:H_2 formation ratio at Fe:MoFe protein ratios below 5, since under these lower flux conditions, the amount of H_2 formed is below the GC limit of quantitation for H_2. While GC is very sensitive for hydrocarbon detection when coupled to FID, H_2 cannot be detected with FID and is instead detected with TCD. In order to fully understand the relationship between electron flux and N_2 reduction efficiency in biological nitrogen fixation, NH_3:H_2 formation ratios must be determined at Fe:MoFe protein ratios well below 5:1. To achieve this, a more sensitive method for H_2 detection must be developed.

2.6 Materials and Methods

2.6.1 Site-directed mutagenesis of A. vinelandii MoFe protein

Genomic mutations were generated in a two-step procedure described previously. Briefly, a plasmid containing a nifK with the codons for N399, K400, and R401 deleted was transformed into competent *A. vinelandii* cells. Bacteria that incorporated this dysfunctional copy of nifK into their genome through double homologous recombination during cell division were screened by their inability to grow in absence of a source of fixed nitrogen. In the second step, plasmids harboring

one or more of the charge reversal mutants (βN399E, βK400E, βR401E) were transformed into competent *A. vinelandii* cells containing the dysfunctional copy of nifK. The bacteria that incorporated this mutation to nifK into their genome through double homologous recombination during cell division were screened by their recovery of the ability to grow in absence of a source of fixed nitrogen.

2.6.2 Expression of nitrogenase proteins

A. vinelandii cells were grown in liquid Burk's medium containing 0.2% sucrose, 0.9 mM $CaCl_2$, 1.67 mM $MgSO_4$, 0.035 mM $FeSO_4$, 0.002 mM $Na_2Mo_2O_4$, 181 mM $C_6H_8O_7$, 10 mM Na_3PO_4, buffered to pH 7.5. For nitrogen-containing Burk's medium, NH_4Cl was added to a concentration of 10 mM. Cells were first grown in a 100-mL nitrogen-containing Burk's medium for 16 h. Then, 10 mL was transferred to a 1-L nitrogen-containing Burk's medium starter culture for fermenter growth. Cells used for nitrogenase expression were grown in a 60-L fermenter (New Brunswick Scientific) containing Burk's medium that was supplemented with 3 mM NH_4Cl rather than 10 mM NH_4Cl. The fermenter growth was initiated with 0.4 L of the 1-L starter culture. Bacteria were harvested by concentration to approximately 5 L using a Pellicon 2 tangential flow membrane (Eppendorf), followed by centrifugation at 5000 rpm to obtain an approximately 100 g cell pellet.

2.6.3 Purification of nitrogenase proteins

All lysis and purification procedures were conducted on a Schlenk line under Ar or inside an anaerobic tent continaing 90% Ar, 10% H_2. Degassed cells were twice resuspended in a solution containing 50 mM Tris, buffered to pH 8.2, 100 mM NaCl, 40% glycerol, 5 mM DT. Cells were subsequently pelleted at 12000 rpm. Swollen cells were resuspended in a second buffered solution of 50 mM Tris, buffered to pH 8.2, 100 mM NaCl, and 5 mM DT, and they were lysed by rapidly shaking with glass

marbles. The lysate was then centrifuged at 12500 rpm. The black supernatant was loaded onto a DEAE Sepharose column and washed with 1-1.5 L of a buffered solution of 50 mM Tris, buffered to pH 7.75, 100 mM NaCl, and 5 mM DT (20% Buffer B). Protein was eluted via a linear gradient using a buffered solution of 50 mM Tris, buffered to pH 7.75 and 5 mM DT, where the NaCl concentration was increased from 100 mM (20% Buffer B) to 500 mM (100% Buffer B). MoFe protein and his-tag Fe protein eluted at 250 mM NaCl and 325 mM NaCl, respectively. Fractions containing MoFe protein and his-tag Fe protein were analyzed by SDS-PAGE, pooled, and concentrated using an Amicon concentrator (Millipore). Proteins were further purified by gel filtration chromatography using a Sepharose 200 column (GE Healthcare) equilibrated with a buffered solution of 50 mM Tris, buffered to pH 8.0, 500 mM NaCl, and 5 mM DT. Fractions containing the respective proteins were identified by SDS-PAGE, pooled, concentrated, and stored in liquid nitrogen in small aliquots in an aqueous solution containing 50 mM Tris, buffered to pH 8.0, 50 mM NaCl, and 5 mM DT.

Though purification of His-tag nitrogenase component proteins using Ni-NTA affinity columns has been reported, His-tag Fe protein in this work was purified via anion exchange followed by size-exclusion chromatography, as described above, just as for wild-type Fe protein, due to issues associated with the interaction of DT with Ni-NTA resin.[56] For a detailed, step-by-step explanation of how to grow and purify nitrogenase component proteins in *A. vinelandii*, refer to the SOPs provided in the Appendix of this dissertation.

2.6.4 Nitrogenase Fe protein activity assays

To measure the specific activity of wild-type and His-tag Fe proteins, the Fe protein concentration was kept constant in each assay at 1.0 μM and the MoFe

concentration was varied between 0 and 4.0 μM. Activity assays were conducted in 1.15-mL solutions contained in sealed 14-mL vials. The activity assay solutions were prepared as follows: 1-mL aliquots of a solution containing 50 mM Tris, buffered to pH 8.0, 50 mM NaCl, 5 mM Na_2ATP, 10 mM $MgCl_2$, 30 mM creatine phosphate, and 0.00125 mg/mL creatine phosphokinase were placed in sealed 14-mL vials and appropriate amounts of a high salt solution (Buffer C: 50 mM Tris, pH 8.0, 500 mM NaCl) were added to maintain a constant volume and ionic strength. Refer to Table 7.2 in the Appendix for an example of the amount of high salt solution to add to each vial. To test the ability of Fe protein to catalyze substrate reduction in the presence of Zn^{2+}, small aliquots of a concentrated $ZnCl_2$ solution were added to each vial at this time.

Solutions were exchanged into an Ar atmosphere using a Schlenk line apparatus. Separately, 2 mmol (0.348 g) DT and 2 mL of a solution of 1.0 M Tris base, to which no acid had been added, so the pH was around 11, were also exchanged into an Ar atmosphere using a Schlenk line apparatus. Next, a solution of 1.0 M DT in 1.0 M Tris base was prepared by anaerobic transfer of 2 mL of Tris base solution to the sealed vial containing DT powder, using a gas tight Hamilton syringe. The solution was shaken until all DT had dissolved. Then, 10-μL aliquots of the 1.0 M DT stock solution were anaerobically transferred to each activity assay vial using a gas tight Hamilton syringe. In a similar manner, 1-mL aliquots were removed from a 1-L flask of pure C_2H_2 gas and added to each activity assay vial. Assay vials contained a final pressure of 0.072 atm C_2H_2 and a final DT concentration of approximately 10 mM.

All activity assay vials were placed in a circulating water bath for 5 minutes at 30°C to equilibrate the solutions. After 5 minutes, appropriate amounts of a solution of MoFe protein were added to each reaction vial anaerobically with a gas tight Hamilton

syringe (refer to Table 7.2 of the Appendix). Reactions were initiated by the anaerobic addition of Fe protein, proceeded for 10 minutes, and were stopped by addition of 0.4 mL glacial acetic acid. All protein concentrations were determined via Fe chelation in 6.4 M guanidine HCl by 2,2-bipyridine using an extinction coefficient of 8650 $M^{-1}cm^{-1}$ at 522 nm on a Hewlett Packard 8452A Diode Array UV-Vis spectrophotometer. When error bars are shown, they represent one standard deviation of the average of at least three independent measurements.

2.6.5 Nitrogenase MoFe protein activity assays

To measure the specific activity of wild-type and mutant MoFe proteins, the MoFe protein concentration was kept constant in each assay at 0.2 μM and the Fe protein concentration was varied between 0 and 12 μM, unless otherwise specified. Reactions were prepared as described above for Fe protein activity assays unless stated otherwise. Table 7.3 in the Appendix provides an example of the volumes of buffer solutions and protein solutions added to each reaction vial. For NaCl dependence experiments, the NaCl concentration was varied from 0 – 600 mM NaCl, while the MoFe protein concentration was kept constant at 0.2 μM and the Fe protein concentration was kept constant at 2.0 μM. For measurement of H^+ reduction, C_2H_2 was omitted from the reaction vials. For experiments designed to measure the ATP/$2e^-$ ratio in the presence of C_2H_2, reactions contained 0.4 μM MoFe protein and 4.0 μM Fe protein. For assays measuring the extent of ATP hydrolysis, reactions were quenched with 0.4 mL of a solution containing 4.0 M NaCl. For the dilution experiment, reactions were let to react for 15 minutes, and the Fe:MoFe molar ratio was kept constant at 4:1, while the MoFe protein concentration was varied from 0 – 0.5 μM.

2.6.6 *Activity assays under an N_2 atmosphere*

Activity assay solutions were prepared as described above with the following modifications: Hepes buffer was used rather than Tris, as Tris buffer interferes with both the colorimetric indophenol and the fluorescence OPA assays. Solutions were made anaerobic on a Schlenk line apparatus containing N_2 gas. For the DT stock solution, a 2-mL aliquot of an aqueous solution of 1.0 M Hepes, buffered to pH 8.0, and 2 mmol (0.348 g) dithionite were placed in two separate, sealed glass vials and also made anaerobic a Schlenk line apparatus containing N_2 gas. After solutions were made anaerobic, 2.0 mL of the 1.0 M Hepes solution were added to anaerobically to 0.348 g ditionite to create a solution containing 1.0 M ditionite and 1.0 M Hepes. A 10 µL aliquot was then added to each reaction vial. Various amounts of Fe protein were added to each vial and vials were shaken at 30°C in a circulating water bath for 5 minutes to equilibrate. Enzymatic reactions were initiated by the addition of 0.4 µM MoFe protein and stopped by the addition of 0.30 mL of 5 M NaCl after 20 minutes. When NH_3 was to be quantified by the modified indophenol method, creatine kinase and phosphocreatine were omitted from the reaction solutions.

2.6.7 *Measurement of C_2H_4 produced by nitrogenase*

C_2H_4 evolution was measured with an SRI 8610C GC containing an alumina column (Alltech) and an FID detector. A 50-µL aliquot of headspace from each activity assay vial was injected onto the alumina column, and the amount of C_2H_4 in each reaction vial was determined from an external calibration curve performed on the same day. The carrier gas was He. For the calibration curve, an evacuated 250-mL round bottom flask was filled with pure C_2H_4 gas and the amount added to the flask was weighted on an analytical balance to 4 significant figures. Then, a 50-µL aliquot of the pure C_2H_4 gas was added to sealed 27-mL glass vial and 10 – 50-µL aliquots

were injected onto the GC. A typical graph of peak area v. nmol C_2H_4 injected yielded a regression line of y = 150 x.

For a detailed explanation of how and why these methods have changed over time, refer to the discussion of activity assay optimizations in Chapter 5 of this dissertation. For a further explanation of how to conduct nitrogenase activity assays and measure reaction products, see SOPs for activity assays provided in the Appendix of this dissertation.

2.6.8 Measurement of H_2 produced by nitrogenase

After quenching enzymatic activity, 500-µL aliquots of headspace from each vial were taken to measure the amount of H_2 formed using GC. Aliquots were injected onto an SRI 8610 GC containing a molecular sieves column (Alltech) and a TCD detector at an oven temperature of 80°C. The carrier gas was N_2. An external calibration was performed. First, an evacuated 500-mL round bottom flask was filled with pure H_2 gas and the amount of H_2 added to the flask was weighted on an analytical balance to 3 significant figures. Then, 100 – 1000 µL aliquots of the pure H_2 were injected onto the GC, and a typical graph of peak area v. nmol H_2 injected yielded a regression line of y = 0.5 x.

For a detailed explanation of how and why these methods have changed over time, refer to the discussion of activity assay optimizations in Chapter 5. For a further explanation of how to conduct these experiments, see SOPs for activity assays provided in the Appendix.

2.6.9 Measuring NH_3 with the indophenol method and UV-Vis spectroscopy

After injection of the reaction headspace into the GC to measure H_2, each reaction vial was opened and 0.5 mL solution was transferred to a Pasteur pipet column packed with activated, equilibrated Dowex-1 resin. DI H_2O was used as the

eluent, and ~ 3.0 mL was collected from each pipet column and weighed on an analytical balance. To 1.0 mL of this collected solution, 40 µL phenol solution, 100 µL sodium nitroprusside, and 40 µL oxidizing solution were added one at a time, with mixing in between each addition, following a procedure detailed previously. Solutions were left to develop in the dark for 1 hour, before measuring their absorbance at 640 nm using a UV-Vis spectrophotometer. An external calibration was also performed. First, a series of standard solutions containing 0 – 500 µM NH_4Cl were prepared in triplicate in a matrix that closely matched the nitrogenase activity assay solution. The matrix included 50 mM Hepes buffer, 50 mM NaCl, 5 mM Na_2ATP, and 10 mM $MgCl_2$. These standards were treated in a manner identical to the experimental samples, including passage over a pipet column. A typical graph of A_{640} v. µM NH_4Cl in the cuvette yielded a regression line of y = 0.009 x. There was a linear response in A_{640} to [NH_4Cl] from 10 – 80 µM NH_4Cl.

2.6.10 Measuring NH_3 with the OPA method and fluorescence spectroscopy

After injection of the reaction headspace into the GC to measure H_2, each reaction vial was opened, 0.5 mL solution was added to a fresh 10 kDa microcon, and samples were centrifuged for 5 minutes at 10,000 rpm. A 200-uL aliquot of solution which had flowed through the 10 kDa filter was mixed with 1.8 mL of the fluorescence reagent and let to react in the dark for 2 hours. Samples were excited at 365 nm, and fluorescence was monitored at 422 nm. To generate the fluorescence reagent, on the day of analysis, a 6 mM sulfite solution was prepared in a solution containing 100 mM P_i buffered to pH 11.0. Also on the day of analysis, a solution of 20 mM OPA in 25% MeOH was made. The fluorescence reagent consisted of equal volumes 6 mM sulfite solution and 20 mM OPA solution that had been mixed immediately before mixing with samples. An external calibration was also performed. A series of standard

solutions containing 0 – 500 μM NH_4Cl were prepared in triplicate in a matrix that closely matched the nitrogenase activity assay solution. The matrix included 50 mM Hepes buffer, 50 mM NaCl, 5 mM Na_2ATP, and 10 mM $MgCl_2$. These standards were treated in a manner identical to the experimental samples, including centrifugation in a fresh 10 kDa microcon. A typical graph of fluorescence v. μM NH_4Cl in each initial standard solution yielded a regression line of y = 0.75 x. There was a linear response in fluorescence to [NH_4Cl] from 0.5 – 5 μM NH_4Cl.

2.6.11 Measurement of ATP hydrolysis as P_i released

ATP hydrolysis was monitored through the quantification of released P_i during the nitrogenase reaction. After product formation was measured by GC, 500 μL of each assay solution was removed and added to 800 μL of a solution containing 200 mM $CaCl_2$ and 50 mM Tris, buffered to pH 8.0. Solutions were mixed and centrifuged for 5 min at 13,000 g. Because the force of pipetting could rupture the soft, white pellet, an aliquot of 1.2 mL of the supernatant fraction was removed, leaving 0.1 mL remaining in the tube with the precipitate, and 1.0 mL DI H_2O was added to the tube. Solutions were centrifuged for an additional 5 min at 13,000 g. An aliquot of 1.0 mL of the supernatant fraction was removed, leaving 0.1 mL remaining in the tube with the precipitate, and 1.0 mL DI H_2O was again added to the tube. This process was repeated for a total of four centrifugation steps. The white pellet was then resuspended in a 1.0 mL solution of 0.2 M HCl, and 100 mL of the resulting suspension was added to 10.0 mL DI H_2O. Then, 1.0 mL of the color reagent was added. The method of Strickland and Parsons was used for the preparation of the color reagent, which contained 4.9 mM ammonium molybdate, 61 mM ascorbate, and 0.42 mM potassium antimonyl tartrate in 1.2 M sulfuric acid.[71] Absorbance of the blue solutions was measured at 885 nm after 1 hour using an Agilent 8453 UV-visible

spectrophotometer.

2.6.12 EDC crosslinking reactions and analysis by electrophoresis

Crosslinking experiments contained, in a final volume of 0.1 mL, 7.5 μM MoFe protein, 45 μM Fe protein, 12.5 mM EDC, and 10 mM Mg^{2+}-ATP in a solution containing 25 mM Hepes, pH 8.0, 60 mM NaCl, and 12.5 mM $Na_2S_2O_4$ under H^+ reduction conditions. The reactions were quenched at 0, 5, and 30-minute time intervals by removing a 10-μL aliquot and mixing it with 190 μL of a solution of 200 mM $NaC_2H_3O_2$. After crosslinking, proteins in each sample were separated using 10% reducing SDS-PAGE and visualized by Ag^+-staining.

2.6.13 Fluorescence measurements

Fluorescence excitation, emission, and polarization experiments were conducted on a Horiba Fluorolog-3 Fluorimeter. To prepare solutions for analysis, Fe protein, with or without Zn-HisZiFiT, was mixed with increasing concentrations of MoFe protein in an anaerobic environment. Solutions contained, in addition to protein, 8.1 mM L-histidine, 2.6 mM ZnO, 10 mM Hepes, 5 mM KCl, 140 mM NaCl, buffered to pH 7.4. Solutions lacked DT and ATP to prevent the enzyme from turning over. Individual mixtures were sealed, removed from the anaerobic tent, and placed under an Ar atmosphere on a Schlenk line apparatus. An empty 2-mL fluorescence anaerobic cuvette was sealed with a rubber septum and made anaerobic on a Schlenk line apparatus. Using a gas tight Hamilton syringe, Fe and MoFe protein mixtures were transferred anaerobically to the cuvette. To determine the wavelength of maximum excitation, solutions were excited from 400 – 540 nm and the fluorescence emission at 560 nm was observed. To determine the wavelength of maximum emission, solutions were excited at 515 or 534 nm and emission intensity was observed from 400 – 600 nm. To monitor the change in fluorescence polarization

upon interaction with MoFe protein, solutions were excited at 534 nm, and the polarization of light emitted at 560 nm was measured. In all cases 5 nm slit widths were utilized.

2.6.14 Fe chelation assays

In an anaerobic quartz cuvette, 6.7 μM Fe protein, 3.3 μM MoFe protein, 5 mM MgATP, 13 mM DT, and 6.25 mM 2,2-bipyridine were mixed together. Under these conditions nitrogenase was active for the reduction of H^+. The reaction was monitored over time at 520 nm, the absorption maximum of the pink $[Fe(bpy)_3]^{2+}$.

2.6.15 Synthesis of HisZiFiT

HisZiFiT was synthesized and purified according to published procedures,[58] with one minor modification to the final step. 2-Pyridinesulfonyl chloride was prepared by the addition of 500 mg 2-mercaptopyridine to 12.5mL of concentrated sulfuric acid over ice, followed by drop wise, slow addition of 50 mL commercial bleach, at an approximate rate of 5 mL/min. This reaction was carried out in a fume hood, since chlorine gas is produced. After the addition of bleach, the reaction was let to stir on ice for one hour. The solution was extracted with DCM. The organic layer was dried over anhydrous sodium sulfate for 30 minutes and then concentrated to less than 5 mL total volume, followed by immediate mixing with 2', 7'diamino-4',5'-dimethylfluorescein dissolved in dry pyridine. Each step of the HisZiFiT synthesis was verified by ESI-MS.

2.6.16 Simulations using Mathematica

C_2H_4, H_2, and NH_3 formation by wild-type and βK400E MoFe proteins was simulated by numerically solving the T-L scheme with Mathematica. The simulations that best describe the C_2H_2 reduction data were determined using a manual grid

search, where k_1 was varied in small intervals. All rate constants were held equal between βK400E and wild-type MoFe protein, except for the respective values of k_1.

2.7 Acknowledgements

The authors would like to thank Dr. Philip Wilson and Professor Gerald Watt from Brigham Young University for kindly providing their Mathematica scripts and insights about the Thorneley-Lowe kinetic model. This work was made possible by assistance from Professor Markus Ribbe of the University of California, Irvine, who kindly provided an *A. vinelandii* strain with an N-terminal His-tag on Fe protein.

Chapter 2 was reproduced in part, with permission, from Owens, C. P.; Katz, F. E. H.; Carter, C. H.; Luca, M. A.; Tezcan, F. A. “Evidence for functionally relevant encounter complexes in nitrogenase catalysis.” *J. Am. Chem. Soc.* **2015**, *137*, 12704–12712.

3 Redox-dependent structural changes suggest functional role for oxygen ligand of P-cluster

3.1 Abstract

Electron transfer through nitrogenase is conformationally gated. *Intramolecular* electron transfer in MoFe protein from the P-cluster to the catalytic FeMoco only occurs in the presence of Fe protein, but it remains unclear precisely what conformational change or changes Fe protein transduces to MoFe protein to make this *intramolecular* electron transfer favorable. It is well established that in MoFe protein from *A. vinelandii* (Av-MoFe), the 2-e^- oxidized P-cluster is ligated by a nearby Ser residue, but it has been assumed this ligation is mechanistically unimportant. Here, MoFe protein from *Gluconacetobacter diazotrophicus* (Gd-MoFe) was crystallized in DT-reduced and IDS-oxidized states, showing a nearby Tyr residue that ligates the 2-e^- oxidized P-cluster when the Ser is absent. Sequence analysis confirmed that, while the Ser is not strictly conserved, all Group 1 nitrogenases contain either a Ser or a Tyr within ligating distance to the P-cluster. Taken together, crystal structures, sequence alignments, and EPR experiments have renewed interest in the role a hard, switchable oxygen ligand of the P-cluster may play in conformationally gating electron transfer through nitrogenase. The application of these findings to improving the yield of photocatalysis by MoFe protein mutants is discussed.

3.2 Introduction

It is established that *intramolecular* electron transfer from the P-cluster to FeMoco occurs before *intermolecular* electron transfer from Fe protein to the P-cluster,[29] that *intramolecular* electron transfer to FeMoco only occurs in the presence

of Fe protein, and that some conformational change or changes precede *intramolecular* electron transfer.[28] ATP hydrolysis and all subsequent dynamic movements in the catalytic Fe protein cycle have been ruled out as the source of these conformational changes, since ATP hydrolysis was recently shown to occur after electron transfer.[26] Indeed, many studies suggest a role for ATP hydrolysis in driving complex dissociation rather than the actual electron transfer steps of turnover.

Chapter 2 discussed experiments that lead to an amended picture of nitrogenase reactivity that now includes more extensive PPI prior to electron transfer steps. Experiments with βK400E MoFe protein revealed the catalytic importance of electrostatic interactions of the Fe and MoFe proteins in *DG1*.[13] While it is unclear exactly how complex formation in *DG1* leads to formation of the activated *DG2* complex, it is plausible that Fe protein explores a large surface area of the β-subunit of MoFe protein during this transition, causing a conformational change or changes that leads to favorable, fast *intramolecular* electron transfer. In principle, any subtle rearrangement within MoFe protein that lowers the reduction potential of the P-cluster, such as electron donation, or increases the reduction potential of FeMoco, such as protonation, could gate electron flow in nitrogenase. Chapter 3 centers on one such example of a conformational change within MoFe protein that may gate *intramolecular* electron transfer from P-cluster to FeMoco.

3.2.1 Conformational changes in A. vinelandii MoFe protein upon oxidation

While Fe protein has been observed crystallographically in many different nucleotide-dependent conformations, few structural changes have been observed within MoFe protein. Up until just a few years ago, the only crystallographically characterized structural change in MoFe protein was a redox-dependent change at the P-cluster.[72] The P-cluster is an 8Fe:7S cluster that bridges the α and β subunits of

MoFe protein and is about equidistant from both the 4Fe:4S cluster of Fe protein and FeMoco in the *DG2* complex.[10,43]

When MoFe protein from *A. vinelandii* (Av-MoFe) is isolated in the presence of DT, the P-cluster is ligated by three Cys residues from the α-subunit, αC62, αC88, and αC154, and three Cys residues from the β-subunit, βC70, βC95, and βC153. When this protein is oxidized, however, the P-cluster gains two additional ligands, the oxygen from the side chain of βS188 and the amide nitrogen of αC88. Figure 3.1 A shows the DT-reduced P-cluster from *A. vinelandii* and its immediate surroundings, and Figure 3.1 B shows the ligation of two additional ligands upon oxidation.[72] The β-subunit of MoFe protein is in purple, and the α-subunit is in light blue. EPR spectroscopy revealed that in this conformation the oxidation state of FeMoco is unchanged but the P-cluster is oxidized by 2-e^-.[72,73] Adding electron density to the P-cluster via ligation of these two ligands could certainly lower the reduction potential of the P-cluster to the degree that electron transfer from P-cluster to FeMoco becomes favorable.

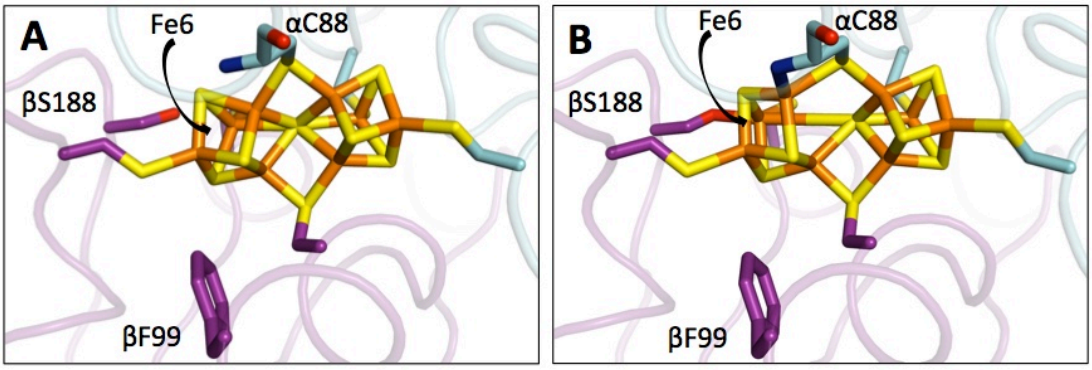

Figure 3.1 The P-cluster and immediately surrounding environment of MoFe protein from *A. vinelandii* in the **A** as-isolated state with DT and **B** 2-e^- oxidized state as initially reported in ref *36*.

Though the changes in Figure 3.1 represent a well-documented, redox-dependent, reversible, and rare ligation of an FeS cluster by a Ser residue that might

seem to have mechanistic importance, βS188 is not conserved among nitrogenase sequences. Because of the lack of conservation of βS188, and the fact that a P-cluster that is 2-e^- more oxidized than the resting state cluster has not been invoked in the mechanism of nitrogenase, the potential importance of this structural change has been largely overlooked.

3.2.2 Motivation for the work

At the same time as the investigations concerning βK400E MoFe protein, efforts were also underway to study nitrogenase from *G. diazotrophicus* in order to streamline the process for constructing nitrogenase mutants. It is notoriously difficult to make permanent, site-directed mutants to nitrogenase proteins from *A. vinelandii*, so there is always interest in developing faster, more facile mutagenesis strategies to study nitrogen fixation. When MoFe protein from *G. diazotrophicus* (Gd-MoFe) was crystallized, however, and overlaid with the structure of MoFe protein from *A. vinelandii* during initial investigation of *G. diazotrophicus* nitrogenase, it was discovered that Gd-MoFe protein, though it lacks βS188, harbors a Tyr residue within 5 Å of the P-cluster that may be able to ligate the cluster. This suspicion was confirmed when Gd-MoFe protein was crystallized in the presence of the oxidizing agent IDS.

Chapter 3 summarizes an investigation into the possible involvement of P-cluster ligation in the conformational gating of electron transfer through nitrogenase using a MoFe protein from the lesser-studied *G. diazotrophicus.* It is proposed that Fe protein may be able to effect subtle structural changes on the β-subunit surface of MoFe protein that are transduced to Ser or Tyr. Subsequently, cluster ligation may be induced, resulting in a decrease of the reduction potential of the P-cluster and favorable *intramolecular* electron transfer to the catalytic cluster, FeMoco. This

proposed mechanism aligns well with the results of Chapter 2 that Fe protein docks onto the β-subunit through electrostatic interactions (*DG1*) before forming the ET-competent complex (*DG2*), and may interact with the residues near the P-cluster on the β-subunit of MoFe protein during turnover.

Efforts to test this mechanistic hypothesis using photocatalytic MoFe protein constructs are also detailed. In 2010, it was shown that a MoFe protein variant, αC45A/L158C, could be covalently modified with the iodoacetamide derivative of $[Ru(bpy)_2(phenIA)]^{2+}$ (Ru-PhenIA), and that when Ru-PhenIA was attached to MoFe protein (Ru-MoFe protein), it enabled reduction of substrates independent of both Fe protein and ATP. The hypothesized location of the photosensitizer is depicted in Figure 3.2. Whereas the ATP-dependence of nitrogenase has made trapping of N_2 reduction intermediates extremely difficult, the uncoupling of ET from ATP hydrolysis is a big step toward generating crystallographically tractable reaction intermediates of biological nitrogen fixation. The motivation for the initial creation of Ru-MoFe protein was to facilitate structural and spectroscopic studies of nitrogenase reaction intermediates, but at only 1% of the specific activity of wild-type MoFe protein, and without a demonstration of N_2 reduction, these applications have not yet been realized. Here the potential of P-cluster alterations to bypass the conformational gating of electron transfer and increase the yield of photoreduction by Ru-MoFe protein is probed.

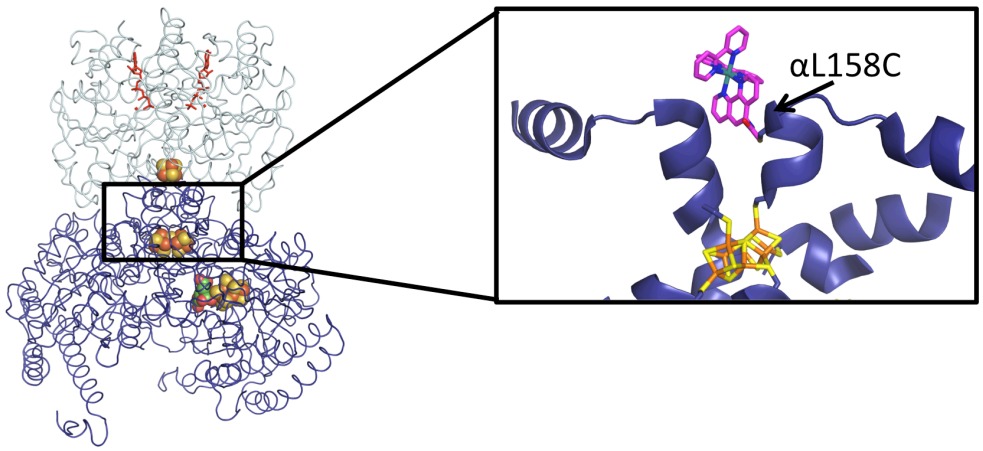

Figure 3.2 Structural model of Ru-PhenIA covalently attached to position αL158C of MoFe protein.

3.3 Results and Discussion

3.3.1 Crystal structures of MoFe protein from G. diazotrophicus

Crystal structures of reduced and oxidized Gd-MoFe protein were determined at 1.83-Å and 2.6-Å resolution, respectively.[74] Comparison of the reduced Gd-MoFe protein structure to that of reduced Av-MoFe protein yielded an overall RMSD of 0.7 Å based on all α-carbons, indicating high similarity between these two proteins. Figure 3.3 A shows the P-cluster from Gd-MoFe when crystallized in the presence of DT, and Figure 3.3 B shows the P-cluster from Gd-MoFe protein when crystallized in the presence of the oxidizing agent IDS. Whereas in oxidized Av-MoFe protein (Figure 3.1 B), the side chain oxygen of βS188 ligates Fe6 of the P-cluster, in oxidized Gd-MoFe protein (Figure 3.3 B), βY98 ligates Fe8. In both oxidized structures the amide backbone of αC88 (*A. vinelandii* numbering) ligates Fe5.

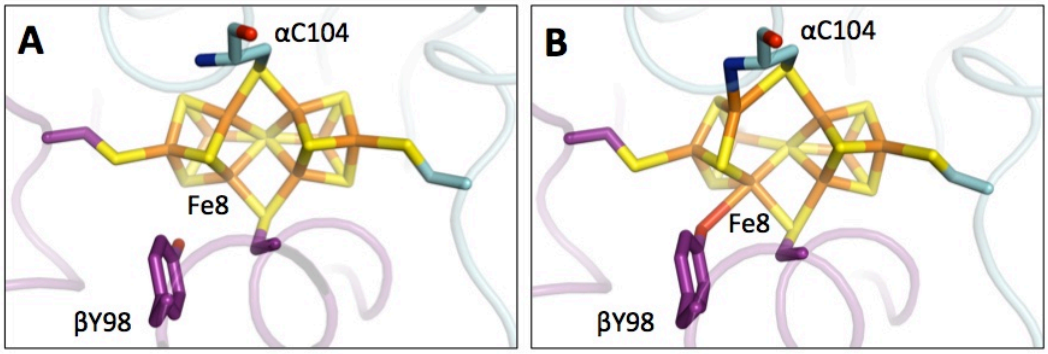

Figure 3.3 The P-cluster and immediately surrounding environment of MoFe protein from *G. diazotrophicus* in the **A** as-isolated state with DT and **B** 2-e^- oxidized state after mixing with IDS.

The redox dependent structural change in Gd-MoFe protein differs from that observed in Av-MoFe protein in the identity and position of the oxygen-containing amino acid that donates electron density to the oxidized P-cluster. Nevertheless, this unexpected result renewed interest in the non-conserved residue βS188.

3.3.2 Group 1 nitrogenases lacking βS188 have βY98

Next, a sequence analysis of nifK genes was conducted to determine whether other diazotrophs that lack βS188 might have a Tyr residue in a similar position as Gd-MoFe protein. Since both *A. vinelandii* and *G. diazotrophicus* were classified as "Group 1" nitrogenases by Howard and Glazer in their extensive phylogenetic mapping,[22] nifK genes from the 43 remaining Group 1 nitrogenases were obtained for further analysis. It was discovered that all 45 Group 1 nitrogenases, including *A. vinelandii* and *G. diazotrophicus,* contain either a Ser at Av-MoFe position β188 or a Tyr at Gd-MoFe position β98, and the results are compiled in Table 3.1. Additionally, when Tyr was present at position β98 (*G. diazotrophicus* numbering), position β188 (*A. vinelandii* numbering) was always an Ala residue, and when Ser was present at position β188 (*A. vinelandii* numbering), position *A. vinelandii* β98 (*G. diazotrophicus*

numbering) was always a Phe residue.

The two exceptions to this trend are two organisms shown to contain both a Ser and a Tyr residue. MoFe protein has never been purified from either of these obligate anaerobic organisms, so amino acid sequences have not been verified by trypsin digest or any other method. Thus, it is possible these anomalies are insignificant and the result of DNA sequencing errors, as the codons for Tyr and Phe differ by only one letter, and the codons for Ser and Ala also only differ by one letter. Nevertheless, sequence analysis established that all Group 1 MoFe proteins, even those that lack βS188, have an oxygen-containing amino acid near the P-cluster that can presumably ligate an oxidized P-cluster.

Table 3.1 Sequence alignment of nifK genes of Group 1 nitrogenases highlights the covariance of A/S at β188 and Y/F at position β99.

	Organism	Ser region (β185-190 *A. vinelandii* numbering)	Tyr region (β95-100 *A. vinelandii* numbering)
1	Acidithiobacillus ferrooxidans ATCC 23270	HTPAFV	CVAYYR
2	Anabaena variabilis ATCC 29413	HTPSFV	CVAYFR
3	Azoarcus sp. BH72	HTPSFV	CVAYFR
4	Azospirillum brasilense Sp245	HTPAFV	CVAYYR
5	Azotobacter vinelandii DJ	HTPSFV	CVAYFR
6	Bradyrhizobium japonicum	HTPAFV	CVAYYR
7	Burkholderia xenovorans LB400	HTPAFV	CVAYYR
8	Calothrix desertica PCC 7102 #	HTPSFV	CVAYFR
9	Chlorogloeopsis fritschii PCC 6912 #	HTPSFV	CVAYFR
10	Cyanothece sp. ATCC 51142	HTPSFV	CVAYFR
11	Desulfitobacterium hafniense DCB-2	NTPSFK	CTAYFR
12	Desulfosporosinus sp. OT	NTPSFK	CAAYFR
13	Fischerella muscicola PCC 7414 #	HTPSFV	CVAYFR
14	Frankia alni ACN14a	HTPSFV	CVAYFR
15	Geobacter sulfurreducens PCA	NTPSFN	CASYYR
16	Gluconacetobacter diazotrophicus PAl 5	HTPAFV	CVAYYR
17	Halorhodospira halophila SL1	HTPSFV	CVAYFR
18	Heliobacterium modesticaldum Ice1	QTPSFV	CAAYFR
19	Klebsiella pneumoniae 342	HTPSFI	CVAYFR
20	Magnetococcus marinus MC-1	HTPSFV	CVAYFR
21	Mesorhizobium loti MAFF303099	HTPAFV	CVAYYR
22	Methylobacterium sp. 4-46	HTPAFV	CVAYYR
23	Methylococcus capsulatus str. Bath	HTPAFV	CVAYYR
24	Methylocystis sp. ATCC 49242	HTPAFV	CVAYYR
25	Nodularia spumigena CCY9414	HTPSFV	CVAYFR
26	Nostoc sp. PCC 7120	HTPSFV	CVAYFR
27	Pectobacterium atrosepticum SCRI1043	HTPSFI	CVAYFR
28	Pelobacter carbinolicus DSM 2380	NTPSFN	CASYYR
29	Polaromonas naphthalenivorans CJ2	HTPAFV	CVAYYR
30	Pseudomonas stutzeri A1501	HTPSFV	CVAYFR
31	Rhodobacter capsulatus SB 1003	HTPAFV	CVAYYR
32	Rhodobacter sphaeroides 2.4.1	HTPAFV	CVAYYR
33	Rhodomicrobium vannielii ATCC 17100	HTPAFV	CVAYYR
34	Rhodopseudomonas palustris CGA009	HTPAFV	CVAYYR
35	Rhodospirillum rubrum ATCC 11170	HTPSFV	CAAYFR
36	Scytonema sp. PCC 7814 #	HTPSFV	CVAYFR
37	Sinorhizobium fredii NGR234]	HTPAFV	CVAYYR
38	Sinorhizobium medicae WSM419	HTPAFV	CVAYYR
39	Synechococcus sp. JA-2-3B'a(2-13)	HTPSFV	CVAYFR
40	Syntrophobotulus glycolicus DSM 8271	NTPSFV	CAAYFR
41	Thermodesulfovibrio yellowstonii DSM 11347	NTPSFT	CVAYFR
42	Trichodesmium erythraeum IMS101	HTPSFV	CVAYFR
43	Wolinella succinogenes	NTPSFK	CVAYFR
44	Xanthobacter autotrophicus Py2	HTPAFV	CVAYYR
45	Zymomonas mobilis subsp. mobilis ZM4	HTPAFV	CVAYYR

3.3.3 Electron paramagnetic resonance spectroscopy

In order to evaluate the extent of cluster P-cluster oxidation in the IDS-oxidized Gd-MoFe, EPR experiments were carried out on oxidized and reduced Gd-MoFe protein. First, perpendicular mode EPR spectra of IDS-oxidized and DT-reduced Gd-MoFe protein were collected and compared to spectra of Av-MoFe protein. The EPR results are displayed in Figure 3.4. Reduced Av-MoFe protein (blue trace, top of Figure 3.4) contains an S = 3/2 signal (g = 4.3, 3.6, and 2.0), which is characteristic of resting-state FeMoco.[75,76] The P-cluster does not contribute to the spectra displayed in Figure 3.4 because the P-cluster is all-ferrous and EPR silent in the as-isolated, DT-reduced state.

Upon oxidation with IDS (light blue trace, second from top in Figure 3.4), the perpendicular mode EPR signal for Av-MoFe does not change because there is no change in the oxidation state of FeMoco in the absence of Fe protein, and the P-cluster has been oxidized to an integer spin system that is not observed in perpendicular mode. As anticipated, the S = 3/2 FeMoco signal is observed in the EPR spectrum of reduced Gd-MoFe protein (orange trace, third from top of Figure 3.4), and no changes are detected in perpendicular mode upon oxidation (pink trace, bottom of Figure 3.4). Interestingly, when the P-cluster has been oxidized by 1-e^- (denoted P^{1+}) in oxidative titrations, small changes in the g = 2 and g = 5 – 8 regions of the perpendicular mode EPR spectrum have been recorded. Figure 3.5 summarizes the results of Tittsworth and Hales,[77] who assigned these small but reproducible signals in Figure 3.5 A to a mixed-spin state P-cluster that has been oxidized by 1-e^- (P^{1+}). Since none of these signals were observed in samples of oxidized Gd-MoFe protein, it was concluded that the IDS-oxidized form of Gd-MoFe

protein did not contain P^{1+} P-clusters.

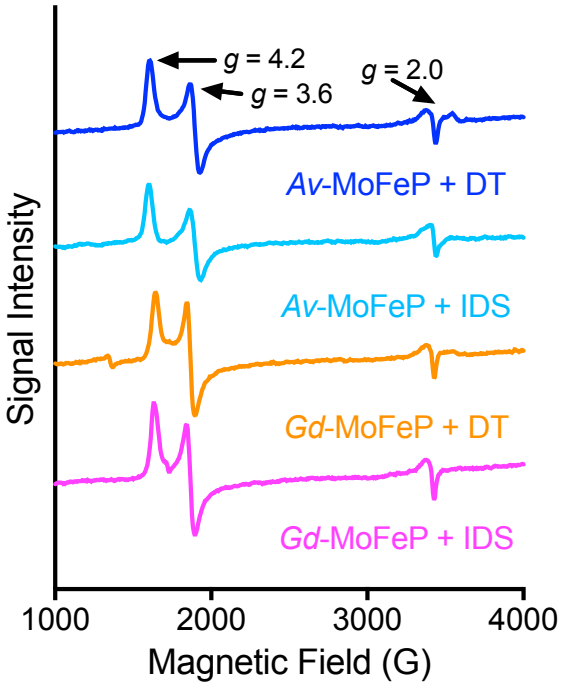

Figure 3.4 Perpendicular-mode EPR spectra of DT-reduced and IDS-oxidized MoFe proteins from *A. vinelandii* (Av) and *G. diazotrophicus* (Gd).

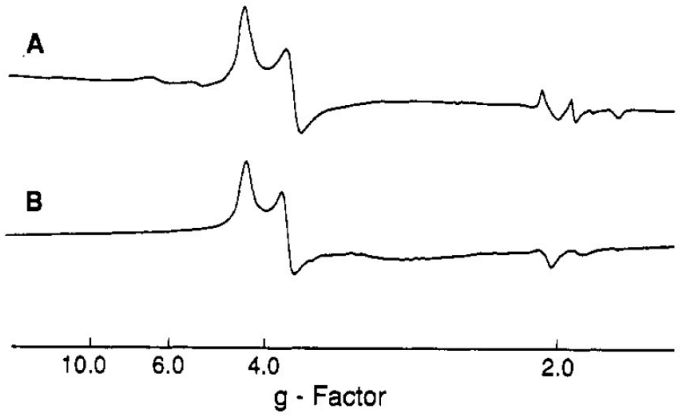

Figure 3.5 Perpendicular-mode EPR spectra collected by Tittsworth and Hales of **A** 2-equivalent-oxidized and **B** as isolated MoFe protein from *A. vinelandii*, adapted from ref *77*.

The integer spin 2-e^- oxidized P-cluster (sometimes referred to as P^{2+} or P^{ox}) has been characterized using parallel mode EPR.[73,78] The 2-e^- oxidized P-cluster from Av-MoFe protein has a low-field peak at g = 12 (light blue trace, second from the top of Figure 3.6). In contrast, oxidized Gd-MoFe protein displayed an even lower-field parallel mode signal at g = 16 (pink trace, bottom of Figure 3.6), and at first it was unclear whether this peak represented the 2-e^- oxidized P-cluster analogous to what is seen in Av-MoFe protein.

Interestingly, not all P^{2+} P-clusters display a parallel mode EPR signal at g = 12. Oxidized MoFe protein from *X. Autotrophicus* (Xa-MoFe), for example, was shown to have a signal at g = 15.6 (Figure 3.7).[73] Like Gd-MoFe protein, Xa-MoFe protein follows the Ala/Tyr motif (Table 3.1). MoFe protein from *C. pasteurianum* (Cp-MoFe), the only MoFe protein shown here that does not have a signal in this region corresponding to the P^{2+} P-cluster, is also the only MoFe protein in this set classified as Group 2 rather than Group 1 by Howard and Glazer.[22] While Cp-MoFe protein contains a Ser that ligates the P-cluster upon oxidation, it contains a His residue where all Group 1 nitrogenases have a Phe or Tyr, and this may help explain the discrepancy in EPR data. In summary, EPR provided evidence that IDS-oxidized Gd-MoFe protein forms a 2-e^- oxidized P-cluster with electronics similar to those of previously characterized MoFe protein P-clusters.

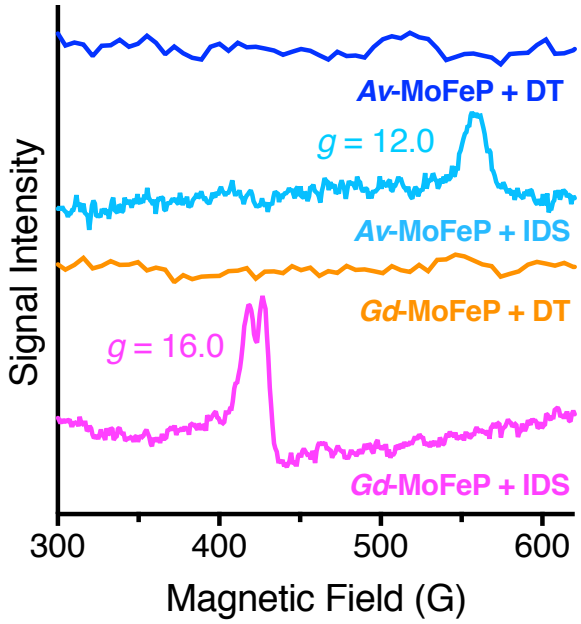

Figure 3.6 Parallel-mode EPR spectra of DT-reduced and IDS-oxidized MoFe proteins from *A. vinelandii* (Av) and *G. diazotrophicus* (Gd).

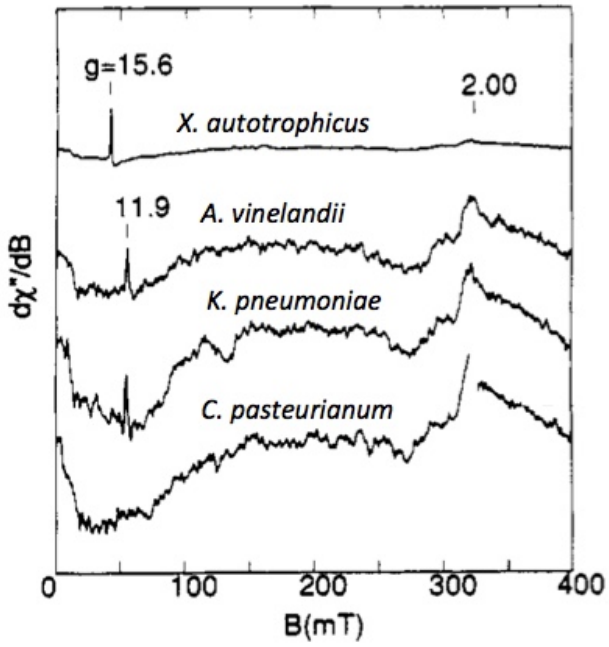

Figure 3.7 Parallel-mode EPR spectra of oxidized MoFe proteins from *X. Autotrophicus*, *A. vinelandii, K. pneumoniae*, and *C. pasteurianum*, adapted from ref *73.*

3.3.4 Application to MoFe protein photoreduction construct

Previously, a MoFe protein variant, αL158C, was created that, when derivatized with the photosensitizer Ru-PhenIA and generating Ru-MoFe protein, could reduce $H^+ \rightarrow H_2$, $C_2H_2 \rightarrow C_2H_4$, and even HCN $\rightarrow CH_4$.[79,80] In this system, FeMoco could receive electrons from light through Ru-PhenIA, eliminating the need for both Fe protein and ATP. There are two main limitations of this photoreduction system, however, that have prevented its application for its intended purpose. First, the overall catalytic activity of the Ru-MoFe protein construct was extremely low, reaching only 1% of the native Fe protein and ATP-dependent nitrogenase. Second, N_2 reduction was never demonstrated, which is the biologically relevant reaction.

The inefficiency of the unimolecular Ru-MoFe system was taken as indirect evidence of the importance of conformational changes in MoFe protein transduced by Fe protein in gating electron flow through nitrogenase. Since Fe protein was absent from the reaction mixture, it could not bind MoFe protein and communicate necessary structural changes within MoFe protein, which are believed to be necessary for efficient electron transfer.

When Gd-MoFe protein was crystallized in the oxidized and reduced states, however, and shown to undergo redox-dependent structural changes at the P-cluster similar to that of Av-MoFe protein, interest was renewed in the possible participation of structural changes at and around the P-cluster in the conformational gating mechanism. Therefore, efforts were undertaken to modulate the P-cluster environment of the Ru-MoFe protein construct in a way that could overcome, or bypass, the conformational gating mechanism in nitrogenase, thereby dramatically increasing the catalytic ability of Ru-MoFe protein and possibly even leading to N_2 fixation.

3.3.5 Recreating Ru-MoFe protein with αC45A/L158C MoFe protein mutant

Before optimization of Ru-MoFe protein, the previous results were reproduced, in order to show conclusively that the Ru-MoFe protein generated in this work was structurally and functionally equivalent to the Ru-MoFe protein utilized previously. Toward this end, Ru-PhenIA was synthesized as described previously.[81,82] In this work, however, Ru-PhenIA was not purified prior to reacting with protein. Instead, after ESI-MS analysis confirmed the presence of Ru-PhenIA in the reaction mixture, the orange liquid was placed under vacuum and all solvent was removed, until an orange solid remained.

A. vinelandii strain harboring αC45A/L158C MoFe protein, which had been generated previously, was sequenced to confirm the mutations were intact, as shown in Figure 3.8. Upon validation of the correct sequence, the strain harboring αC45A/L158C MoFe protein was grown, and αC45A/L158C MoFe protein purified according to published procedures.

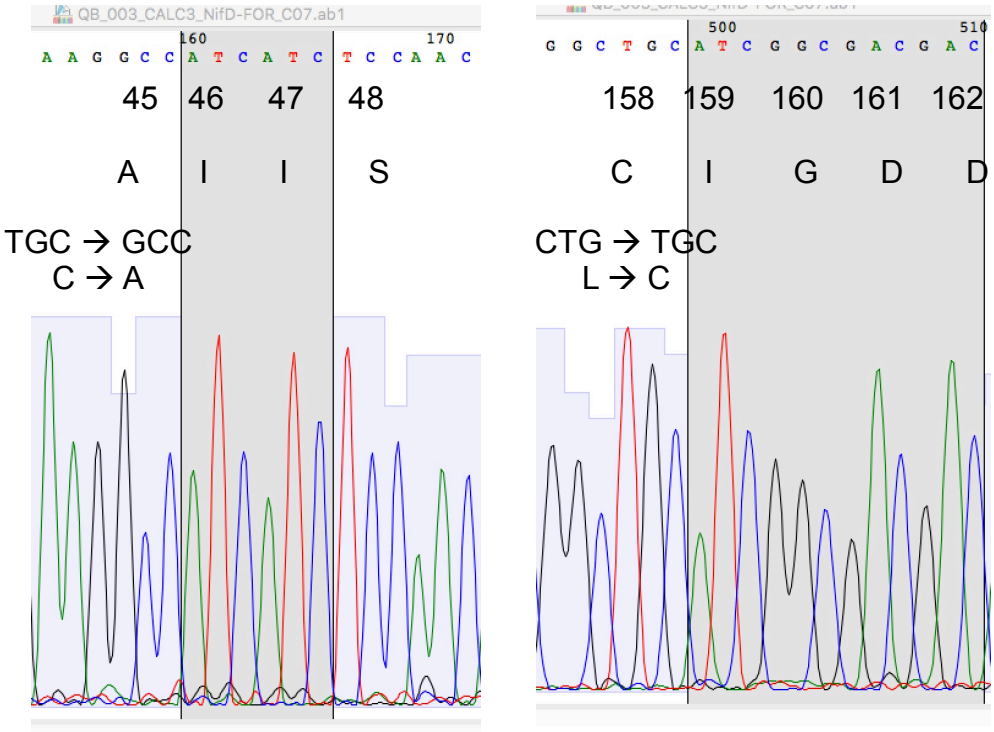

Figure 3.8 Sequencing chromatograms of the nifD regions including the codon for αC45, which has been previously mutated to an Ala, and αL158, which has previously been mutated to a Cys, showing that both mutations are intact in the strain utilized in this work.

Subsequently, αC45A/L158C MoFe protein was mixed with an excess of crude Ru-PhenIA to label the protein at position α158C. Ru-MoFe protein was characterized qualitatively by UV-Vis spectroscopy and SDS-PAGE and quantitatively by ICP-MS. As reported in previous work, Ru-MoFe protein has a unique absorption spectrum, with absorption maxima at 415 and 451 nm. Figure 3.9 shows the absorption spectrum of Ru-MoFe protein generated in this work. Ru-MoFe protein was also analyzed by separation with SDS-PAGE, and fluorescent pink bands were observed under a UV light source. An 8% SDS-PAGE experiment achieves effective separation of the α- and β-subunits of MoFe protein, and the gel results shown in Figure 3.10 confirm that the α-subunit of Ru-MoFe protein has been labeled with Ru-PhenIA, while the β-subunit remains unaltered.

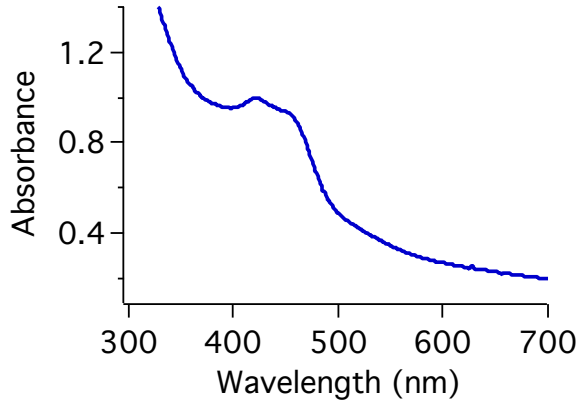

Figure 3.9 Absorption spectrum of αC45A/L158C Ru-MoFe protein, showing absorption maxima of 414 and 451 nm.

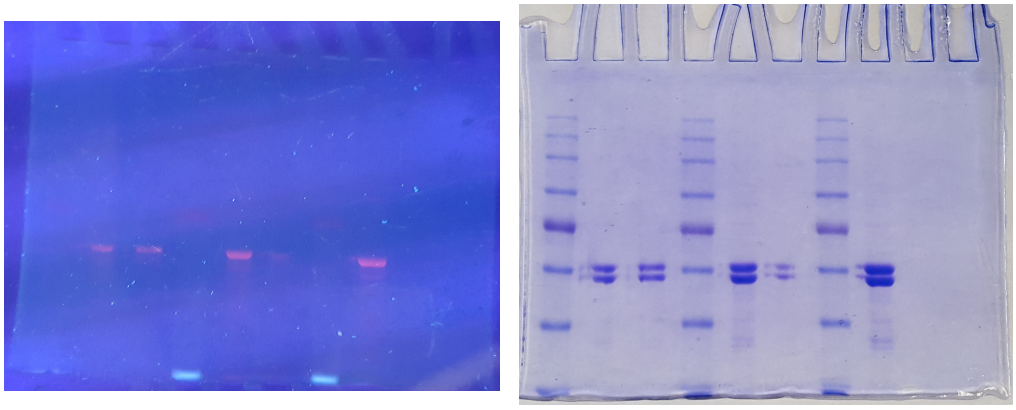

Figure 3.10 Gel from 8% SDS-PAGE analysis of multiple concentrations of αC45A/L158C Ru-MoFe protein under fluorescent light prior to Coomassie staining (left) and after Coomassie staining (right).

ICP-MS was performed to quantify the efficiency of labeling. Since ICP-MS allows for the determination of multiple metal concentrations simultaneously, this technique was used to evaluate both the Ru:Mo ratio, providing information about the efficiency of labeling, and the Fe:Mo ratio of the same sample, providing information about the integrity of the metal clusters within MoFe protein. Typical ICP-MS results are summarized in Table 3.2 and indicate that samples of αC45A/L158C Ru-MoFe protein contain approximately 2 Ru atoms per Mo atom, which is more than what is

expected for a sample that contains two FeMo-cofactors and two reactive Cys residues per tetramer. A ratio of 2 Ru:Mo could be either the result of labeling at an additional, unknown site, or from less than 100% incorporation of metal cofactors into each MoFe protein by *A. vinelandii* during synthesis of active nitrogenase.

Unexpectedly, however, ICP-MS analysis also revealed a slight decrease in the Fe:Mo ratio in Ru-MoFe protein as compared to unlabeled αC45A/L158C MoFe protein and wild-type MoFe protein. Because Ru-MoFe protein may not contain as many Fe atoms as unlabeled MoFe protein, a colorimetric Bradford assay, which detects the amount of polypeptides in solution, is not a reliable measure of active Ru-MoFe concentration. Fe chelation assays were the most reliable measure of active Ru-MoFe protein, and when concentration was determined using this method, Ru-MoFe protein generated by the above labeling strategy routinely reached a specific activity of 20 nmol min^{-1} mg^{-1}, for the reduction of C_2H_2 to C_2H_4, which is 1% of the maximum specific activity of wild-type nitrogenase and in line with previously reported results.[79] This activity was achieved when Ru-MoFe protein was irradiated with a 150W Xe arc lamp. Specific activities between 8 – 12 nmol min^{-1} mg^{-1} were measured for the reduction of C_2H_2 to C_2H_4 when Ru-MoFe protein was irradiated with a less powerful 455-nm blue light from an LED light source, which also matches previous reports well. The results of typical experiments are summarized in Figure 3.11.

Table 3.2 ICP-MS results of Fe, Mo, and Ru concentrations in wild-type and αC45A/L158C-MoFe proteins.

	Fe (ppm)	Mo (ppm)	Ru (ppm)	Fe:Mo (molar ratio)	Ru:Mo (molar ratio)
Wild-type MoFe	237 ± 5	24.1 ± 0.6	0.04 ± 0.004	16.9	0.001
αC45A/L158C MoFe	235 ± 5	22.6 ± 0.7	0.06 ± 0.01	17.8	0.003
αC45A/L158C Ru-MoFe	113 ± 3	13.0 ± 0.5	25.5 ± 2.5	14.9	1.9

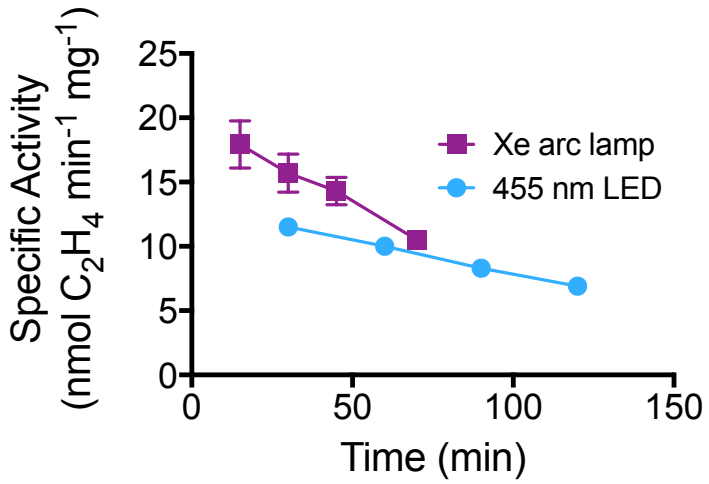

Figure 3.11 Specific activities for photoreduction of C_2H_2 to C_2H_4 by Ru-MoFe protein when irradiated with the Xe arc lamp or the 455 nm LED light source.

The only significant difference observed between the proteins utilized previously and those utilized in this work is in measurements of Fe protein and ATP-dependent turnover experiments, the results of which are summarized in Table 3.3. Previously, αC45A/L158C MoFe protein was shown to be just as active as wild-type MoFe protein for the Fe protein and ATP-dependent reduction of C_2H_2 to C_2H_4. When αC45A/L158C MoFe protein was purified and assayed in this work, however, it never exceeded a specific activity of 1500 nmol C_2H_4 min^{-1} mg^{-1}, even with a 40-fold molar excess of Fe protein. Additionally, Ru-MoFe protein was shown in prior work to maintain its ability to catalyze Fe protein and ATP-dependent reduction of substrates. The maximum specific activity of Ru-MoFe protein for the reduction of C_2H_2 was 2400 nmol C_2H_4 min^{-1} mg^{-1}, but in the present work, Ru-MoFe protein never reached a specific activity above 50 nmol C_2H_4 min^{-1} mg^{-1}.

This discrepancy may be due to the fact that a proper calibration procedure was not in place when these measurements were conducted previously. The results

obtained in this work can be rationalized according to what is known about the mechanism of nitrogenase. When a non-polar surface-exposed residue Leu, which, at position α158, lies at the α/β interface where Fe protein binds, is replaced with a polar Cys residue, PPI during turnover will likely be perturbed, so it is unsurprising that the overall maximum specific activity of αC45A/L158C MoFe protein is less than wild-type MoFe protein. Furthermore, when a large molecule such as Ru-PhenIA is attached at position α158, Fe protein may be completely unable to bind MoFe protein. The extremely low observed specific activity of 50 nmol min^{-1} mg^{-1}, which is a mere 2% of the maximum wild-type activity, may in fact be the result of substrate reduction by unlabeled MoFe protein.

Table 3.3 Maximum specific activites for Fe protein and ATP-dependent C_2H_2 reduction achieved by wild-type, αC45A/L158C, and αC45A/L158C Ru-MoFe proteins in units of nmol C_2H_4 min^{-1} mg^{-1} MoFe protein.

	2012	2017
Wild-type MoFe	2500	2500
αC45A/L158C MoFe	2400	1500
αC45A/L158C Ru-MoFe	2400	50

3.3.6 Optimization of photoreduction reaction conditions

Previously, a specific activity of 20 nmol C_2H_4 min^{-1} mg^{-1} could only be achieved by αC45A/L158C Ru-MoFe protein with 200 mM DT as the terminal electron source. Specifically, the reported reaction solutions all contained 100 mM Hepes, buffered to pH 7.75, 200 mM NaCl, and 200 mM DT. When the Ru-MoFe protein generated in this work was initially tested for its ability to reduce $C_2H_2 \rightarrow C_2H_4$ in the reported reaction solution, no activity was detected, even though UV-Vis, SDS, and ICP-MS analyses had all confirmed successful labeling of the protein with Ru-PhenIA. The pH of the reaction solution was determined after these tests did not yield the

anticipated results, and the pH was found to be between 2 – 3, rather than the reported 7.75, due to the high concentration of DT, which significantly acidifies aqueous solutions when dissolved.

Typically, for standard activity assays containing Fe protein and ATP, the 1.0 M DT stock solution is created by adding 2 mL of an anaerobic solution of 1.0 M Tris base (at pH ~11) to 2 mmol (0.348 g) DT. Then, 10-µL aliquots of this stock solution are transferred to activity assays solutions of ~ 1 mL. In this procedure, DT is mixed with a very basic solution to neutralize the DT, and the DT stock solution is diluted about 100-fold into the final activity assay solution, so the pH of the activity assay solution is unchanged by the addition of DT.

To create the photoreduction reaction solution, however, 2 mL of an anaerobic solution of 100 mM Hepes, at pH 9.0 with 200 mM NaCl, is added to 2 mmol (0.348 g) DT. Then, 1.0 mL of this solution is added to every 4.0 mL of a solution containing 100 mM Hepes, pH 7.75, 200 mM NaCl, in the hopes of creating a solution of 100 mM Hepes, 200 mM NaCl, and 200 mM DT at a final pH of 7.75. When solutions were prepared according to this procedure, however, the actual measured pH of these solutions was between 2 – 3 rather than 7.75, explaining why Ru-MoFe protein was not active.

To address this issue, photoreduction assays were carried out in a variety of buffers, at multiple pH values, and with various concentrations of DT. In the end, it was discovered that in a solution containing 50 mM DT and 100 mM P_i, buffered to pH 7.0, Ru-MoFe protein was most active and reached a specific activity for C_2H_2 reduction of ~ 20 nmol min^{-1} mg^{-1}. Furthermore, tests with alternative reductants showed that ascorbate, and not just DT, could be used as the terminal electron source for these photoreduction assays, as shown in Figure 3.12. Ultimately, it was

concluded that the large and specific requirement of DT as the electron source was about pH and not the identity or amount of reductant.

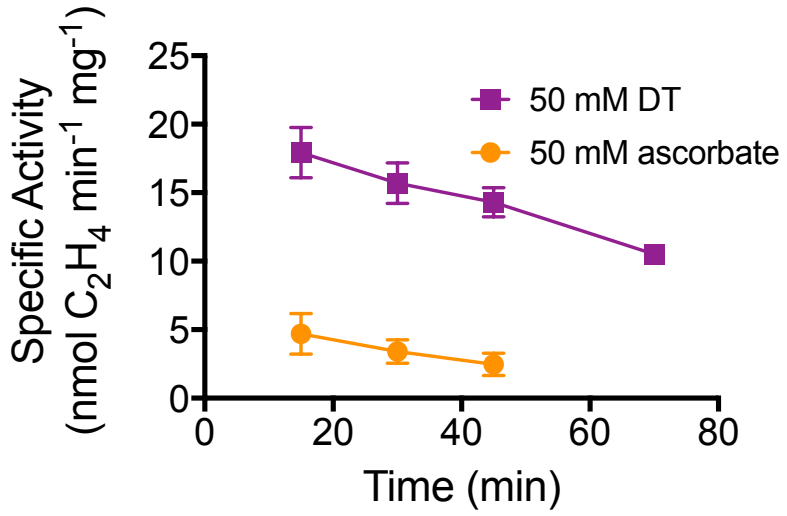

Figure 3.12 Specific activities for photoreduction of C_2H_2 to C_2H_4 by Ru-MoFe in the presence of 50 mM DT or 50 mM ascorbate.

3.3.7 Site-directed mutagenesis to generate P-cluster Ru-MoFe protein variants

Having established that the Ru-MoFe protein construct generated in this work was similar in structure and function to that made by previous researchers, site-directed mutagenesis efforts were undertaken to create the P-cluster variant αC45A/L158C/βS188C MoFe protein. It was hypothesized that replacement of βSer188 with Cys would add electron density near the P-cluster, thereby decreasing its reduction potential, such that electron transfer from P-cluster to FeMoco would become much more favorable.

Initial results proved unsuccessful, and the reasons for this are discussed extensively in Chapter 4, which is wholly devoted to method development in the area of site-directed mutagenesis in *A. vinelandii*. Briefly, mutagenesis of nitrogenase structural proteins in *A. vinelandii* is necessarily a two-step process. In the first step,

the region in which the mutation will be made must be deleted from the *A. vinelandii* genome, and in the second step, exogenous DNA containing the mutation of interest is introduced into *A. vinelandii* and incorporated into the genome, fixing the deletion.

Because *A. vinelandii* harbors multiple copies of its single chromosome,[83] if the DNA region of interest is not removed from every single copy of the chromosome, then the "deletion strain," upon stress, readily reverts to the wild-type genotype. Since all *A. vinelandii* deletion strains are N^-, meaning they are unable to fix N_2 and rely on external fixed nitrogen to survive, successful creation of *A. vinelandii* deletion strains cannot be screened using N^- media, a traditional screening technique. Instead, potential transformants can only be identified by sequence analysis to confirm the gene sequence. Thus, detecting loss of N_2 fixation ability is much more time-consuming than screening for the ability to fix N_2.

Eventually, after repeated failure in creating the *A. vinelandii* deletion strain αC45A/L158C/ΔβS188, the precursor deletion strain required to make αC45A/L158C/βS188C MoFe protein, an extensive literature search and correspondence with nitrogenase researchers from another lab led to the successful implementation of a much quicker and reliable method for making nitrogenase mutants in *A. vinelandii.* The details of this process are discussed in Chapter 4, and extensive procedural details can be found in the Appendix.

In the end, general, all-purpose *A. vinelandii* deletion stains, which did not revert to a wild-type genotype under stress, were kindly provided by Professor Dennis Dean (Virginia Tech). These all-purpose deletion strains each had large portions of nifH, nifD, and/or nifK removed from the genome, and as such, could be used to create nearly any mutation to nifH, nifD, or nifK. One of these deletion strains was DJ11, which lacks nearly all of nifH, all of nifD, and most of nifK. Because DJ11 is missing the entire region between and including αC45A and βS188C, it was chosen

as the deletion strain precursor to use to create αC45A/L158C/βS188C MoFe protein. First, a plasmid was created that contained the entire nifHDK region, and then all three mutations of interest were inserted into the plasmid. Finally, the plasmid was transformed into DJ11, but again, efforts to create αC45A/L158C/βS188C MoFe protein were unsuccessful. It was determined that this was most likely due to the large size (nifHDK is > 5000 nucleotides) of DNA that needed to incorporate into the chromosome during cell replication. Indeed, there is no published report of any MoFe protein variant that has mutations to both the α- and β-subunits of MoFe protein, due to the inherently low probability of incorporation of such large stretches of DNA.

It was hypothesized that, since DJ33 has a shorter deletion than DJ11, the chances of successful transformation would improve if using DJ33 rather than DJ11. The region around αC45A is not deleted in DJ33, so attempts were made to construct αL158C/βS188C and leave the extra surface-exposed Cys intact. Unfortunately, αL158C/βS188C could not be created using DJ33, either. One hypothesis to explain this failure is that a MoFe protein with both αL158C and βS188C mutations is unable to reduce N_2 to NH_3. If this were the case, incorporation of exogenous DNA may have occurred, but the transformed cells would be unable to grow on media lacking a source of fixed nitrogen, so there would be no way to screen for success. Support for this hypothesis comes from the fact that it was possible to create a strain harboring αL158C/βS188A from DJ33, so length of DNA incorporation was not the prohibitive factor. Figure 3.13 shows relevant portions of the DNA sequencing chromatogram for αL158C/βS188A, which was created by transformation of DJ33 with a plasmid harboring nifHDK.

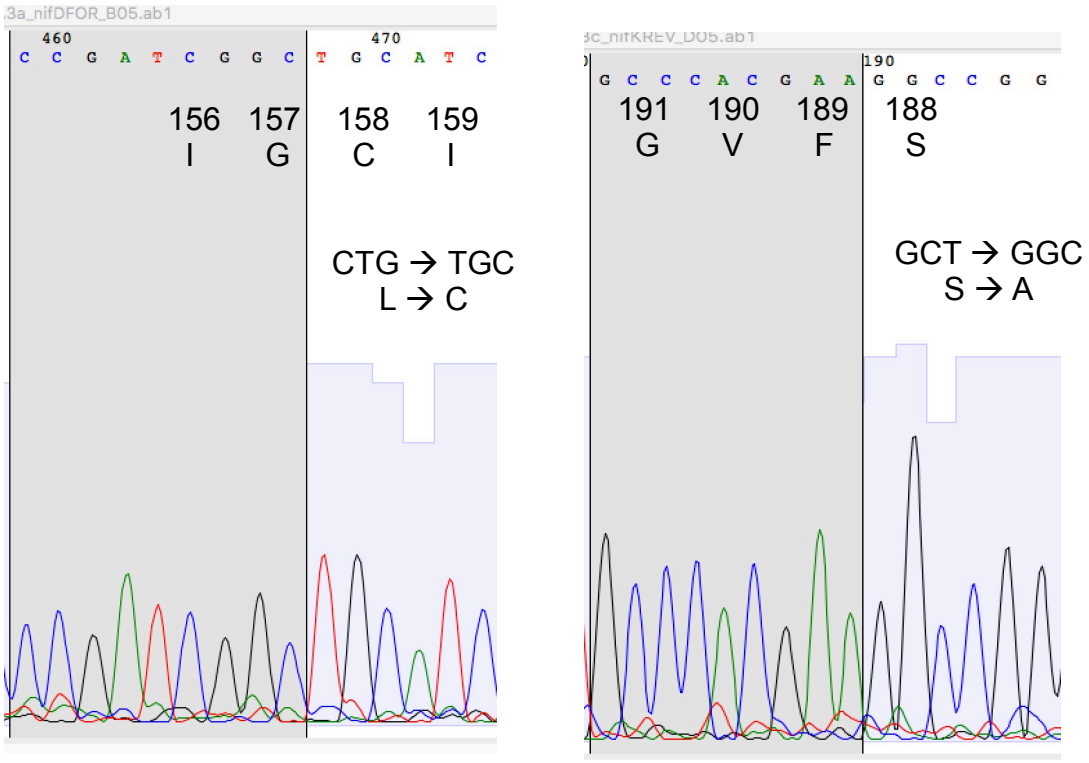

Figure 3.13 Sequencing chromatograms of the nifD and nifK regions including the codon for αL158, which has been mutated to an Cys in this work, and βS188, which has been mutated to an Ala in this work, showing that both mutations are intact in the strain created in the current work.

3.3.8 Modification of βV157C MoFe protein

When mutagenesis efforts to create a strain harboring αL158C and βS188C proved unsuccessful, βV157 was explored as a location for covalent attachment of Ru-PhenIA. It was shown previously that Ru-PhenIA could label Cys residues near the P-cluster, including αL158C, but also αI159C and βV157C, yielding photocatalytic Ru-MoFe protein constructs. Before growing the strain harboring βV157C MoFe protein, however, the nifK gene was sequenced and the desired mutation was not fully present. Instead, as is clear from Figure 3.14, the strain is in the process of reverting to a wild-type genotype, since it had been constructed using an impure deletion strain. Utilizing deletion strain DJ200, which had been provided by the Dean

lab, a plasmid containing βV157C was readily transformed into DJ200. The DNA sequencing chromatogram of the stable, permanent mutation at position β157 is shown in Figure 3.15. Additionally, nifK mutants such as βV157C/βS188C, βV157C/βS188A, and βV157C/βF99Y were readily made with the deletion strain DJ200. Figure 3.16 shows sequencing chromatograms for the regions containing the codons for β99Y and β157C, which show successful mutagenesis and maintenance of the mutations after multiple rounds of growth on media lacking a source of fixed nitrogen.

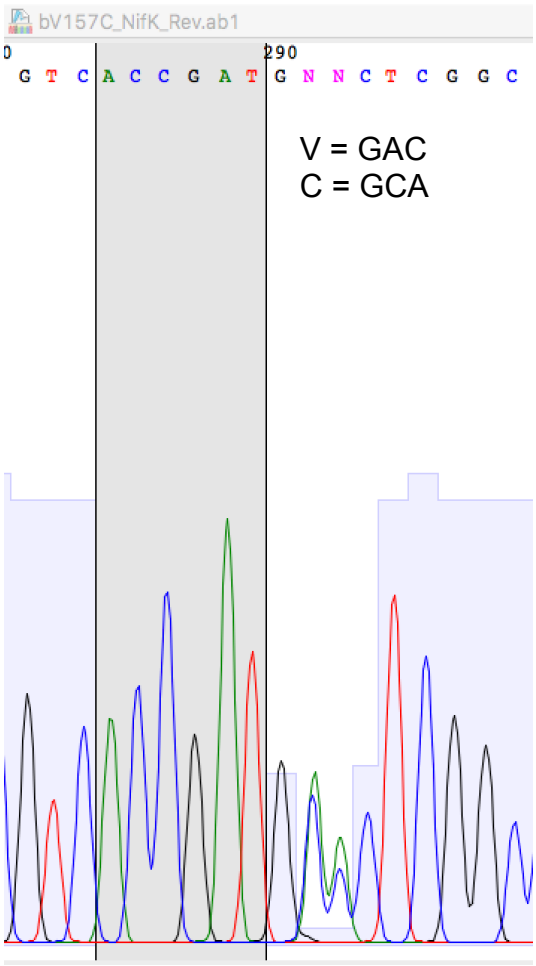

Figure 3.14 DNA sequencing chromatogram in the reverse direction of strain βV157C created previously, which is in the process of reverting to wild-type because it was made with a “deletion strain” still containing some wild-type DNA.

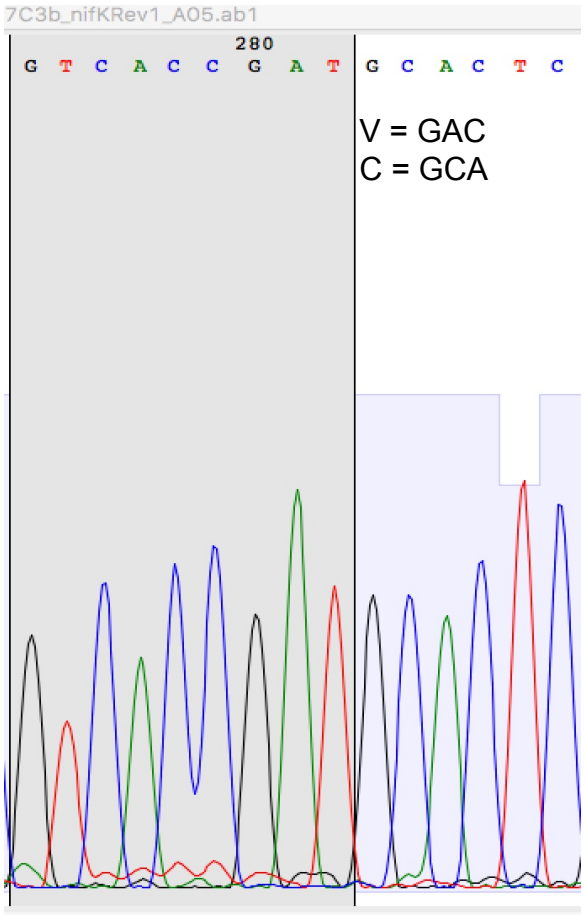

Figure 3.15 DNA sequencing chromatogram in the reverse direction of strain βV157C created in this work, which was created from transformation of plasmid DNA into DJ200.

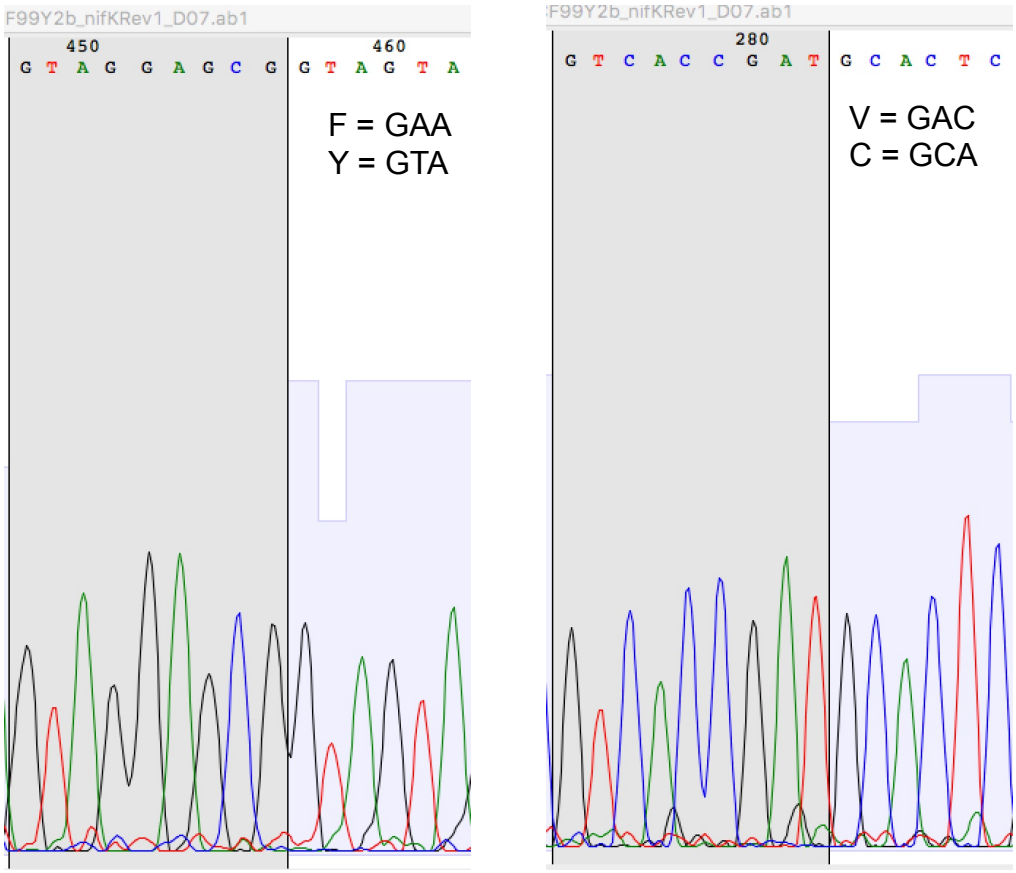

Figure 3.16 DNA sequencing chromatogram in the reverse direction of strain βF99Y/V157C created in this work, which was created from transformation of plasmid DNA into DJ200.

Surprisingly, βV157C Ru-MoFe protein was not active in the reduction of H^+ → H_2 or C_2H_2 → C_2H_4. Further analysis revealed that βV157C Ru-MoFe protein was only labeled with the photosensitizer Ru-PhenIA on one subunit, the α-subunit. Visualization of βV157C Ru-MoFe protein on an 8% SDS-PAGE gel under UV light should reveal two fluorescent bands, if indeed position β157C has been labeled. However, βV157C Ru-MoFe protein appears indistinguishable from wild-type Ru-MoFe (which can be labeled at αC45) protein on an 8% SDS-PAGE gel, as shown in Figure 3.17, suggesting βV157C Ru-MoFe protein has been labeled on the α but not the β subunit, explaining its lack of photoreduction activity.

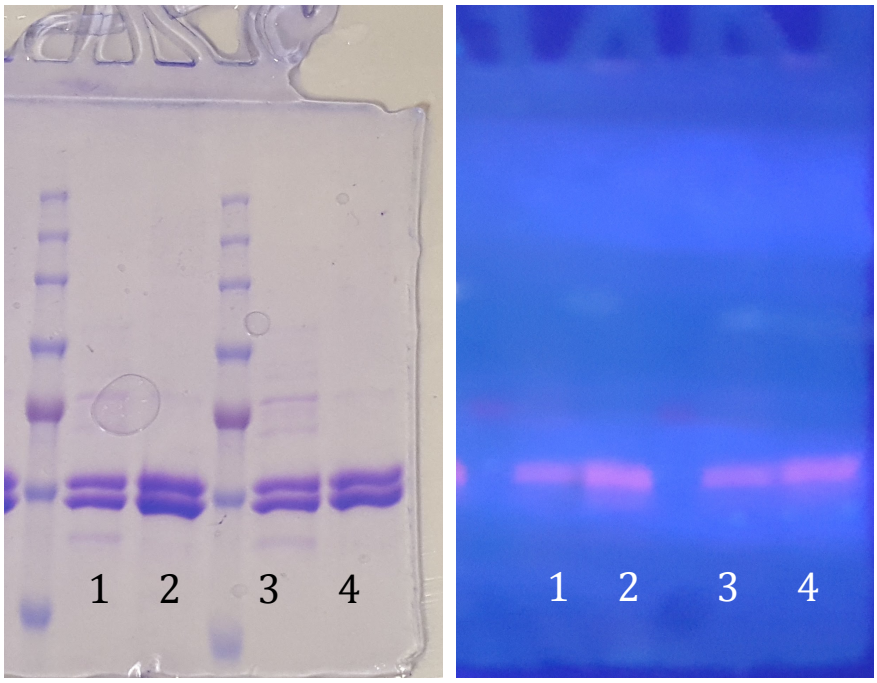

Figure 3.17 An 8% reducing SDS gel after (right) and prior (left) to staining with Coomasie Brilliant Blue dye highlights separation of α- and β-subunits of MoFe protein, with the image on the right taken under UV light to show the fluorescence of the Ru label. Both 1 and 3 are wild-type MoFe protein after reaction with Ru-PhenIA, and 2 and 4 are βV157C MoFe protein after reaction with Ru-PhenIA.

As a follow-up test, βV157C MoFe protein was mixed with two different fluorophores, IAEDANS and maleimide-derivatized Eosin, to evaluate whether molecules smaller than Ru-PhenIA could access and label the Cys residue at position β157C. These tests, shown in Figure 3.18, confirmed that β157C MoFe protein could be labeled on both α- and β- subunits by molecules smaller than Ru-PhenIA. These results support the hypothesis that the Cys at position β157 is not surface exposed enough to be accessed by a large molecule like Ru-PhenIA, and the protein must be perturbed to increase the solvent accessibility of the Cys at position β157 in order to achieve labeling with Ru-PhenIA. Thus, labeling reactions were carried out at increasing reaction temperatures and reaction times, but no labeling could be accomplished, even at 40°C and for 24 hours.

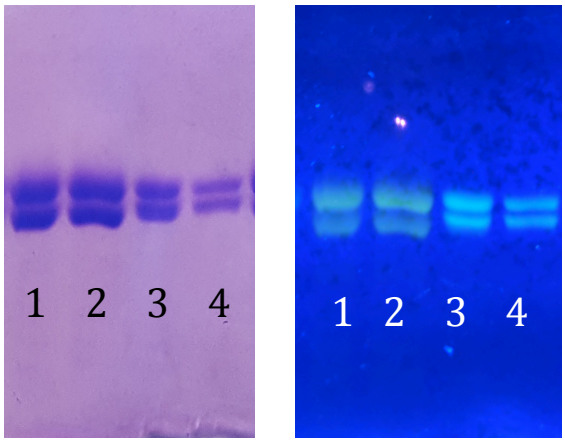

Figure 3.18 An 8% reducing SDS gel after (right) and prior (left) to staining with Coomasie Brilliant Blue dye highlights separation of α- and β-subunits of βV157C MoFe protein, with the image on the right taken under UV light to show the fluorescence of the Ru label. Both 1 and 2 are reactions of βV157C MoFe protein with maleimide-derivatized Eosin, and 3 and 4 are reactions of βV157C MoFe protein with IAEDANS.

3.4 Conclusions

To summarize, MoFe proteins, which lack Ser at position β188, still contain a nearby oxygen ligand capable of ligating the P-cluster, and all Group 1 nitrogenases lacking βS188 have βY98. This finding, coupled with the rarity of non-Cys amino acids as ligands for biological FeS clusters, strongly suggests a functional role for an oxygen ligand near the P-cluster. One possible mechanistic hypothesis comes from the differences in electron donor characteristics of oxygen compared to sulfur. While oxygen is a hard ligand that will preferentially bind hard Fe^{3+} rather than softer Fe^{2+} species, sulfur is a softer, larger, more polarizable donor that will bind both ferrous and ferric Fe. Thus, oxygen may be capable of acting as a redox switch where sulfur is not. Whether oxygen ligates the P-cluster could be dictated by the position and dynamics of nearby amino acid residues in MoFe protein.

A possible theory for the mechanism of conformational gating of electron transfer in nitrogenase is that, as Fe protein explores the surface of MoFe protein in

the transition from *DG1* to *DG2*, Fe protein communicates some structural change or changes to the MoFe region surrounding the P-cluster, causing either βS188 or βY98 to move into a proper binding distance and orientation relative to the P-cluster, and this subtle change provides enough additional electron density at the P-cluster to lower its reduction potential below that of FeMoco, allowing *intramolecular* electron transfer to proceed.

Extensive attempts were made to optimize the photocatalytic Ru-MoFe protein based on the above hypothesis about the role of the P-cluster in conformational gating of electron transfer. A MoFe protein, when derivatized with a Ru-photosensitizer near the P-cluster, was able to deliver electrons to FeMoco and ultimately reduce substrates using light and without the need for ATP or Fe protein. Though still the only example of a unimolecular, photocatalytic nitrogenase system, unfortunately, the overall yield of any reaction with this construct is extremely low compared to the native biological system, and it produced exclusively H_2 and no NH_3 under and N_2 atmosphere. It was suggested that this inefficiency might be due to the fact that, in the absence of Fe protein, an important conformational change is not taking place within MoFe protein that would lead to more favorable electron flow to FeMoco. Because P-cluster ligation by βS188 may be a part of that conformational gate in *A. vinelandii*, mutations which might lower the reduction potential of the P-cluster, such as βS188C, were pursued as an addition to the light-driven MoFe protein construct in an attempt to subvert, or permanently open, the conformational gate. It was hypothesized that this could lead to huge increases in photoreduction efficiency and also potentially enable the challenging N_2 reduction, however, difficulties in mutagenesis and alternative labeling sites prevented comprehensive testing of this hypothesis.

3.5 Future Directions

There are many exciting avenues of investigation that should be explored to follow-up on the insights gained from the experiments discussed in Chapter 3. First, amino acid residues along surface of the Fe-MoFe protein interface between *DG1* and *DG2* should be individually and collectively mutated to probe their potential involvement in signal transduction from the surface of Fe protein to the P-cluster. Examples of such residues include βF189 and γR100, which are shown in Figure 3.19 to lie in close proximity to one another and the residues surrounding the P-cluster. Interaction between βF189 and γR100 could cause a movement of βS188 that permits it to ligate the P-cluster, offering a mechanism by which movement from *DG1* to *DG2* could activate ET. Thus, βF189 should be mutated to smaller (Ala or Gly) and more polar (Tyr, Lys, or Glu) residues, since P-cluster oxidation could reasonably be triggered by interaction between βF189 on the surface of MoFe protein and γR100 on the surface of Fe protein. Mutation of γR100 has previously been shown to dramatically decrease nitrogenase activity, so a decrease in catalytic activity resulting from mutation of βF189 could provide biochemical support for this mechanism.

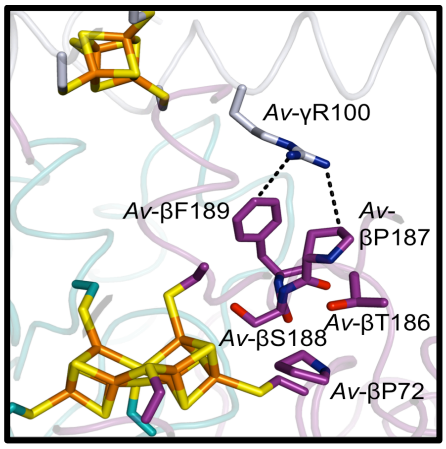

Figure 3.19 Amino acid residues near the 4Fe:4S cluster of Fe protein and the P-cluster of MoFe protein in the DG2 crystal structure, highlighting the proximity of residues βF189 and γR100.

Second, mutations should be made to Av-MoFe protein at and around the P-cluster such that it more closely resembles the P-cluster environment of Gd-MoFe protein. One example of this type of mutation is the double Av-MoFe mutant βS188A/βF99Y, which would convert Av-MoFe protein from the F/S motif to the Y/A motif. Two important pieces of evidence could be gained from this “Gd-like” Av-MoFe protein. If *A. vinelandii* strains harboring this mutation can still grow in the absence of a source of fixed nitrogen, this would indicate that whatever conformational change or changes Fe protein transduces to MoFe protein either do not actually involve the P-cluster or they can be accomplished even when the F/S motif is replaced with the Y/A motif. Next, cross-reactivity studies between the “Gd-like” Av-MoFe protein with actual Gd-Fe protein would reveal whether a switch to the Y/A motif alone is sufficient to increase the cross-reactivity of Av-MoFe protein with Gd-Fe protein.

Finally, the optimization of the light-driven MoFe protein can be continued with improved mutagenesis strategies. When the αC45A/αL158C/βS188C MoFe protein construct could not be obtained, βV157C/βS188C was created instead, based on previous work demonstrating photoreduction activity by a MoFe protein variant derivatized at position β157C instead of α158C. Unfortunately, the analysis detailed here shows that β157C can be covalently labeled with small fluorophores but not the bulky Ru-PhenIA ligand. Thus, improved mutagenesis strategies are needed to facilitate rapid generation of MoFe protein variants containing mutants in both the α- and β-subunits, in order to create a MoFe protein that can be derivatized by Ru-PhenIA that also contains an altered P-cluster.

3.6 Materials and Methods

3.6.1 Expression and purification of nitrogenase proteins from A. vinelandii

An *A. vinelandii* strain harboring genes coding for wild-type nitrogenase proteins was expressed and cells harvested according to the procedures reported in Chapter 2. Wild-type Av-MoFe protein was purified as described in Chapter 2, with some modifications. Instead of using glycerol-containing solutions to induce cell rupture by osmotic shock, here cells were ruptured by shear forces using a microfluidizer (Microfluidics Corporation) under a stream of Ar. The lysate was degassed and centrifuged for 1 hour at 12500 rpm. Clarified cell lysate was then loaded onto a DEAE Sepharose column and purified as detailed in Chapter 2.

3.6.2 Expression of G. diazotrophicus nitrogenase

G. diazotrophicus cells were grown in media containing 10% glucose, 0.14 mM $CaCl_2$, 0.81 mM $MgSO_4$, 0.036 mM $FeSO_4$, 0.008 mM $Na_2Mo_2O_4$, 10 mM Na_3PO_4 pH 6.0.[84] Solid media contained in addition 20 g/L agar and 5 mL/L of a 0.5% bromophenol blue solution. For nitrogen-containing media, $(NH_4)_2SO_4$ was added to a concentration of 0.5 mM. Cells were first grown in a 100-mL nitrogen-containing starter culture for 48 hours. To start the expression culture, 20 mL of cells were transferred into 2 L of nitrogen-containing media in a 6-L Erlenmeyer flask. Cells were grown for 5-7 days at 30°C and shaken at 200 rpm. Nitrogenase activity was monitored by measuring whole cell reduction of C_2H_2 to C_2H_4, and cells were harvested when nitrogenase activity peaked. The cells were harvested by centrifugation at 5000 rpm to collect a visible brown pellet of approximately 2 g per L of culture.

3.6.3 Purification of nitrogenase proteins from G. diazotrophicus

All lysis and purification procedures were conducted on a Schlenk line apparatus under Ar or inside an anaerobic chamber under 90% Ar, 10% H_2. Cells were ruptured using a microfluidizer (Microfluidics Corporation) under a stream of Ar. The lysate was degassed and centrifuged for 1 h at 12500 rpm. Clarified cell lysate was then loaded onto a DEAE Sepharose column and washed with an aqueous solution containing 50 mM Tris, buffered to pH 7.75, 100 mM NaCl, and 5 mM DT, until the flow through was clear. Protein was eluted with a linear gradient using an aqueous solution containing 50 mM Tris, buffered to pH 7.75, and 5 mM DT, in which the NaCl concentration was increased from 100 mM to 500 mM. Gd-MoFe protein and Gd-Fe protein eluted together around 350-400 mM NaCl. Gd-MoFe protein and Gd-Fe protein were further purified by gel filtration chromatography using a Sepharose 200 column (GE Healthcare) equilibrated with an aqueous solution containing 50 mM Tris, buffered to pH 8.0, 500 mM NaCl, and 5 mM DT. Fractions containing the respective protein were identified by SDS-PAGE, pooled, concentrated, and stored in liquid nitrogen in small aliquots. Purified Gd-MoFe protein typically had C_2H_2 reduction activities between 1000-1500 nmol/mg/min, in line with the previous report.[85]

3.6.4 Crystallization of Gd-MoFe proteins

Gd-MoFe protein crystals were grown using the sitting drop method. A 2-μL aliquot of a solution containing 170 μM (40 mg/mL) Gd-MoFe protein, as well as 25 mM Tris, buffered to pH 8.0 and 100 mM NaCl, was mixed with 2 μL of well solution in the drops. Reduced Gd-MoFe protein crystals were grown against 0.25 mL well solution containing 45% MPD, 300 mM NaCl, 100 mM sodium cacodylate, buffered to

pH 6.5, 1 mM Spermine, 0.1% Zwittergent, and 5 mM DT. X-ray diffraction data were collected at SSRL beamline 9-2 at 77 K at a wavelength of 0.98 Å.

Crystals of oxidized Gd-MoFe protein were grown against 0.25 mL well solution containing 50% MPD, 300 mM NaCl, 100 mM sodium cacodylate, buffered to pH 6.5, 1 mM Spermine, and 0.43 mM IDS. X-ray diffraction data were collected at 77 K on SSRL beamline 14-1 at a wavelength of 0.98 Å. X-ray data were indexed and integrated in XDS, scaled and merged in Aimless, and converted into Amplitudes in Truncate. The structure of reduced Gd-MoFe protein was solved by molecular replacement with 1M1N as search model using phenix.MR, and oxidized Gd-MoFe protein was solved using reduced Gd-MoFe protein as a search model. The structure was refined by automated refinement using refmac, phenix.refine, and manual refinement using coot. Final data collection and refinement statistics for reduced and oxidized Gd-MoFe proteins are found in Table 3.4.

Table 3.4 X-ray data collection and refinement statistics with statistics for the highest-resolution shell shown in parentheses.

	Reduced Gd-MoFe	Oxidized Gd-MoFeP
Wavelength	0.98 Å	0.98 Å
Resolution range	39.73 - 1.83 (1.895 - 1.83)	39.59 - 2.592 (2.684 - 2.592)
Space group	P 41 21 2	P 41 21 2
Unit cell	202.598 Å × 202.598 Å × 132.567 Å 90° × 90° × 90°	201.569 Å × 201.569 Å × 132.208 Å 90° × 90° × 90°
Total reflections	6537704 (662790)	1897797 (176858)
Unique reflections	240200 (23851)	84437 (8009)
Multiplicity	27.2 (27.8)	22.5 (21.5)
Completeness (%)	100 (100)	100 (99)
Mean I/sigma(I)	12.85 (1.64)	17.97 (2.61)
Wilson B-factor	14.27	37.65
R-merge	0.4208 (1.434)	0.411 (1.65)
R-meas	0.4288 (1.46)	0.4206 (1.689)
CC1/2	0.976 (0.815)	0.986 (0.548)
CC*	0.994 (0.948)	0.996 (0.842)
Reflections used in refinement	240146 (23850)	84169 (8009)
Reflections used for R-free	11943 (1208)	4243 (419)
R-work	0.1396 (0.1933)	0.1811 (0.3098)
R-free	0.1613 (0.2308)	0.2137 (0.3436)
CC(work)	0.967 (0.912)	0.955 (0.521)
CC(free)	0.960 (0.890)	0.948 (0.508)
Number of non-hydrogen atoms	17789	16070
as part of macromolecules	15690	15616
as part of ligands	120	96
Protein residues	1986	1981
RMS(bonds)	0.037	0.044
RMS(angles)	1.88	1.63
Ramachandran favored (%)	97	97
Ramachandran allowed (%)	2.6	3.3
Ramachandran outliers (%)	0.2	0.2
Rotamer outliers (%)	1.6	3.4
Clashscore	2.35	2.07
Average B-factor	18.59	40.29
macromolecules	17.08	40.52
ligands	15.37	36.27
solvent	30.75	31.21

3.6.5 Electron Paramagnetic Resonance Spectroscopy

EPR experiments were carried out with purified Gd-MoFe and Av-MoFe proteins at 10 K on a Bruker EMX X-band spectrometer equipped with an Oxford ESR 900 cryostat. Solutions contained 50 μM protein. Parallel mode spectra were recorded with a microwave frequency of 9.36 GHz, a modulation amplitude of 10.02 Gauss, and a microwave power of 6.4 mW. Perpendicular mode spectra were recorded with a microwave frequency of 9.64 GHz, a modulation amplitude of 10.02 Gauss, a microwave power of 6.4 mW.

3.6.6 Synthesis of Ru-PhenIA

PhenIA was synthesized as reported previously with minor modifications.[81] Briefly, iodoacetic acid anhydride was synthesized by mixing 3.4 g N,N'-dicyclohexylcarbodiimide (Alfa Aesar) with 6.5 g iodoacetic acid (Alfa Aesar) in 75 mL ethyl acetate. The solution was stirred at room temperature in the dark for two hours, at which point the solution was filtered. The orange filtrate was concentrated to < 2 mL in a rotary evaporator. The orange solution contained both iodoacetic acid anhydride and ethyl acetate, but as the melting temperatures of iodoacetic acid anhydride is < 50°C, iodoacetic acid anhydride was utilized in liquid form. Iodoacetic acid anhydride was immediately mixed with 0.5 g 5-amino-1,10-phenanthroline (Sigma-Aldrich) in 50 mL acetonitrile. The reaction proceeded overnight, in the dark, and at room temperature. The product was collected by filtration, washed with 5% sodium bicarbonate, and dried overnight under vacuum.

Ru-PhenIA was synthesized as reported previously with a minor modification.[82] Briefly, 50 mg $Ru(bpy)_2Cl_2$ (Sigma-Aldrich) was mixed with 40 mg PhenIA in 25 mL methanol and refluxed overnight in the dark. The orange solution

was filtered and the filtrate evaporated to dryness. Crude Ru-PhenIA was stored as a solid at -20°C and used without further purification.

3.6.7 Modification of MoFe protein with photosensitizers and fluorophores

To label MoFe protein with Ru-PhenIA, αC45A/L158C MoFe protein was first transferred to an aqueous solution buffered with P_i rather than Tris, and lacking DT, since primary amines and reductants can both inhibit the reaction of iodoacetamide with Cys thiols. Additionally, the P_i solution was buffered to pH 7.8. Then, dilute αC45A/L158C MoFe protein (1 – 5 mg/mL) was mixed with approximately a 100-fold excess of crude Ru-PhenIA product. The solution was let to react anaerobically in the dark for at least 2 hours, and passing the reaction solution over a 10-DG column stopped the labeling reaction. Visible separation of brown protein from excess orange Ru-PhenIA was always accomplished. The 10-DG column was equilibrated with an aqueous solution buffered to pH 7.0 with 100 mM P_i, which was determined in this work to be the pH of optimum photocatalytic activity, and also included 100 mM NaCl and 5 mM DT. If the 10-DG column did not contain at least 5 mM DT, then Ru-MoFe protein was susceptible to oxygen damage, resulting in substantial loss in activity over time. The Ru-MoFe protein construct was then concentrated in 10 kDa microcons. A clear flow-through confirmed full removal of excess Ru-PhenIA from the labeled protein.

The same procedures were followed to modify MoFe protein with the fluorophores IAEDANS and maleimide-derivatized Eosin, except only a 50-fold molar excess of fluorophores was used. To test the effect of reaction temperature on labeling efficiency, reactions were carried out on a heating stir plate that also had a temperature probe and digital readout in a vial containing 20 mL H_2O to approximate

the temperature of the reactions. Reactions were iteratively carried out from 30°C – 40°C at 2°C intervals.

3.6.8 Site-directed mutagenesis of nitrogenase proteins in A. vinelandii

A concentrated stock of *A. vinelandii* strain DJ11 was removed from the -80°C freezer and slowly thawed on ice. A 100-uL aliquot of this cell stock was sterily plated on solid Burk's media containing a source of fixed nitrogen (10 mM NH_4Cl) but lacking Fe (N^+/Fe^-) and incubated at 30°C. After two days, a portion of the lawn growth was sterily transferred to a fresh plate, also containing a source of fixed nitrogen (10 mM NH_4Cl) but lacking Fe (N^+/Fe^-) and incubated at 30°C. After two days, a portion of the lawn growth was sterily transferred to a fresh plate for a 3rd round of Fe-starvation. When bright green colonies appeared, 3 – 5 single colonies were sterily transferred to 50 mL Burk's media (low Ca/N^+/Fe^-) in a 125 mL Erlenmeyer flask. This Burk's media contained 0.09 mM Ca^{2+}, which is 10% of the Ca^{2+} in standard Burk's media. Cultures were let to shake for 20 hours at 30°C and 150 rpm. After 20 hours of growth, the $O.D._{600}$ was monitored until the liquid culture achieved an $O.D._{600}$ between 0.25 – 0.5. DJ11 cells that had turned fluorescent green and achieved a sufficient $O.D._{600}$ were used for transformations.

Transformations were initiated by sterily adding 50 µL of DJ11 liquid culture to 50 µL of a sterile solution containing 20 mM MOPS buffer and 20 mM $MgSO_4$, buffered to pH 7.2, and 2 – 5 µg plasmid DNA. Solutions were placed in a 30°C incubator for 30 minutes, then diluted with 400 µL Burk's media (low Ca/N^-), and subsequently plated on Burk's media lacking a source of fixed nitrogen (N^-). Single colonies first appeared after 3 – 5 days of incubation at 30°C. Single colonies were streaked on Burk's media (N^-), before performing colony PCR to confirm the presence of the desired mutation. After confirmation of incorporation of the

mutation(s) of interest, newly-created mutant strains were stored in small, concentrated aliquots containing 7% v/v DMSO, flash frozen in liquid N_2, and stored at -80°C until further use. This procedure never proved successful for the generation of an *A. vinelandii* strain harboring the three mutations αC45A/αL158C/βS188C, most likely due to the large amount of DNA that needed to be incorporated into the genome, and the strong possibility that an *A. vinelandii* strain harboring the three mutations αC45A/αL158C/βS188C may be completely impaired in its ability to fix nitrogen. The mutagenesis procedure described here, however, was successful for the generation of *A. vinelandii* strains harboring βV157C/βS188C and βV157C/βF99Y using the smaller deletion strain DJ200.

3.6.9 Photoreduction assays with Xe arc lamp

The catalytic ability of Ru-MoFe protein was assessed by irradiating samples with a 150W Xe arc lamp housed in an LS Series light source (Abet Technologies). The position of the lamp was adjusted to maximize the number of photons that reached the Ru-MoFe protein sample. Ru-MoFe protein was let to react in a 4-mL solution contained in a 10-mL glass vial, sealed with a rubber septum. This 10-mL vial was placed at the center of a stir plate in a small water bath, as shown in Figure 3.20.

Reactions contained, in a final volume of 4.0 mL, 100 mM P_i, buffered to pH 7.0, 100 mM NaCl, 50 mM DT, and 0.1 – 0.2 mg/mL Ru-MoFe protein. Solutions lacking protein and DT were placed in sealed vials with a stir bar and exchanged into an Ar atmosphere using a Schlenk line apparatus. Separately, 2 mmol (0.348 g) DT and 2 mL of a solution of 100 mM P_i, buffered to pH 7.0, with 100 mM NaCl, were also exchanged into an Ar atmosphere using a Schlenk line apparatus. Next, a solution of 1.0 M DT in 100 mM P_i, buffered to pH 7.0, with 100 mM NaCl, was prepared by anaerobic transfer of 2 mL of the P_i buffered solution to the sealed vial

containing DT powder, using a gas tight Hamilton syringe. The solution was shaken until all DT had dissolved. Then, 200-µL aliquots of the 1.0 M DT stock solution were anaerobically transferred to each photoreduction assay vial using a gas tight Hamilton syringe. In a similar manner, 0.5-mL aliquots were removed from a 1-L flask of pure C_2H_2 gas and added to each photoreduction assay vial. Finally, an aliquot of the Ru-MoFe protein stock solution was added anaerobically using a gas tight Hamilton syringe. Assay vials contained a final pressure of approximately 0.05 atm C_2H_2, a final DT concentration of 50 mM, and final protein concentration of between 0.1 – 0.2 mg/mL Ru-MoFe protein. For assays monitoring the photoreduction of $H^+ \rightarrow H_2$, the C_2H_2 gas was omitted. For reactions containing alternative reductants, such as acorbate, solid reductants were made anaerobic on the Schlenk line apparatus and 1.0 M stock solutions were prepared in the same P_i buffered solution.

Reactions were initiated by irradiation with light and stirred at room temperature for 10 – 90 minutes. Reactions were terminated at various times when samples were removed from the light source, and a 500-µL aliquot of reaction headspace was injected onto the GC to quantify product formation.

To monitor the photocatalytic ability of Ru-MoFe protein over time, a 500-µL aliquot of headspace was removed and injected onto the GC to monitor product formation, and the reaction vial was returned to the water bath for irradiation. No more than 3 500-µL aliquots of the 6-mL headspace were removed from the same vial for these time-course experiments.

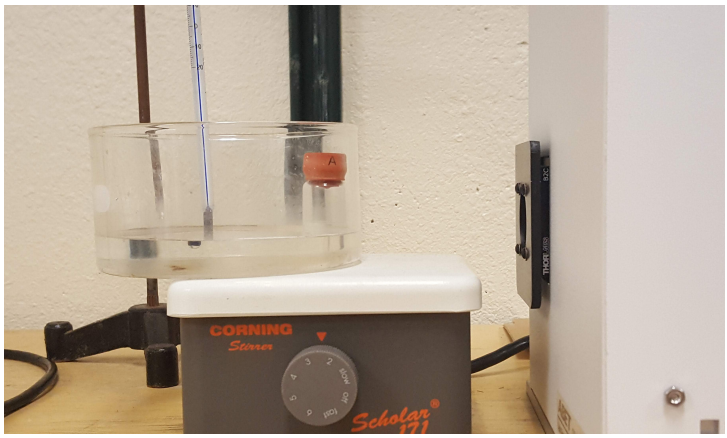

Figure 3.20 Photoreduction assay set-up with Xe arc lamp.

3.6.10 Photoreduction assays with LED light

Alternatively, photoreduction assays were also carried out under irradiation with a 455-nm LED light (Thor labs). The set-up for this experiment is shown in Figure 3.21. The reaction solution preparation was identical to samples irradiated with the Xe arc lamp.

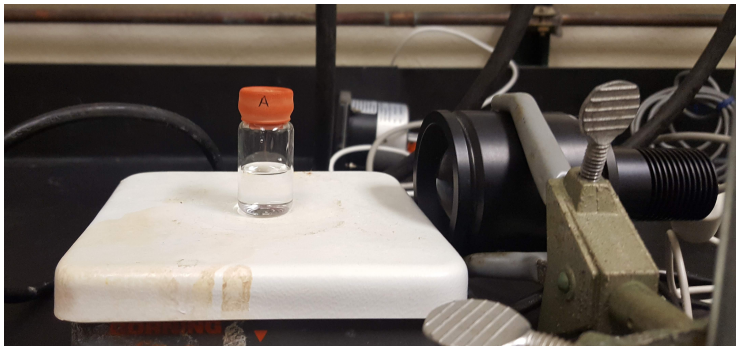

Figure 3.21 Photoreduction assay set-up with 455-nm LED light source.

3.6.11 Quantification of C_2H_4 formed by GC

C_2H_4 was measured as described in Chapter 2, except 500-µL rather than 50-µL aliquots of reaction headspace were analyzed.

3.6.12 Quantification of H_2 formed by GC

H_2 was measured as described in Chapter 2.

3.7 Acknowledgements

The authors would like to thank Valeria Cash and Professor Dennis Dean from Virginia Tech for kindly providing all-purpose deletion strains and quick, succinct answers to numerous questions over the years. The authors would also like to thank Professor Andy Borovik for assistance with EPR and Dr. Richard Cochran for assistance with ICP-MS.

Chapter 3 was reproduced in part, with permission, from Owens, C. P.; Katz, F. E. H.; Carter, C. H.; Oswald, V. F.; Tezcan, F. A. “Tyrosine-coordinated P-cluster in *G. diazotrophicus* nitrogenase: evidence for the importance of O-based ligands in conformationally gated electron transfer.” *J. Am. Chem. Soc.* **2016**, *138*, 10124–10127.

4 Methods for site-directed mutagenesis of nitrogenase proteins in *A. vinelandii*

4.1 Abstract

In order to pursue many different research questions about nitrogenase reactivity, it is of paramount importance to quickly and routinely generate permanent site-directed mutants in *A. vinelandii*. Though many studies, including work discussed in this dissertation, include analyses of nitrogenase mutants, the actual creation of these mutants is an extremely challenging and often poorly understood process than can take years. The future directions proposed in this dissertation necessitate the generation of many nitrogenase mutants. This chapter details the molecular biology of how permanent changes to the genome of *A. vinelandii* can be made and successful efforts in this lab to implement facile mutagenesis procedures. The average time of the mutagenesis process has been shortened from years to weeks.

4.2 Introduction

4.2.1 History of mutagenesis in A. vinelandii

In the 1970's and 1980's, there was great interest in developing procedures for genetic transformation of a multitude of organisms, but there was specific interest in genetically manipulating *A. vinelandii* to further understand biological nitrogen fixation. Toward this end, successful transformation of *A. vinelandii* with exogenous DNA was first reported in 1976 by Page and Sadoff.[86] Subsequent studies by these and other researchers tested a variety of conditions to optimize the efficiency of uptake of exogenous DNA by *A. vinelandii*. They also figured out that while in some cases, *A. vinelandii* could stably maintain the exogenous DNA in plasmid form for many generations, in some cases the external DNA was maintained because it was

incorporated into the genome of *A. vinelandii*, and it is this latter mechanism, incorporation of exogenous DNA into chromosomal DNA, that has allowed for hundreds of mutants of *A. vinelandii* nif genes to be created, purified, and characterized over the last 30 years.

4.2.2 Motivation for the work

The βK400E MoFe protein construct took years to create, and at a rate of years per mutant, none of the future aims posed in this dissertation will be feasible. Thus, the investigation and troubleshooting discussed here was carried out in order to shorten the process of site-directed mutagenesis of nitrogenase structural proteins, in order to propel a variety of different research aims forward.

4.3 Summary of the creation of βK400E MoFe protein

First, it is necessary to explain how βK400E MoFe protein was created in the first place and why each step was so laborious and time consuming, to contextualize the amended procedures developed in this chapter. In the first step of the creation of βK400E MoFe protein, a plasmid containing *nif*K was created that had a short sequence of interest deleted. In this case the three codons coding for the amino acids βN399, βK400, and βR401 were deleted. After amplification of the plasmid in competent *E. coli* XL-1 blue cells, purification of the plasmid, and confirmation of the correct sequence, the plasmid *nif*K-Δβ399-401 was co-transformed into competent wild-type *A. vinelandii* cells along with a plasmid containing rifampicin resistance. Single colonies that grew were screened for incorporation of this deletion into the genome first by their ability to grow in the presence of 5 μg/mL rifampicin. Colonies that grew on rifampicin-containing media were then screened for loss of their ability to fix nitrogen by plating on N^+ and N^- media in parallel. Assuming that this deletion of three codons prevented the organism from synthesizing an active nitrogenase,

successful transformants should grow on N^+ but not N^- media, whereas wild-type *A. vinelandii* that did not incorporate the deletion should retain the ability to grow in the absence of a source of fixed nitrogen. After the deletion strain *A. vinelandii* Δβ399-401 was isolated, it was used for part two of the mutagenesis process.

Meanwhile, a plasmid containing *nif*K was created that had the codon for Lys at position β400 replaced with the codon for Glu. After amplification of the plasmid in competent *E. coli* XL-1 blue cells, purification of the plasmid, and confirmation of the correct sequence, the plasmid nifK-βK400E was transformed into competent *A. vinelandii* Δβ399-401 cells generated in the first step. Successful transformation was detected by screening on N^- media, assuming that incorporation of a plasmid containing the codons for amino acids 399, 400, and 401 restored the ability of the cells to fix nitrogen, even when βK400 was replaced with β400E.

The biggest bottleneck in this process was the successful creation of the *A. vinelandii* deletion strain. *A. vinelandii* has a single chromosome, but each cell can contain up to 100 copies of this single chromosome, depending on its stage of growth.[87] A successful transformation, then, must incorporate the desired deletion into every copy of the chromosome. If this does not occur, if even one copy of wild-type DNA remains, the deletion strain can eventually "revert" back to a wild-type genotype when it is challenged by an environment lacking a source of fixed nitrogen.

In step two of the mutagenesis, *A. vinelandii* Δβ399-401 was transformed with the plasmid containing nifK-βK400E. Single colonies that grew on N^- media should contain the desired mutation, βK400E, but this was not always the case. Many times, the single colonies instead contained exclusively wild-type DNA because there had been wild-type DNA remaining in the "Δβ399-401" stain. Thus, when the cells were challenged on N^- media, the trace wild-type DNA was amplified so the cells could fix nitrogen and survive, and no transformation actually took place. When this happened,

the process would have to start over again, in order to create a more pure deletion strain.

Eventually, after many years of work, an *A. vinelandii* Δβ399-401 strain was isolated that was completely free of wild-type DNA, stable for many generations, and was used to successfully create the following mutations described in Chapter 3: βN399E, βK400E, βR401E, βN399E/R401E, and βN399E/βK400E/βR401E. However, other labs seem to complete this process much more quickly. The Dean lab, for example, has generated hundreds of nitrogenase mutant proteins. When it became evident just how many mutations would need to be made to continue the research on the role of the P-cluster and associated ligands in the conformational gating of electron transfer, as well as the optimization of Ru-MoFe protein, it became essential to figure out how to complete this process in a more timely manner.

4.4 Site-directed mutagenesis as carried out by the Dean lab

One of the most readily apparent things in literature from the Dean lab was that they did not create a new deletion strain every time they wanted to make a nitrogenase mutant. Instead, they relied on a handful of tried and true deletion strains that had large portions of nifH, nifD, and/or nifK deleted. Of the hundreds of nitrogenase mutants created, most were made using one of the following deletion strains: “ΔnifH,” “ΔnifD,” “ΔnifK,” or “ΔnifDK.” However, these deletion strains had not worked for Tezcan group members in the past. Specifically, the ΔnifD deletion strain hadn’t worked for the creation of αC45A MoFe protein, used as a control for the photoreduction construct, and the ΔnifK deletion strain hadn’t worked for the creation of βK400E or any of the other *DG1* mutations.

What became evident after a thorough review of the literature was that these strains hadn’t achieved the desired goals because the names of the deletion strains

were a bit misleading. ΔnifD, also named DJ100, is only a deletion between the two Kpn1 cut sites in nifD, removing codons for the amino acids 102-276 of the α-subunit of MoFe protein, and ΔnifK, also named CA13, is only a deletion between the two Pst1 cut sites in nifK, removing codons for the amino acids 135-292 of the β-subunit of MoFe protein. Thus, ΔnifD was never an appropriate choice of deletion strain for making αC45A MoFe protein because it isn't missing the codon for αC45, so while transformation of a plasmid may incorporate the missing part of nifD through double homologous recombination, position 45 will always remain a Cys. Similarly, ΔnifK was never an appropriate choice of deletion strain for making βK400E because it isn't missing the codon for βK400.

Valerie Cash, the lab manager of the Dean lab, confirmed this hypothesis as to why ΔnifD and ΔnifK strains hadn't worked for Tezcan lab members in the past, and suggested they would work in the future if making a mutation within the region that had been deleted. Dennis Dean at Virginia Tech kindly provided a variety of all-purpose deletion strains, which are described in Figure 4.1. Strains DJ1192 and DJ200 have a gene coding for kanamycin resistance replacing the missing nif sequence, while DJ764, DJ33, DJ11, and DJ13 simply contain large gaps in their nif genes. Sequencing chromatograms for two of the deletion strains used in the work of this dissertation, DJ33 and DJ200, are shown in Figures 4.2 and 4.3, respectively. Figure 4.2 shows how the codon for residue αI101 is followed by the palindromic sequence of a Kpn1 cut site and then the codon for residue βW309. Figure 4.3 shows the Pst1 cut site where the DJ200 deletion was created and the poly-G sequence beginning the sequence inserted to confer kanamycin resistance. The sequences of all deletion strains were verified before use in a transformation.

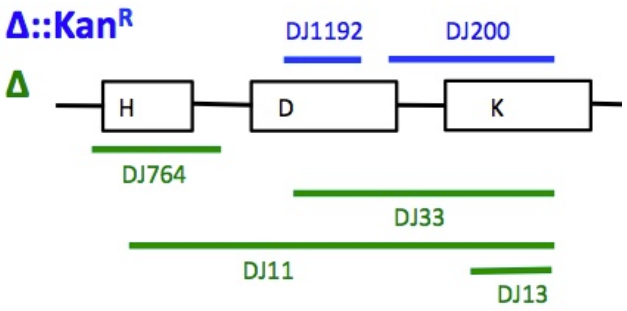

Figure 4.1 Schematic representation of six all-purpose deletion strains received from the Dean lab.

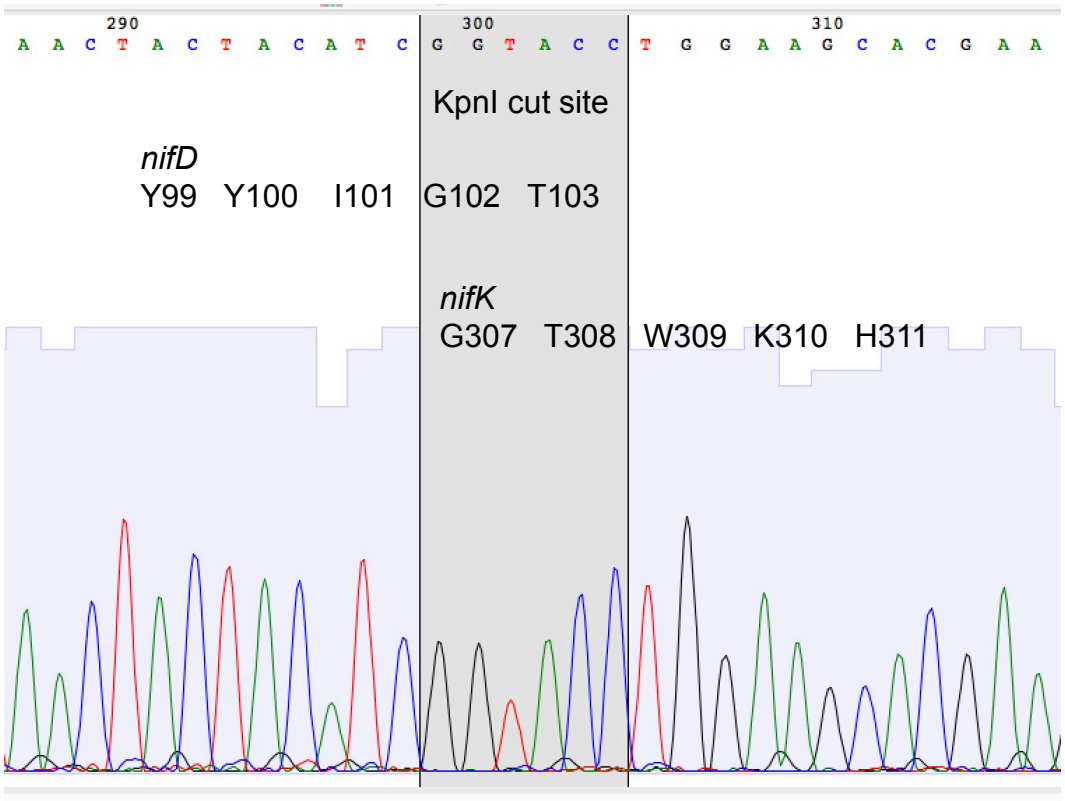

Figure 4.2 Sequencing chromatogram of DNA sequencing of *A. vinelandii* deletion strain DJ33.

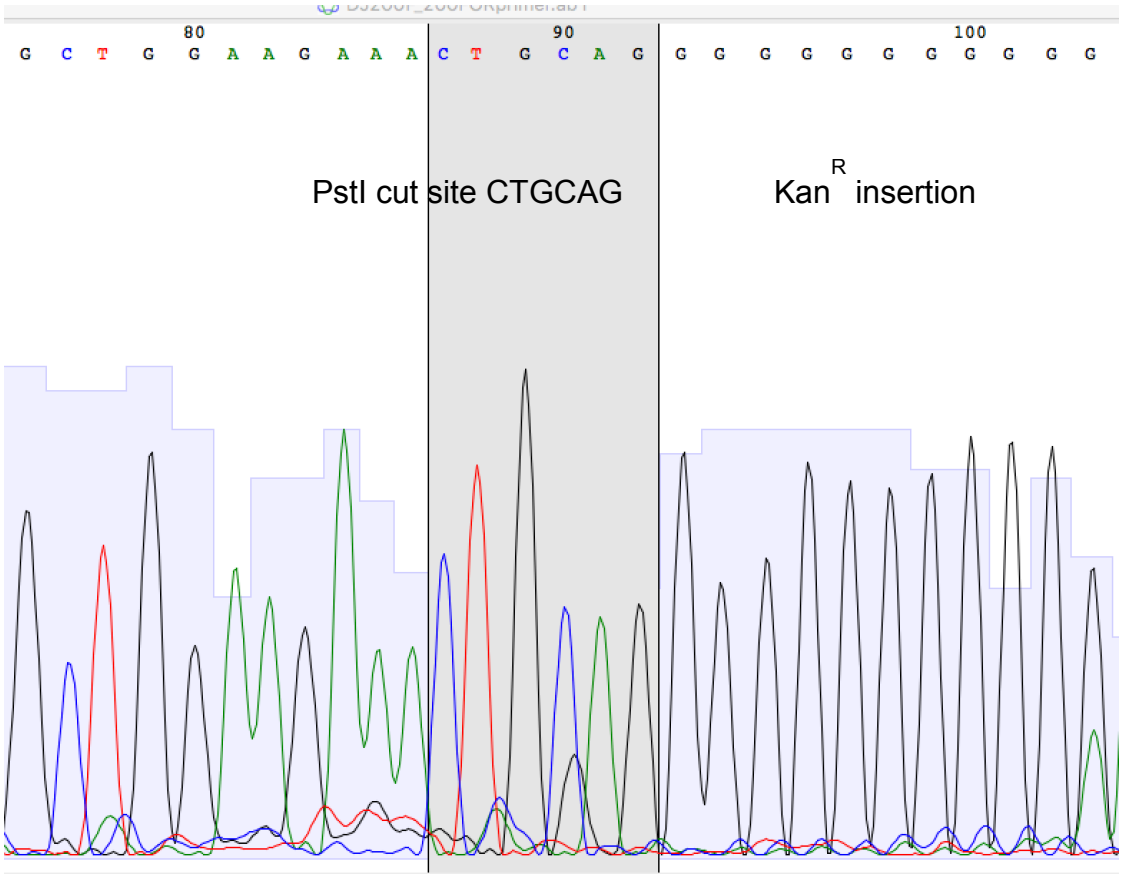

Figure 4.3 Sequencing chromatogram of DNA sequencing of *A. vinelandii* deletion strain DJ 200 showing the Pst1 cut site and the poly-G sequence that beings the kanamycin resistance insertion.

Creation of βK400E MoFe protein took years because a unique deletion strain was made for mutagenesis when ΔnifK proved unsuccessful. While Figure 4.1 shows that none of the deletion strains received from the Dean lab would be successful in the generation of βK400E MoFe protein, it is a waste of time to create a new, unique deletion stain for a proposed nitrogenase mutant if one of the above deletion strains encompasses the amino acid residue(s) of interest in its deleted region.

4.5 Two-step procedure for site-directed mutagenesis in *A. vinelandii*

Site-directed mutagenesis of *A. vinelandii* is necessarily a two-step process.[88] To summarize, a deletion strain of *A. vinelandii* is first created that is impaired in its

ability to fix nitrogen (N^- phenotype).[89,90] In many cases, one of the six strains depicted in Figure 4.1 is chosen and no new deletion strain is actually created, since it is this step that is the most time consuming and difficult part of *A. vinelandii* mutagenesis. Then, exogenous plasmid DNA, which contains the mutation of interest, is incorporated into the genome of the *A. vinelandii* deletion strain during cell replication through double homologous recombination, restoring the organism's ability to fix nitrogen. Successful transformants can be screened on media lacking a source of fixed nitrogen. When creating a site-directed mutant that cannot fix nitrogen (i.e., ΔLeu127-Fe protein), the deleted region must be replaced with some antibiotic resistance cassette, typically kanamycin resistance. Then, successful incorporation of exogenous plasmid DNA into the *A. vinelandii* deletion strain genome during cell replication can be screened by a loss of kanamycin resistance.

4.6 Creating competent *A. vinelandii* cells

There are many factors that affect the generation of *A. vinelandii* cells competent for the uptake of exogenous DNA and successful incorporation of that DNA into the *A. vinelandii* chromosome. First, cells must be stressed through both Fe and O_2 limitation. Fe starvation is accomplished by omitting Fe from Burk's media. Often, a deletion cell line is passed multiple times over solid Fe-free Burk's media prior to transformation to enhance Fe-starvation. *A. vinelandii* excretes a fluorescent siderophore under these conditions, and when sufficiently starved of Fe, *A. vinelandii* cultures will appear fluorescent green, as shown in Figure 4.4. O_2 is limited by slow shaking of cell cultures; cells are left to shake overnight at 150 rather than 200 rpm. It is also critical that the Ca content of this growth media is low (no more than 0.1 mM) to maximize DNA uptake. Finally, this media must contain a source of fixed nitrogen, since the deletion strains are unable to fix nitrogen.

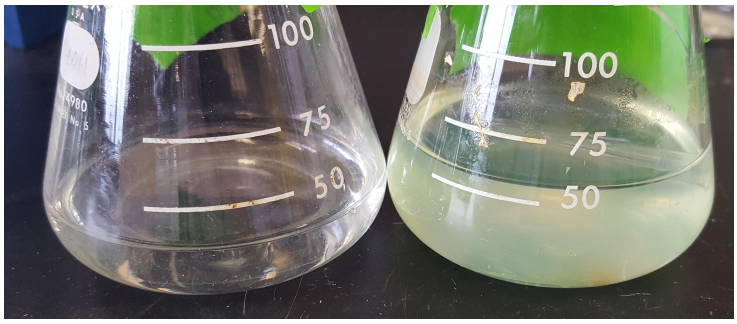

Figure 4.4 Color comparison of clear Burk's media (left) with opaque, light green Fe-starved *A. vinelandii* cells (right).

While the above considerations are important for obtaining cells that will receive exogenous DNA, because *A. vinelandii* harbors so many copies of its single chromosome,[83] the probability of correct incorporation of this DNA into every single copy of the *A. vinelandii* chromosome is extremely low. Thus, it is imperative to transform cells with exogenous DNA only when the $O.D._{600}$ of the cell culture is between 0.2 – 0.5. At this early exponential phase, cells have fewer copies of their genetic information,[87] greatly improving the chances of incorporation of exogenous DNA into every single chromosome copy. Figure 4.5 shows the relationship between cell culture density and transformation efficiency, as noted by Page and co-workers.[86]

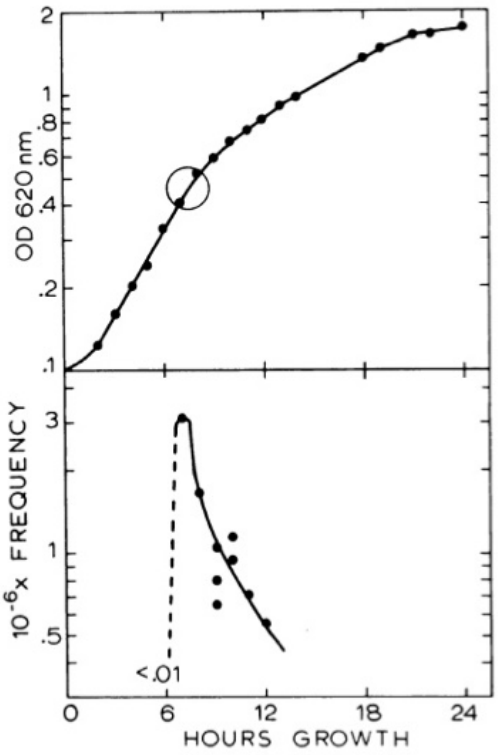

Figure 4.5 Correspondence of density of cell culture and transformation frequency as observed by Page, adapted from ref *86*.

To set-up a transformation, competent, fluorescent green *A. vinelandii* cells with an $O.D._{600}$ between 0.2 – 0.5 are mixed with an equal volume of an aqueous solution of MOPS, buffered to pH 7.2 and containing 20 mM Mg^{2+}. Then exogenous DNA is added to the mixture, and the components are let to interact at 30°C for 30 minutes, at which time cells are plated. It has been demonstrated experimentally that 30°C, pH 7, and a final concentration of 10 mM Mg^{2+} maximize transformation frequency, and these results as determined by Page and co-workers are summarized in Figure 4.6.[91]

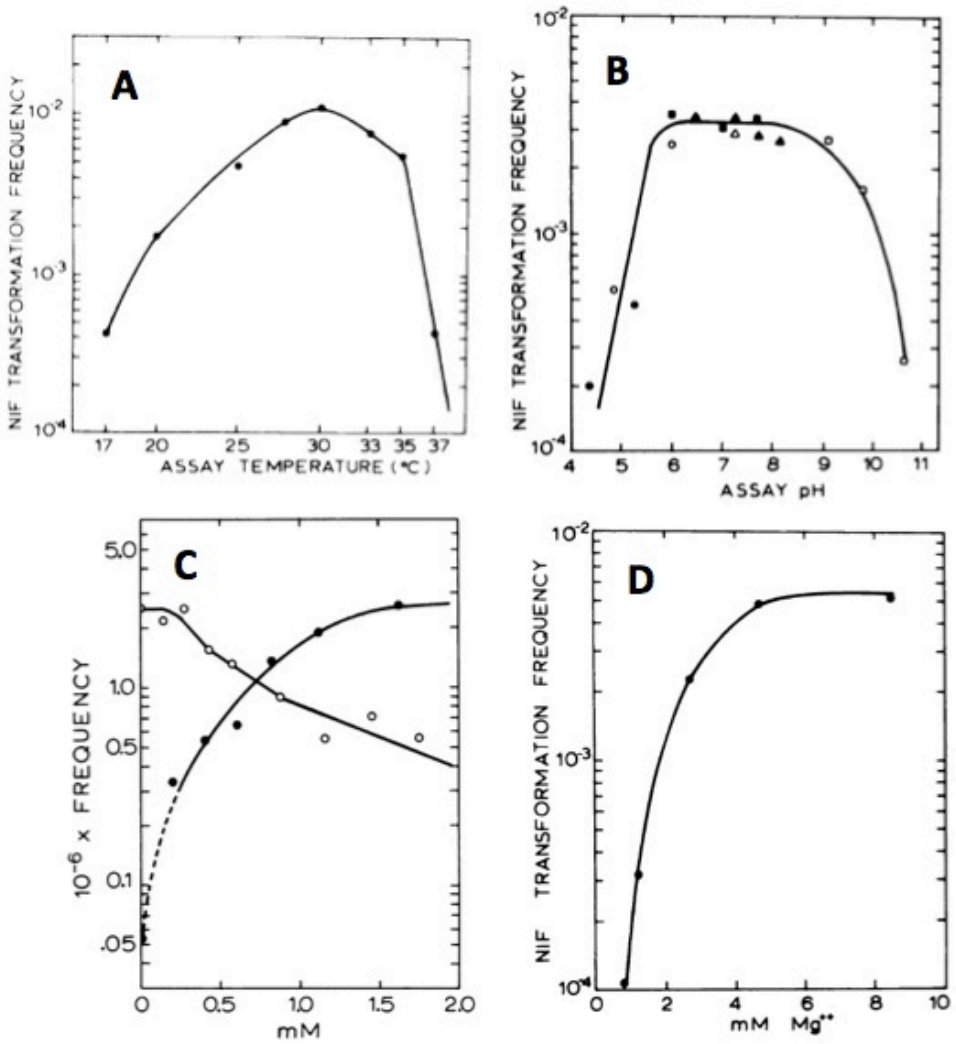

Figure 4.6 Transformation frequency versus **A** temperature, **B** pH, **C** Mg^{2+} (solid) and Ca^{2+} (hollow), and **D** Mg^{2+}, adapted from ref *91.*

4.7 Conclusions

In this work, a thorough review of the literature and assistance from members of the Dean lab were utilized to implement a quick procedure for creating mutations of nitrogenase structural proteins, shortening the time of the procedure from years to weeks. Additionally, the rationale behind each step is explained, to aid future researchers. Since implementing more practical processes for mutagenesis in *A.*

vinelandii, many mutants with altered P-cluster environments have been created, expressed, purified, and undergone initial characterization.

4.8 Future Directions

While the deletion strains obtained from the Dean lab and discussed here are making the process of mutagenesis much quicker for many mutant strains, because the deletion strains to not cover ever single amino acid of Fe and MoFe proteins, there are some protein mutants that are not possible to make without first making additional deletion strains. Future research efforts should be geared toward creating deletion strains covering these regions. These deletion strains should be generated to contain antibiotic resistance in place of the deleted nif region, as this will provide a handle for screening deletion strain success.

4.9 Acknowledgements

This work was made possible by assistance from Valeria Cash and Professor Dennis Dean from Virginia Tech, who kindly provided all-purpose deletion strains and quick, succinct answers to numerous questions over the years.

5 Methods for measuring the specific activities of nitrogenase proteins

5.1 Abstract

The consensus equation for nitrogenase reactivity dictates that, at a minimum, 2 molecules of ATP will be hydrolyzed for each electron transferred to substrate, and a maximum of 75% of those electrons will be used to reduce N_2. Despite the critical importance of these limiting conditions in building a model for nitrogenase reactivity, NH_3, H_2, and ATP hydrolysis by nitrogenase are almost never measured from the same reaction vial. This chapter explains the rationale behind and troubleshooting of methods for measuring many different nitrogenase reaction products, enabling the measurement of H_2 production, NH_3 formation, and ATP hydrolysis by nitrogenase under fully active conditions from a single reaction vial. These methods are also applicable to investigations of other biochemical systems.

5.2 Introduction

5.2.1 Consensus stoichiometry for biological nitrogen fixation

Most research articles discussing nitrogenase begin with a description of nitrogenase reactivity in terms of Equation 3, which is given in Chapter 1. The equation captures decades of research confirming the absolute requirement of ATP for biological nitrogen fixation and the inability of high pressures of N_2 to completely eliminate H_2 evolution during N_2 reduction by purified nitrogenase proteins. The equation, however, skips over the extensive debates as to whether Fe protein is a 1- or 2-e^- donor, which determines whether 1 or 2 ATP molecules must be hydrolyzed for the transfer of one electron to substrate.[92-96] Additionally, this equation masks the

nuance of nitrogenase reactivity for allocating electrons to N_2 versus H^+ reduction. Nitrogenase does not produce exactly 2 NH_3:H_2 under all experimental conditions.

5.2.2 Motivation for the work

Unfortunately, since this equation is generally considered consensus stoichiometry, few researchers bother to validate the equation by measuring the amount of NH_3 produced, H_2 evolved, and ATP hydrolyzed from a single nitrogenase activity assay. Only one publication has reported the specific activities of wild-type nitrogenase from *A. vinelandii* for H_2 evolution, NH_3 formation, and ATP hydrolysis from a single reaction under fully active conditions, which includes DT as the electron source and creatine kinase and phosphocreatine to regenerate ATP and prevent nitrogenase inhibition by ADP.[97] These researchers obtained a specific activity for H_2 formation of 570 nmol min^{-1} mg^{-1} MoFe protein, a specific activity for NH_3 formation of 930 nmol min^{-1} mg^{-1} MoFe protein, and a specific activity for ATP hydrolysis of 3900 nmol min^{-1} mg^{-1} MoFe protein, leading to a NH_3:H_2 of 1.6 and an ATP/$2e^-$ of 5.4. These values, however, were only measured for one MoFe protein concentration (2 μM) and one Fe:MoFe protein molar ratio (40:1).

During the investigation of the surface charge reversal mutant βK400E MoFe protein, it was important to determine whether this mutation had a similar, less pronounced, or more pronounced effect on N_2 reduction as compared to its effect on H^+ and C_2H_2 reduction in the absence of N_2. Since βK400E MoFe protein displayed a minor drop in activity for C_2H_2 → C_2H_4 reduction as compared to wild-type MoFe protein, it was critical to measure not only NH_3, but also H_2 production by βK400E MoFe protein under an N_2 atmosphere to evaluate whether a decrease in NH_3 production was a decrease in total electron flow or a “loss” of electrons to H_2 evolution. Since the effect of βK400→E on reduction of C_2H_2 was more pronounced

at low concentrations of protein and low electron flux (Fe:MoFe molar ratio), it was imperative to evaluate the ability of βK400E MoFe protein to reduce N_2 under these conditions. A thorough literature search revealed no data for wild-type nitrogenase proteins from *A. vinelandii* at such low protein concentrations and low flux, which are needed to compare to results from βK400E MoFe protein.

Here, a strategy was developed to measure H_2, NH_3, and ATP hydrolysis as P_i released from the same nitrogenase reaction vial. The aim was to measure the NH_3:H_2 and ATP/$2e^-$ ratios at low protein (0.4 μM MoFe protein) and low flux (5 – 30 fold molar excess of Fe:MoFe protein) for wild-type nitrogenase from *A. vinelandii*, since this has never been done before, and then to use these results to interpret the effect of βK400→E on the ability of nitrogenase to reduce the biologically relevant substrate N_2. The biggest reason these three products are so rarely measured in tandem is because of the time-consuming and technically challenging nature of each of these measurements. This chapter details 5 years of efforts to improve the reliability and ease of measuring all the reaction products of nitrogenase, including C_2H_4, and also H_2, NH_3, and ATP hydrolysis, in order to routinely measure the NH_3:H_2 and ATP/$2e^-$ ratios of nitrogenase reactivity and assess small changes in these ratios resulting from site-directed mutagenesis.

5.3 Results and Discussion

5.3.1 General GC considerations for C_2H_4 analyses

All H_2 and C_2H_4 production measurements in the proceeding work were carried out on an SRI 8610C GC. Previously in the Tezcan lab, a 5’ x 1/8” activated alumina column was utilized for separation of C_2H_2 from C_2H_4 with He as a carrier gas. An FID was used to detect the hydrocarbons after elution from the column, and experiments were carried out at an oven temperature of 150 °C. This set-up regularly

suffered from delayed C_2H_4 retention times caused by contaminants stuck to the alumina column, most likely H_2O. A gas purifier was purchased to remove all possible H_2O from the He carrier gas before it was passed over the column, but the retention times remained inconsistent, most likely due to the small amounts of H_2O present in the headspace injections from activity assays. For a typical assay measurement, 50 µL of headspace from a 10-mL vial containing 1.5 mL aqueous solution was injected onto the alumina column. Switching to a 6' x 1/8" HayeSep N packed column, available from SRI Instruments (PN 8600-PKDB) has solved all retention time issues. Since the HayeSep N material is slightly less polar than the alumina, less H_2O injected onto the column is retained. Using an oven temperature of 110 °C, the typical retention time for C_2H_4 is 1.9 min, and the typical retention time for C_2H_2 is 2.7 min.

5.3.2 External calibration for GC analyses of C_2H_4

Previously in the Tezcan lab, no external standard was implemented to calibrate C_2H_4 measurements. Instead, C_2H_4 was estimated by first assuming the FID response to C_2H_2 and C_2H_4 were equivalent, and then averaging the C_2H_2 peak areas, assuming that exactly 1.00 mL of 1.00 atm C_2H_2 was always added to every single activity assay vial. While this strategy sufficed when determining whether or not purified proteins were active, it did not yield precise enough measurements to determine whether site-directed nitrogenase mutants had a lowered specific activity for C_2H_2 reduction relative to the wild-type proteins. In this strategy, to create the C_2H_2 stock for activity assays, a 1-L round bottom flask was evacuated, filled with C_2H_2, and then "vented" to atmospheric pressure, which yields a flask that is at about 1 atm, but can vary significantly from researcher to research, and is not 1.00 atm. An external calibration strategy was implemented to address this issue at the outset of the investigation of βK400E MoFe protein. Pure C_2H_4 was purchased from Airgas and

used to fill a pre-weighed, evacuated 250-mL round bottom flask. The weight of the C_2H_4 added to the sealed flask was measured. Then, after making a serial dilution of that gas into smaller vials, various but known amounts of C_2H_4 were injected onto the GC column. Over the past four years, the slope of the standard curve of peak area v. nmol C_2H_4 injected has varied depending on the age and integrity of the column, but in general the sensitivity of a clean column yields a slope of 150 when graphing peak area versus nmol C_2H_4 injected.

5.3.3 External calibration for GC analyses of H_2

The efficiency of electron transfer through the nitrogenase component proteins to products is, according to the T-L model and decades of research, independent of the substrate being reduced. Thus, the maximum specific activity of wild-type MoFe protein for C_2H_2 reduction should be equal to the maximum specific activity of wild-type MoFe protein for H_2 formation, since both are 2-e^- processes. In initial characterization of βK400E MoFe protein and other mutants in the *DG1* region, it was critical to establish this condition for wild-type MoFe protein and evaluate whether this assumption about electron transfer efficiency held true for the mutant proteins.

At first, however, data collected were not precise enough to provide an answer to this question because a proper standardization method for the H_2 activity assay was not in place. In previous experiments, small aliquots of 10%/90% H_2/Ar mixed gas were injected onto the molecular sieve column to estimate the sensitivity of the TCD detector to H_2, but this technique lacked the required precision because the ratio of H_2/Ar varied from tank to tank and even over the lifetime of one tank. Additionally, this type of estimation assumed that an evacuated 1-L round bottom filled with 10%/90% H_2/Ar mixed gas always contained 1.00 atm gas, after the “venting” procedure mentioned above, which is not the case. To address this imprecision, an

external H_2 calibration curve was constructed before each day's experiments using pure H_2 gas rather than the 10%/90% H_2/Ar mixture, and the nmol H_2 injected onto the GC was determined by weight, as was done for C_2H_4, rather than by using a rough estimation of the pressure of a "vented" flask.

A pre-weighed, evacuated 500-mL round bottom flask was filled with pure H_2 gas, and the weight of the H_2 added to the sealed flask was measured. Then, after making a serial dilution of that gas into smaller vials, various but known amounts of H_2 were injected onto the GC column. Over the past four years, the slope of the standard curve of peak area v. nmol H_2 injected has varied from 0.5-1.5, depending on the carrier gas used, but in general the sensitivity yields a slope of about 1.0.

A variety of carrier gases can be used to separate H_2 from other gases over a molecular sieve column, including He, Ar, and N_2. Whereas the slope of the standard curve of pure H_2 gas when N_2 is the carrier gas is about 0.5, changing the carrier gas to Ar increased the slope of the curve of peak area v. nmol H_2 to about 1.5. Using Ar as a carrier gas works for H_2 production assays, when no other substrate was present for nitrogenase to reduce, and Ar was the primary gas present in the headspace.

When the Schlenk line is switched from Ar to N_2 to conduct N_2 reduction assays, though, and measure H_2 and NH_3 formation under an N_2 atmosphere, a small peak is detected by the TCD that overlaps with the H_2 peak and has a slightly faster retention time. Since He and Ne are the only permanent gases that can have a shorter retention time than H_2 on a molecular sieve column, the source of this peak was determined to be the result of slight differences in He or Ne content of the Ar carrier gas and the N_2 Schlenk gas. This peak disappeared and the problem was resolved by reconfiguring the gas tanks leading to the Schlenk lines and GC. The GC and Schlenk line are now set-up such that when Ar is going to the Schenk line, the same Ar tank is also the carrier gas for the molecular sieve column, and when N_2 is

going to the Schlenk line, the same N_2 tank is the carrier gas for the molecular sieve column.

A 10' x 1/8" packed, washed molecular sieve (5A 80/100) column is still used to separate H_2 at an oven temperature of 80 °C and a TCD to detect H_2 after elution. However, the improvements in external calibration and choice of carrier gas have substantially increased the reproducibility of H_2 measurements for activity assays.

5.3.4 ATP hydrolysis assay development

Many assays have been developed to measure enzymatic ATP hydrolysis, and they focus primarily on measuring the amount of ADP formed or P_i released as a result of ATP hydrolysis. In assays that quantify ADP, ADP must be separated from unused ATP with chromatography. HPLC can be coupled to quantification of ADP based on its absorbance of ultra-violet light.[52] Alternatively, radiolabeled ATP can be added to enzymatic assays and, after enzymatic activity is quenched, ATP and ADP can be separated using TLC and ADP quantified by measuring the ratio of radioactivity of the ADP to ATP spots.[98] Unfortunately, since nitrogenase can only be studied under conditions of maximal activity when an ATP-regeneration system is added to the nitrogenase activity assay, and this constantly reforms ATP from ADP and phosphocreatine, ATP hydrolysis by fully active nitrogenase cannot be determined by measuring ADP formed.

Methods to measure ATP hydrolysis as P_i released are in principle compatible with the ATP-regeneration system added to nitrogenase assays and generally employ some variation of a method based on the complexation of P_i with molybdic acid to yield a colored analyte.[99] These methods, however, often measure total phosphate content of the reaction mixture rather than true P_i released from enzymatic ATP hydrolysis, leading to substantial errors in measurements of ATP hydrolysis activities.

The sections that follow detail the development of a method for quantifying ATP hydrolysis that achieves the precision of chromatographic methods for ADP determination and also maintains the simplicity of colorimetric methods for P_i determination. Importantly, this analysis is compatible with all the elements of the standard nitrogenase activity assay, including the ATP-regeneration system, and the method is also applicable to measuring nucleotide hydrolysis by other enzymes, such as GTP hydrolysis by a GTPase.

5.3.5 Measuring ATP hydrolysis by nitrogenase as ADP formed

First, an extensive effort was made to measure ATP hydrolysis by nitrogenase as ADP formed using a procedure commonly-cited in nitrogenase literature.[52] Nitrogenase assays were carried out in which the ATP-regeneration system was omitted. After quenching the reaction with acetic acid, 500-μL aliquots of each reaction headspace were injected onto the GC molecular sieve column to determine the number of electrons transferred to evolve H_2. Subsequently, all reaction vials were opened, and small aliquots were injected onto an RP-HPLC column 35 cm in length. Figure 5.1 shows RP-HPLC traces for seven standard solutions of 0 – 6 nmol ADP in the presence of 1 nmol ATP. The area under these curves plotted versus nmol ADP can be used to obtain a standard curve.

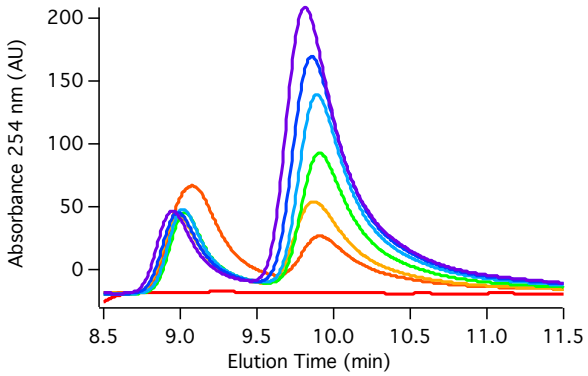

Figure 5.1 RP-HPLC traces of standard solutions containing 1 nmol ATP, which elutes around 9 minutes, and 0 – 6 nmol ADP, which elutes around 10 minutes.

Unfortunately, though the ATP/$2e^-$ ratio was calculated from the collected data, summarized in Table 5.1, it was evident that nitrogenase was substantially less active than it is in the presence of the ATP-regeneration system. Table 5.1 shows the specific activity for H_2 formation and the ATP/$2e^-$ ratio for 4 separate trials of 0.2 μM MoFe protein mixed with a 40-fold excess of Fe protein, which should lead to a maximum specific activity between 2200 – 2500 nmol H_2 min^{-1} mg^{-1}. Furthermore, baseline separation of ATP and ADP was difficult to achieve in a reasonable about of time. Thus, measuring ATP hydrolysis by nitrogenase as P_i released was pursued instead.

Table 5.1 Specific Activities and ATP/$2e^-$ for nitrogenase assays conducted in the absence of the ATP-regeneration system.

	Sp. Ac. H_2	ATP/$2e^-$
1	1520	3.9
2	1420	4.9
3	1630	4.5
4	1420	4.6

5.3.6 Rationale for ATP hydrolysis assay development

The colorimetric determination of phosphate was popularized by Fiske and Subbarow in 1925.[100] They mixed phosphate solutions with molybdic acid and a yellow color formed. Since their pioneering work, many optimizations to this colorimetric detection have been reported. One of the most common modifications is reduction of the yellow phosphomolybdate complex with ascorbate to form a blue color. For the following experiments, the color development procedure of Strickland and Parsons was utilized, which involves molybdic acid, ascorbate, and potassium antimonyl tartrate, which increase color stability and assay sensitivity.[71]

Figure 5.2 A shows that standard solutions of 0-20 μM P_i made in DI H_2O turned blue when mixed with the color reagent containing ammonium molybdate, ascorbate, and potassium antimonyl tartrate in sulfuric acid. Though this procedure works as advertised with P_i standards made in DI H_2O, when P_i standards were instead made up in the nitrogenase activity assay solution, all solutions quickly turned dark blue (Figure 5.2 B). The nitrogenase activity assay contains many compounds with acid-labile, terminal phosphate groups, such as ATP and phosphocreatine, and both of these molecules are present in mM quantities, while the analyte of interest, P_i, is present at a 1000-fold lower concentration. Phosphomolybdate complex formation only occurs in acidic conditions and is typically performed in 0.25 M sulfuric acid. Organic phosphate compounds (OPCs) such as ATP and phosphocreatine undergo rapid acid-catalyzed hydrolysis under these conditions, releasing mM quantities of free phosphate. Thus, while only 0 – 20 μM P_i was added to each standard solution, when the color reagent is added to the nitrogenase assay matrix, the effective phosphate concentration skyrockets to mM quantities, and the solutions turn dark blue.

In order to use a colorimetric P_i method for quantifying ATP hydrolysis by nitrogenase, and be able to study fully active nitrogenase in the presence of the ATP-regeneration system, the true P_i released from enzymatic hydrolysis must be separated from the OPCs prior to addition of the acidic color reagent. Inspiration for achieving this separation came from additional work of Fiske and Subbarow, who popularized the colorimetric determination of P_i as a phosphomolybdate complex. In 1929, just a few years after their paper detailing how to measure phosphate, they published the first isolation and characterization of phosphocreatine.[101] Scientists had hypothesized the existence of such a molecule, but because it was so susceptible to hydrolysis, forming P_i and creatine, the existence of phosphocreatine had not been confirmed. One of the steps in Fiske and Subbarow's isolation of phosphocreatine involved the addition of Ca^{2+} salts to precipitate the P_i in the solution while leaving the phosphocreatine behind. A few quick tests in the laboratory confirmed that the addition of excess $CaCl_2$ to a solution containing P_i and phosphocreatine selectively precipitated the P_i and left the phosphocreatine behind in solution. Whereas Fiske and Subbarow capitalized on the low solubility of $Ca^{2+}P_i$ to get rid of P_i, in this experiment, the low solubility of $Ca^{2+}P_i$ was used to get rid of the phosphocreatine and other OPCs. Indeed, addition of excess $CaCl_2$ to a solution containing P_i in the presence of both phosphocreatine and ATP led to the formation of small white pellets upon centrifugation (Figure 5.2 C). After removing the supernatant, the white precipitate was resuspended in weak acid (~0.2 M HCl), and the color development of these P_i standards (Figure 5.2 D) matched that of the P_i standards made in DI H_2O (Figure 5.2 A).

Since the $Ca^{2+}P_i$ pellets are soft and easily broken, fine-tuning of this procedure led to a series of centrifugation steps. If the entire supernatant shown in Figure 5.2 C was removed via pipet, the white pellet was frequently disturbed, and

this would lead to irreproducible results. Reproducible results were obtained when 90-95% of the supernatant fraction was removed, replaced with water, and the centrifugation step repeated. This sequence of events was repeated four times to remove enough of the nitrogenase assay matrix that P_i could be measured without interference from OPCs.

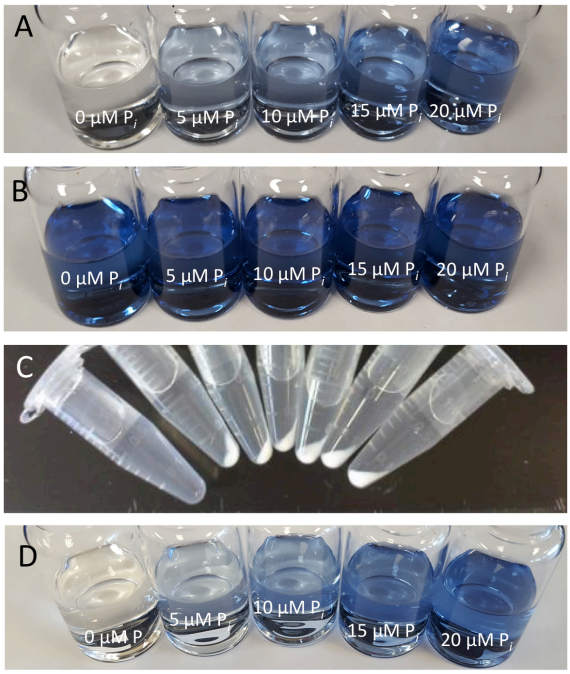

Figure 5.2 Blue phosphomolybdate complex formation of P_i standard solutions in **A** DI H_2O and **B** a mock nitrogenase activity assay solution. **C** Solutions containing P_i after addition of excess $CaCl_2$ and centrifugation. **D** Blue phosphomolybdate complex formation after implementation of new procedures.

Next, the rate of phosphomolybdate complex formation was measured. The absorbance of a P_i standard solution, when made up in a complex matrix containing an excess of OPCs, continues to increase with time due to continuous release of labile P_i from OPCs, as shown in Figure 5.3 A. In contrast, when true P_i is separated from OPCs by precipitation with Ca^{2+} prior to addition of the acidic color reagent, the blue color stabilizes after about 1 hours, since no OPCs remain in solution to release additional P_i. Standard curves of P_i diluted to a final concentration of 0 – 20 µM P_i

made in DI H_2O and those made in the nitrogenase activity assay matrix, which includes a large excess of OPCs, are within one standard deviation of one another (Figure 5.3 B). These experiments firmly establish that the Ca^{2+} precipitation procedure is effective at separating labile OPCs from true P_i. Furthermore, quantitative recovery of P_i is achieved by this procedure, since there is no change in the absorbance of P_i standards made in DI H_2O whether or not the Ca^{2+} precipitation step is used. P_i was quantitatively recovered whenever the white precipitate was visible.

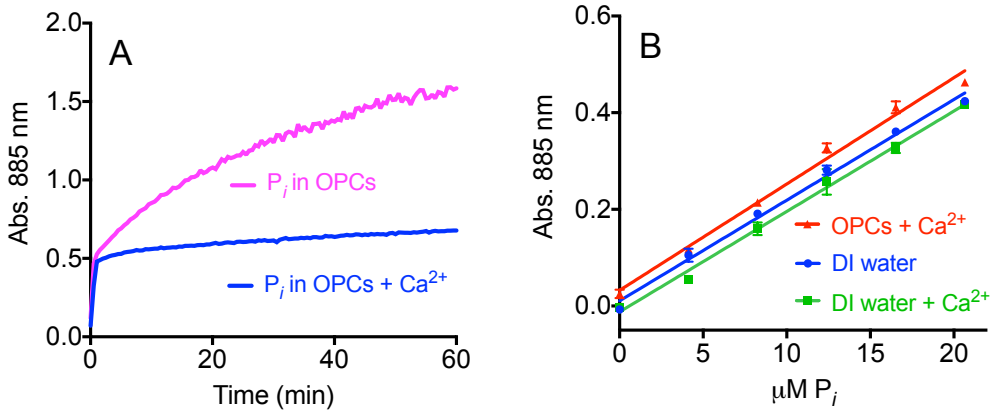

Figure 5.3 **A** Phosphomolybdate complex formation over time and **B** P_i standards in DI H_2O (blue), DI H_2O and treated with the Ca^{2+} precipitation step (green), and in the nitrogenase activity assay matrix that has been treated with the Ca^{2+} precipitation step (red).

The first iteration of this method only worked when at least 1.0 mM P_i was present. If less than 1.0 mM P_i was present, a precipitate would form when $CaCl_2$ was added, but the pellet was so small it was invisible to the naked eye. Thus, the four centrifugation, removal, and water addition steps could not be performed without inadvertently disturbing the pellet and removing some P_i along with the supernatant. To lower the minimum amount of P_i required for visible $Ca^{2+}P_i$ pellets, K_2CO_3 was added to precipitate $CaCO_3$ in addition to $Ca^{2+}P_i$ and thereby increase the size of the

white pellet. Using this technique, as little as 100 μM P_i was routinely pelleted and quantitatively recovered.

Prior to mixing P_i solutions with the color reagent, a dilute HCl solution is added to resuspend the Ca/P_i pellet. When K_2CO_3 is present in the samples, though, addition of this HCl alters the final pH of the sample relative to samples that do not contain K_2CO_3 because CO_2 is produced. Because the formation of the phosphomolybdate complex is pH dependent, samples containing K_2CO_3 did not turn as dark blue as samples that did not contain K_2CO_3. Figure 5.4 shows that the color development still increases linearly with P_i concentration in the presence of K_2CO_3, but the method becomes slightly less sensitive to P_i, so the P_i concentration of samples analyzed with the K_2CO_3 step must be calculated from a standard curve of solutions also treated with K_2CO_3.

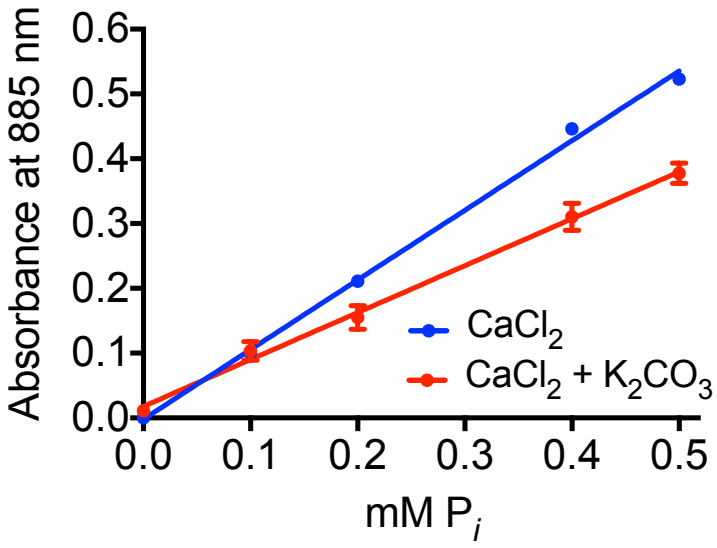

Figure 5.4 Absorbance of the phosphomolybdate complex versus P_i concentration for standard solutions in which P_i was precipitated with $CaCl_2$ alone (blue) or $CaCl_2$ and K_2CO_3 (red).

5.3.7 Measuring elevated ATP/2e⁻ ratio in the presence of cyanide

To assess the ability of the method to quantify ATP hydrolysis during nitrogenase turnover, the ATP/2e⁻ ratio for wild-type nitrogenase under standard assay conditions was measured and compared to previously published results. Experimentally, ratios of 4-5 are typically measured, but with %RSDs that are often not reported or exceed the mean.[50,96,102,103] First, nitrogenase activity assays were quenched with 5 M NaCl rather than concentrated acid, base, chelator, or detergent. The number of electrons productively transferred to C_2H_2 to produce C_2H_4 by wild-type nitrogenase was quantified using GC. Then, $CaCl_2$ was added to the assay solutions to capture released P_i in a white precipitate. Assay solutions were subjected to centrifugation, the supernatant fraction removed, the white pellet resuspended, and an aliquot of each activity assay solution was added to the acidic color reagent. After measuring the absorbance of these solutions at 885 nm, this method yielded an ATP/2e⁻ value of 4.8 ± 0.3 with a RSD of 5.3% (Table 5.2). Thus, the method is able to reproduce the accepted ATP/2e⁻ literature value in the presence of the regeneration system, which contains a large excess of OPCs, with a substantial increase in precision.

As a further validation, the ATP/2e⁻ ratio for wild-type nitrogenase was also measured under a condition known to cause uncoupling of ATP hydrolysis from electron transfer. CN^- is known to inhibit nitrogenase activity by uncoupling the hydrolysis of ATP from productive ET to substrate. The ATP/2e⁻ increases with increasing [CN^-] and plateaus at about 18 when [CN^-] ≥ 80 μM.[104] The ATP/2e⁻ for wild-type nitrogenase proteins was measured in the presence of 5 mM NaCN at pH 8.0, so the effective [CN^-] would be much larger than 80 μM. Though CN^- is a reversible inhibitor of nitrogenase activity, HCN is a substrate of nitrogenase. Thus, in order to measure the number of electrons transferred to product, both the C_2H_4

formed from 2-e^- reduction of C_2H_2 and the CH_4 formed from 6-e^- reduction of HCN to CH_4 and NH_3 were measured. As expected, the ratio of ATP/2e^- under these conditions, 16 ± 1.1, as measured by the NaCl/Ca^{2+}/P_i assay, lies within the range of previously reported values (Table 5.2).

Table 5.2 ATP/2e^- values for nitrogenase under standard assay conditions and in the presence of 5 mM NaCN at pH 8.0.

	ATP/2e^- (in literature)	ATP/2e^- (this work)
Wild-type nitrogenase, standard conditions	4-5 (%RSDs >100% reported)	4.8 ± 0.3 (5.3% RSD)
Wild-type nitrogenase with 5 mM NaCN at pH 8.0	17-18 (%RSDs not reported)	16 ± 1.1 (6.7% RSD)

5.3.8 Measuring GTP hydrolysis by EF-G

As an independent validation of the NaCl/Ca^{2+}/P_i assay, ribosome-dependent GTP hydrolysis by EF-G was evaluated using the method. EF-G is a ribosome factor that participates in protein synthesis. Translocation of mRNA and tRNA along the ribosome is coupled to the binding and hydrolysis of GTP by EF-G.[105] In order to interrogate how the hydrolysis of GTP is coupled to the efficient synthesis of proteins, it is crucial to precisely measure GTP hydrolysis by wild-type EF-G and site-directed mutants. An established method for measuring GTP hydrolysis by EF-G requires the use of radiolabeled GTP.[106] Each activity assay is initially spiked with ^{32}P-γ-GTP. After the enzyme activity is quenched, ^{32}P-γ-GTP and $^{32}P_i$ are separated by TLC and the ratio of radioactivity counts is used to extrapolate the extent of hydrolysis. While this assay offers a substantially higher sensitivity than colorimetric measurements, radiolabeled nucleotides are expensive, hazardous, and have a short shelf life.

To establish that the NaCl/Ca^{2+}/P_i assay was also applicable to GTPase activity measurements, steady-state Michaelis-Menten parameters for ribosome-

dependent GTP hydrolysis by EF-G were determined using two techniques. First, GTP hydrolysis was evaluated using the established ^{32}P-γ-GTP method, and the k_{cat} for ribosome-dependent GTP hydrolysis was shown to be 5.0 ± 0.3 s^{-1} and the K_m to be 8.7 ± 0.8 μM (Table 5.3). Subsequently, 70S ribosome-dependent GTP hydrolysis by EF-G was measured under the same reaction conditions using the NaCl/Ca^{2+}/P_i colorimetric method. Like nitrogenase assays, these EF-G activity assays were quenched with 5 M NaCl rather than acid or detergent. Using this method, the k_{cat} for ribosome-dependent GTP hydrolysis was 3.1 ± 0.7 s^{-1} and the K_m was 9.4 ± 3.5 μM. It is important to note that though these k_{cat} values lie within two standard deviations of one another, both fall well within the range of previously reported k_{cat} values for ribosome-dependent GTP hydrolysis by EF-G.[106-108]

Additionally, while the K_m values determined by these techniques are slightly higher than what has been reported previously, which can be explained by the inherent preparation-to-preparation variance in ribosome purity among laboratories,[107,109] they are within one standard deviation of one another. Figure 5.5 shows the Michaelis-Menten curves obtained in this work. Because the standard ^{32}P-γ-GTP assay and the new NaCl/Ca^{2+}/P_i method yielded overall similar steady-state kinetic parameters, while achieving a decrease in cost, hazard, and time, this new method is well suited to assess changes in the GTP hydrolysis activity of EF-G, for example, due to mutagenesis.

Table 5.3 Steady-state Michaelis-Menten kinetic parameters for 70S ribosome-dependent GTP hydrolysis by EF-G.

	K_m (μM)	k_{cat} (s^{-1})
^{32}P-γ-GTP method (this work)	8.7 ± 0.8	5.0 ± 0.3
Ca^{2+}/P_i method (this work)	9.4 ± 3.5	3.1 ± 0.7

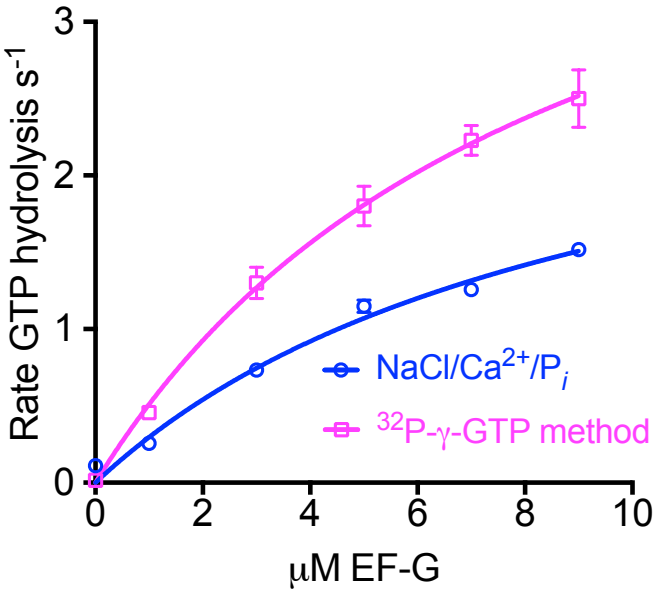

Figure 5.5 Michaelis-Menten curves for 70S ribosome-dependent GTP hydrolysis ribosome factor EF-G.

5.3.9 Colorimetric NH_3 detection with modified indophenol assay

Since previous members in the Tezcan lab encountered many difficulties implementing fluorescence-based detections methods for NH_3 produced by nitrogenase, in this work the indophenol assay was initially explored as a way to measure differences in nitrogen fixation rates between wild-type and βK400E MoFe proteins. The indophenol reaction is a well-documented colorimetric method for the quantification of NH_3, in which NH_3 is reacted with phenol and bleach in the presence of catalyst to accelerate the rate of indophenol formation.

Indeed, when solutions containing increasing concentrations of NH_3 are mixed with bleach, phenol, and a sodium nitroprusside catalyst, and let to react in the dark for 1 hour, solutions containing NH_3 develop a turquoise-green color, as seen in Figure 5.6, and these solutions have a maximum absorption at 640 nm. When NH_3

standard solutions are made up in DI H_2O, the indophenol method yields a linear response in absorbance with increasing NH_3 from about 10 – 100 μM NH_3, as evidence by the representative standard curve shown in Figure 5.7.

Figure 5.6 Aqueous solutions containing 0 – 80 μM NH_3 after addition of indophenol color reagents and 1 hour of color development.

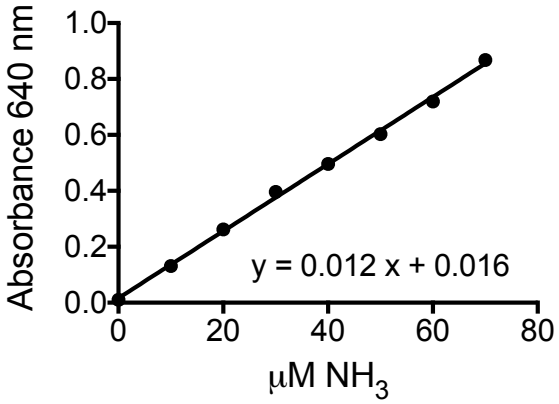

Figure 5.7 Absorbance at 640 nm versus NH_3 concentration for NH_3 standard solutions made up in DI H_2O when no interfering substances are present.

Before the indophenol method was used to measure NH_3 formed by nitrogenase, the effects of each component of the nitrogenase activity assay solution on A_{640} were assessed. First, it was established that DT inhibits color development, but inhibition is relieved if solutions are aerated prior to mixing with the color reagents. Figure 5.8 shows indophenol reactions in 1.7 mL Eppendorf tubes to compare the color formation of solutions containing 50 μM NH_3 with and without DT

and with short and long periods of aeration. Figure 5.8 shows, from left to right, NH_3 in DI H_2O, NH_3 in a solution containing 10 mM DT with 10 minutes aeration prior to color reaction, NH_3 in H_2O, and NH_3 in a solution containing 10 mM DT with 40 minutes of aeration prior to color reaction.

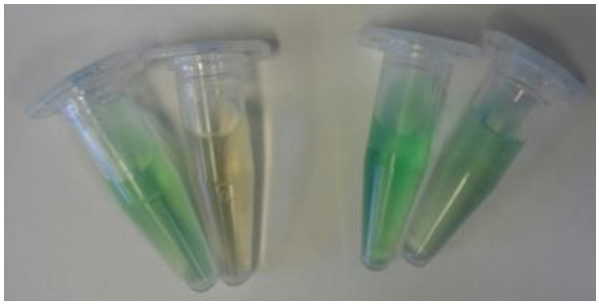

Figure 5.8 Solutions of 50 μM NH_3 after 1-hr color development. Preparation of NH_3 solutions from left to right: NH_3 in DI H_2O, NH_3 in a solution containing DT with 10 minutes aeration prior to color reaction, NH_3 in H_2O, NH_3 in a solution containing DT with 40 minutes aeration prior to color reaction.

Next, the effect of Hepes buffer on color development was evaluated. Standard procedures for nitrogenase activity assays in the Tezcan lab utilize either Tris or Hepes as a buffering agent. Since Tris contains a primary amine functionality, Hepes was chosen as the buffering agent in these experiments. Unfortunately, it is evident from the solutions in Figure 5.9 that the presence of even 1 mM Hepes significantly effects color development, preventing quantification of NH_3. Because many other components of the activity assay matrix, including creatine, phosphocreatine, and nucleotides, all had similar effects on color development as those depicted in Figure 5.9, the chromatography modification first reported by Eady et al. was implemented.[66] Following this procedure, each NH_3 standard solution and each reaction sample were individually passed over the pipet columns shown in Figure 5.10. Each NH_3 standard solution was made up in a mock activity assay solution containing 50 mM Hepes, buffered to pH 8.0, 1.0 M NaCl, to mimic the high-

salt quench of activity, 10 mM creatine, to mimic the creatine formed from regeneration of ATP during the assay, 10 mM phosphocreatine, and an excess of creatine kinase, to mimic the amount of polypeptides present from not just creatine kinase but also Fe and MoFe proteins. An aliquot of each flow-through was then mixed with bleach, phenol, and nitroprusside and let to react for 1 hour in the dark.

Figure 5.9 Solutions of 50 uM NH_3 after 1-hr color development. Preparation of NH_3 solutions from left to right: NH_3 in 20 mM Hepes, 10 mM Hepes, 5 mM Hepes, 2.5 mM Hepes, 1 mM Hepes.

Figure 5.10 Pipet columns containing Dowex anion exchange resin used to separate NH_3 from interfering substances in the nitrogenase activity assay matrix prior to reacting with indophenol reagents.

Even with the chromatography modification, the A_{640} of standard solutions prepared in this manner was much high than the A_{640} of standard solutions prepared

in DI H_2O. Only when creatine was omitted did the A_{640} of standard solutions made in the mock assay solution that had been separated using chromatography begin to resemble the A_{640} of standard solutions made in DI H_2O. When all components of the ATP regeneration system were omitted from the mock activity assay solution, the color development of NH_3 standard solutions was linear with increasing NH_3 concentration, as shown in the Eppendorf tubes in Figure 5.11 and the standard curve in Figure 5.12. In summary, the indophenol method can be used to measure the amount of NH_3 formed in nitrogenase activity assays when the ATP regeneration system is absent, either for photoreduction assays or when it is not necessary to study fully-active nitrogenase proteins. However, the indophenol method is not sufficient to quantify NH_3 produced by fully active nitrogenase in ATP- and Fe protein-dependent catalysis.

Figure 5.11 Aqueous solutions containing 0 – 80 μM NH_3 after elution from the Dowex pipet columns, addition of indophenol color reagents, and 1-hr color development.

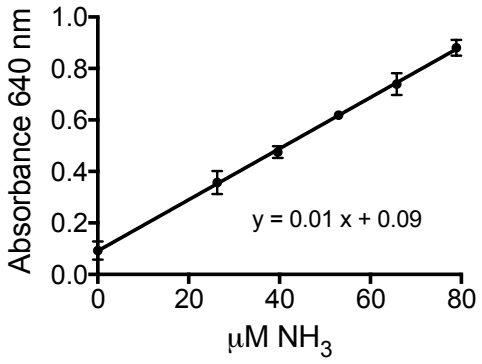

Figure 5.12 Absorbance at 640 nm versus NH_3 concentration for NH_3 standard solutions made up in mock nitrogenase activity assays and then individually passed over pipet columns prior to reaction with indophenol reagents.

5.3.10 Fluorometric NH_3 detection with modified OPA assay

When it became evident that the indophenol method, though appropriate for monitoring NH_3 production by nitrogenase in the absence of creatine, was not appropriate for use with the ATP regeneration system, fluorescence detection of NH_3 produced by nitrogenase was explored. Previously, it was reported that NH_3, when mixed with BME and OPA, forms a fluorescent complex with a maximum fluorescence emission at 470 nm when excited at 410 nm.[110] A quick, 2-min OPA-HPLC assay was reported in which aliquots of quenched nitrogenase activity assays were mixed with the OPA/BME reagent, passed over a reverse-phase C_{18} column, and the amount of NH_3 present determined from the fluorescence intensity at 470 nm.[69]

No liquid chromatography systems in the Tezcan lab were set up for fluorescence detection, but a Shimadzu fluorescence detector was available that was compatible with a Bio-Rad FPLC workstation. The fluorescence detector was connected to an FPLC, and initial tests of the fluorescence quantification of NH_3 were conducted using a small reverse-phase column hooked up to an FPLC.

First, the stability of the reagent mixture was evaluated, and it was determined that BMA and OPA must be mixed immediately before addition of a solution containing NH_3. If OPA and BME were left together overnight, even at 4°C and in the dark, the fluorescence of NH_3 standard solutions was significantly decreased. Figure 5.13 shows the fluorescence intensity at 470 nm of samples upon excitation at 410 nm versus the elution time. The dashed line is the elution profile of an aliquot of an NH_3 standard solution when mixed with day-old OPA/BME reagent, which contained 10 mM P_i, buffered to pH 6.8, 10 mM BME, and 5 mM OPA, compared to the elution profile of the same concentration of NH_3 when mixed with freshly-prepared OPA/BME reagent, which is shown as a solid line. Typical FPLC experiments were carried out with a flow rate of 3 mL/min using 50/50 v/v mixture of 10 mM P_i, pH 6.8/acetonitrile as the mobile phase. Using fresh reagent, a standard curve of fluorescence versus [NH_3] could be constructed from the FPLC data shown in Figure 5.14. Figure 5.14 shows the absorbance at 410 nm and fluorescence emission at 470 nm of standard solutions of 0 – 400 μM NH_3.

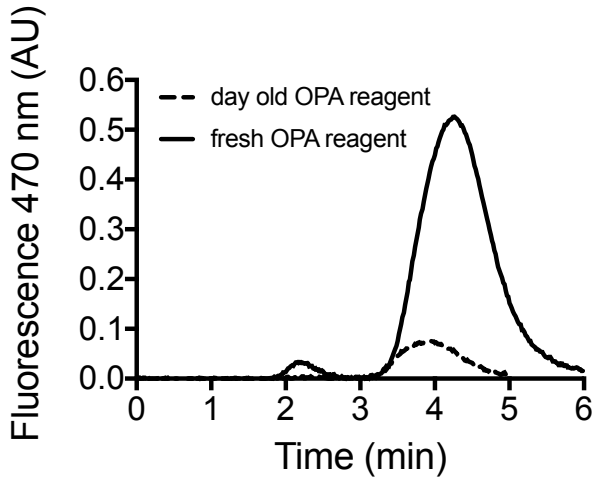

Figure 5.13 FPLC trace of fluorescence versus time for NH_3 standard solutions reacted with old and fresh OPA reagent.

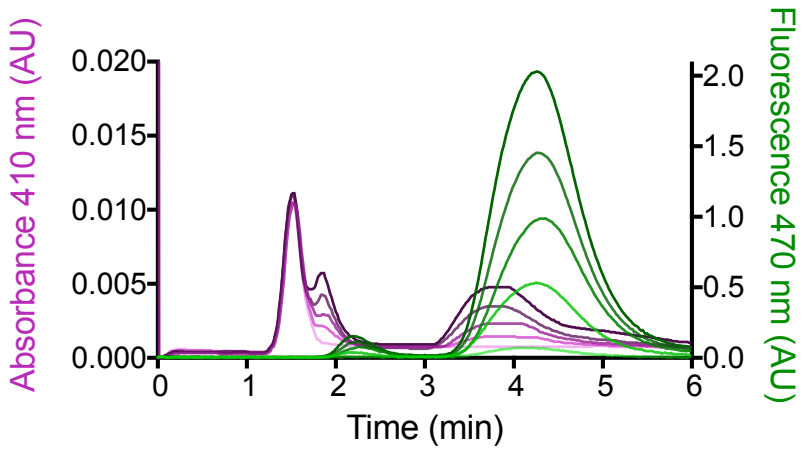

Figure 5.14 FPLC trace of absorbance and fluorescence versus time for NH_3 standard solutions reacted with fresh OPA reagent.

Since creatine caused such a significant interference in the color development of the indophenol assay, it was imperative to characterize the effect of creatine on the fluorescence detection of NH_3 with BME and OPA. Typical activity assays might contain 50 – 500 μM NH_3 and 5 – 10 mM creatine, which is not an initial component of the ATP regeneration system but rather a product, formed by creatine kinase in the regeneration of ATP from ADP and phosphocreatine. Thus, as an initial experiment, the peak area of fluorescence intensity at 470 nm resulting from a standard solution of 200 μM NH_3 was compared to an identical solution, which differed only in the addition of 8 mM creatine. Figure 5.17 shows that the addition of creatine causes a broadening of the peak at 4 minutes and an increase in the total peak area.

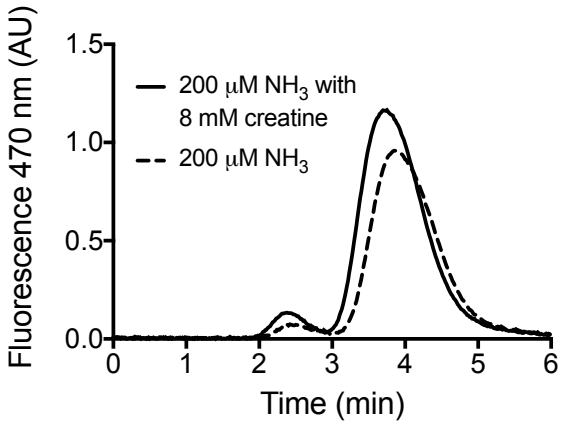

Figure 5.15 FPLC trace of fluorescence versus time for NH_3 standard solutions with and without added creatine and reacted with fresh OPA reagent.

Interestingly, when the OPA-HPLC method was first reported for nitrogenase, the method was checked for compatibility with creatine kinase, phosphocreatine, DT, and nucleotides, but creatine was never explored as a potential interfering substance.[69] Nevertheless, it is clear from Figure 5.15 that the amount of creatine generated over the course of a nitrogenase activity assay is enough to interfere with the fluorescence quantification of NH_3. Since every nitrogenase activity assay can contain a unique proportion of creatine:NH_3, depending on the concentration of Fe protein, DT, reaction temperature, and reaction time, a single standard curve would not be sufficient to determine the amount of NH_3 in all of a day's activity assays. Instead, a unique set of standards would need to be created for every single reaction sample, and this is simply not feasible. However, by running a slow gradient of increasing acetonitrile, rather than an isocratic run of 50/50 v/v 10 mM P_i, pH 6.8/acetonitrile as the mobile phase, the fluorescence associated with NH_3 can be separated from the fluorescence associated with creatine. Unfortunately, as shown in Figure 5.16, this separation takes 40 minutes to achieve, even at a flow rate of 3

mL/min. Since a normal day's experiment would require a minimum of 20 runs, performing an acetonitrile gradient is not a realistic solution to the creatine problem.

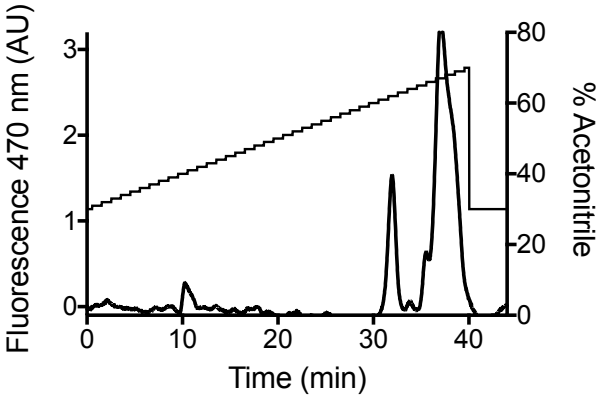

Figure 5.16 FPLC trace of percent acetonitrile in the mobile phase and fluorescence versus time for and NH_3 standard solution containing 200 μM NH_3 and 8 mM creatine.

Rather than separate the creatine-associated fluorescence from the NH_3-associated fluorescence using chromatography, the creatine-associated fluorescence was eliminated by modifying the OPA reagent. Replacement of BME with sulfite has been shown to increase the selectivity of this OPA method for NH_3.[70] When this modified OPA reagent is used, which contains 50 mM P_i, buffered to pH 11, 3 mM sulfite, and 10 mM OPA, the fluorescence intensity of NH_3 standard solutions at 422 nm when excited at 365 nm is unaffected by large excesses of creatine. Figure 5.17 shows how the fluorescence intensity of H_2O is within one standard deviation of the fluorescence intensity of an aqueous solution containing 100 μM creatine. Additionally, the fluorescence intensity of a solution of 2 μM NH_3 is within one standard deviation of the fluorescence intensity of a solution of 2 μM NH_3 and 100 μM creatine. Further tests were conducted to evaluate the effect of each component in the activity assay matrix on the fluorescence intensity at 422 nm. The only other component that caused interference was protein, which can be easily removed by

filtration. When this modified OPA reagent is used, which contains sulfite rather that BME, and protein is removed by filtration prior to mixing with the OPA reagent, the standard curve of NH_3 solutions made in H_2O is indistinguishable from the standard curve of NH_3 solutions made in a mock nitrogenase activity assay matrix (Figure 5.18). This modified OPA method for fluorimetric determination of NH3 is not only selective for NH_3 in the presence of creatine, it is also substantially faster than all prior methods for measuring NH_3 produced by fully active nitrogenase, since it avoids the chromatographic step entirely.

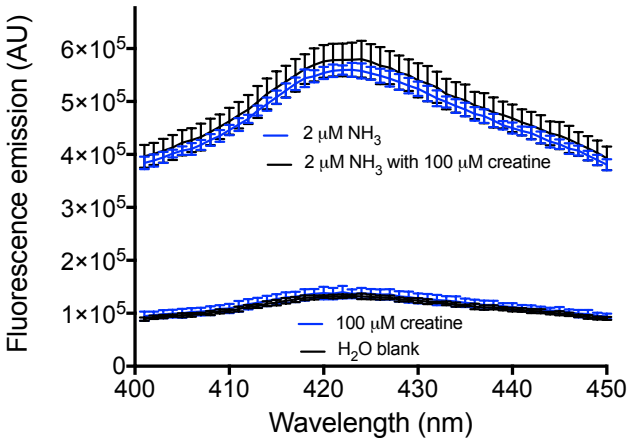

Figure 5.17 Fluorescence intensity of samples excited with 365 nm light.

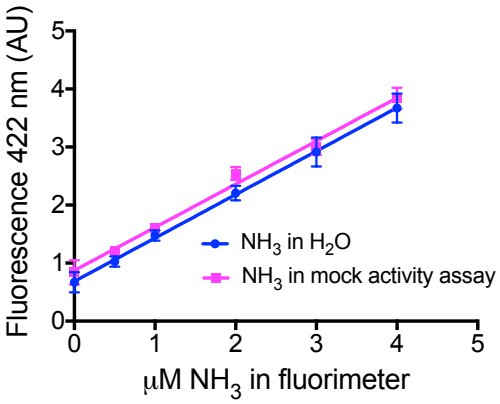

Figure 5.18 Fluorescence intensity versus NH_3 concentration of standard solutions made up in either H_2O (blue) or a mock activity assay solution (pink).

5.3.11 Protein purity and integrity of metal clusters for Fe protein and MoFe protein

Though the concentration of many proteins can be measured to 2-3 significant figures by measuring the absorbance at 280 nm and using Beer's Law to calculate the concentration, given a known ε_{280}., this is not a viable option for determining the concentration of nitrogenase component proteins, Fe protein and MoFe protein, because both contain Fe:S clusters which absorb strongly in that region. Additionally, solutions of pure component proteins always contain 5 mM DT, which also absorbs in this region, to protect the proteins from degredation by O_2.

The most information can be gained about the purity, activity, and integrity of the nitrogenase component proteins by assessing their concentration by a variety of techniques, including the Bradford assay, Fe-chelation assay, and ICP-MS. Step-by-step procedures for these techniques are provided in the Appendix. A Bradford assay measures the total protein concentration in the solution, while Fe-chelation measures the total Fe content of the solution, which gauges the amount of active protein in solution, and ICP-MS provides the Fe:Mo molar ratio to verify that metal cofactors are intact.

Typically, the Bradford assay and the Fe-chelation assay should agree within two standard deviations for pure Fe protein solutions. Since MoFe protein has 30 Fe atoms per heterotetramer, while Fe protein has only 4 Fe atoms per homodimer, even small amounts of MoFe protein impurity present in the Fe protein solution will cause an erroneously large number from the Fe-chelation assay as compared to the Bradford assay.

For pure MoFe protein solutions, the Bradford assay and the Fe-chelation assay should agree within one standard deviation. If this does not occur, it is possible the MoFe protein does not have full incorporation of its metal clusters. Occasionally, MoFe protein mutants will have lowered metal incorporation, most likely due to a

perturbation near the site of cluster insertion. If the Bradford and Fe-chelation assay numbers do not match well, ICP-MS analysis can be performed to determine the Fe:Mo ratio in the protein. The theoretical Fe:Mo ratio for wild-type MoFe protein is 15:1, since one heterotetramer contains two 8Fe:7S P-cllusters and two 7Fe:9S:1Mo:1C FeMo-cofactors. An Fe:Mo ratio substantially above 15:1 can indicate incomplete FeMoco incorporation, while a Fe:Mo ration substantially below 15:1 can indicate incomplete P-cluster incorporation.

5.3.12 Optimizations to photoreduction assays

Nitrogenase photoreduction experiments conducted in the Tezcan lab prior to 2013 utilized a 400-W Xe arc lamp placed in a housing (Oriel arc lamp housing 66023) paired with a power supply (Oriel universal power supply 68920). Because the Xe arc lamp in this housing emits ozone, all photoreduction experiments were carried out in a fume hood. Before the experiments described in Chapter 3 were undertaken, however, the Tezcan lab moved to a new lab space, and there was no longer sufficient fume hood space that could be dedicated to the arc lamp housing and power supply. It was determined that the most cost-effective solution was to purchase an ozone-free Xe arc lamp compatible with the housing and power supply. The only ozone-free Xe arc lamp compatible with the Oriel lamp housing and power supply was a 1000-W lamp. After purchase an installation of the 1000-W lamp, it was discovered that, though the power supply could ignite the old 400-W lamp, it was no longer powerful enough to repeatedly ignite the 1000-W lamp. Since the Oriel components were so old, replacement parts were not available, either from the manufacturer or eBay.

The cost of a new Oriel lamp housing and power supply compatible with the 1000-W ozone-free Xe arm lamp was in excess of $10,000, so a new Xe arc lamp,

housing, and power supply unit was purchased from Abet Technologies for a much lower price. This piece of equipment can only hold up to a 150-W lamp, but this setup is still able to deliver just as many if not more photons to the nitrogenase photoreduction sample. Though the 150-W lamp is less powerful than the 1000-W lamp, in the new setup it can be focused much more than either the 1000-W or 400-W lamps in the old housing. Ru-MoFe protein photoreduction assays are conducted in small, cylindrical 10 – 27 mL glass vials with radii of < 1 cm and heights of < 10 cm. In the old housing, lamps could not be focused to the point that all of the lamp output hit the sample, while it is possible to accomplish this with the 150-W lamp in the new housing.

Similar to the experiments conducted by previous members of the Tezcan lab, photoreduction experiments described in Chapter 3 were placed in small water baths to help maintain a constant temperature over the course of the reaction, despite being in close proximity to a hot lamp. Both the water bath and reaction sample contained stir bars and were stirred slowly during the experiment. In every experiment, the initial and final temperature of the water bath was monitored, and the temperature was never raised above 30°C, so there was no heat-inactivation of Ru-MoFe protein.

Additional changes to the photoreduction system were concerned with the solution conditions for photoreduction, including buffer choice, reaction pH, concentration and identity of reductant, and concentration of Ru-MoFe protein. The primary goals were to maintain maximal photoreduction activity of Ru-MoFe protein while minimizing the amount of protein used in each experiment and achieving product formation rates in the linear range of the detection methods. As mentioned briefly in Chapter 3, the original method described for preparing photoreduction reaction solutions yielded an extremely acidic solution, in which Ru-MoFe protein was not active for the reduction of C_2H_2 or H^+. An alternative buffer system was used and

the concentration of DT substantially reduced, in order to create solutions with a neutral pH in which Ru-MoFe protein would be active.

When the first photoreduction experiments were carried out, the catalytic ability of Ru-MoFe protein seemed to decrease over the course of the day's reactions. Typically, gas tight Hamilton syringes, which are used to perform anaerobic transfer of Ru-MoFe protein stock solutions to photoreduction reaction vials, were made anaerobic by inserting syringes into the rubber septum sealing a side-arm Erlenmeyer flask, which was attached to a Schlenk line apparatus. The flask was evacuated for four minutes and then filled with Ar, and this process was repeated four times. When syringes handled in this manner were used to aliquot Ru-MoFe protein more than a few minutes after the degassing procedure, Ru-MoFe protein specific activity dropped.

In contract, when the degassing procedure was repeated and syringes used immediately, the specific activity of the same Ru-MoFe protein stock increased. Figure 5.19 shows the specific activity for photoreduction of C_2H_2 versus time for four identical photoreduction trials that differ only in the order in which they were initiated. The results highlight how the activity of Ru-MoFe protein decreased in trials 2 and 3 as compared to the first trial (trial 1), but that, when syringes were degassed again immediately before use in trial 4, the protein's activity returned to the rate observed at the beginning of the day in trial 1. In the end, a procedure was implemented in which degassed Hamilton syringes were left under vacuum after the degassing procedure rather than left in an Ar atmosphere, and the Erlenmeyer flask was only filled with Ar immediately before the syringes were used.

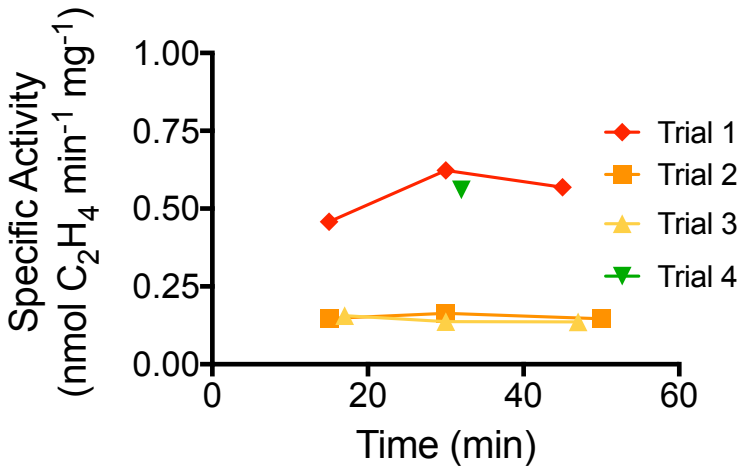

Figure 5.19 Photoreduction activity depends on how gas tight Hamilton syringes are made anaerobic.

During the course of optimization, it was also discovered that a higher concentration of DT did not always result in a higher specific activity for photoreduction by Ru-MoFe protein. Figure 5.20 shows the specific activity versus time for photoreduction reactions that differ only in the concentration of the electron source, DT. As mentioned in Chapter 3, solid DT acidifies aqueous solutions when dissolved, so the concentration of DT can dramatically alter the final pH of a reaction solution. It is likely that previous experiments determined 200 mM DT to facilitate maximum photoreduction activity because the addition of 200 mM DT helped to achieve the optimal reaction pH. When the reaction pH is lowered by use of a more appropriate buffer system, such as P_i or Tris, rather than Hepes, increasing the concentration of DT does not have the same positive impact on activity. In the work discussed in this dissertation, the maximum specific activity of Ru-MoFe protein for the production of C_2H_4 was achieved with just 50 mM DT.

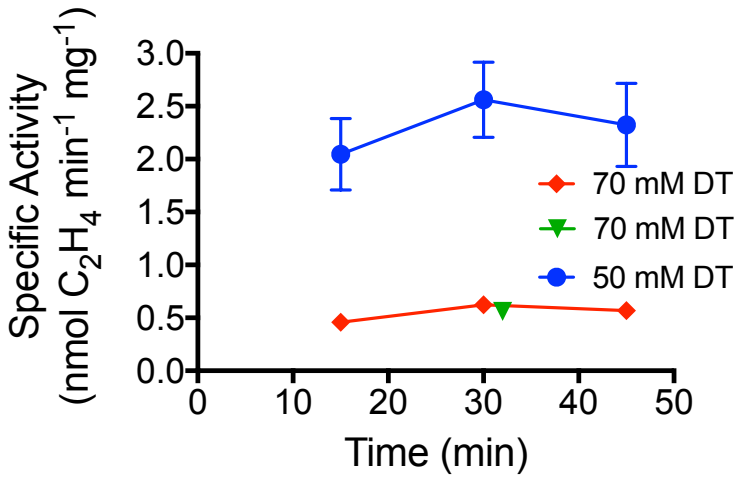

Figure 5.20 Less DT leads to higher specific activities for photoreduction.

While a typical experiment assessing the specific activity of wild-type MoFe protein for an Fe protein and ATP-dependent reaction might be conducted in a 1 – 1.5 mL reaction volume housed in a 10 – 14 mL sealed glass vial, adjustments to this standard set up were made to account for the lower specific activity of Ru-MoFe for photocatalysis as compared to wild-type MoFe protein in ATP and Fe protein-dependent reactions. When standard vials, which contain 0.2 – 0.4 μM MoFe protein (0.05 – 0.1 mg/mL) in 1 – 1.5 mL, are let to react for 10 minutes, a 50-μL aliquot of the reaction headspace is more than enough to achieve a peak area of C_2H_4 within the linear range of the GC. In order to achieve total amounts of C_2H_4 in the vial headspace of photoreduction assays that would also be within the linear range of GC-FID detection methods, initial photoreduction experiments in 2010 were designed as large reaction volumes in small glass vials, creating a small headspace. These were normally 9-mL reactions in 14-mL glass vials.

Additionally, to further increase the amount of C_2H_4 in the reaction headspace, previous experiments contained a higher concentration of catalytic MoFe protein (0.25 – 0.5 mg/mL) than used for Fe protein and ATP-dependent experiments. In the

present work, however, it was determined that both of these adjustments, increasing reaction volume and increasing catalyst concentration, actually have a detrimental effect on the observed specific activity of Ru-MoFe protein.

Because the new Abet Technologies lamp set up can achieve a much greater focus of the Xe arc lamp it houses, if the reaction volume is too large, light will not reach the entire sample, causing a decrease in the observed specific activity of the bulk reaction. Figure 5.21 shows how, when the reaction volume is decreased from 16 mL to 4 mL, the specific activity of Ru-MoFe protein, that is, the amount of product formed per catalyst per unit of time, substantially increases. Whereas 16 mL reactions in 27 mL glass vials reach a maximum specific activity of around 2 nmol C_2H_4 min^{-1} mg^{-1}, 4 mL reactions housed in 10 mL glass vials achieve a maximum specific activity around 20 nmol C_2H_4 min^{-1} mg^{-1}.

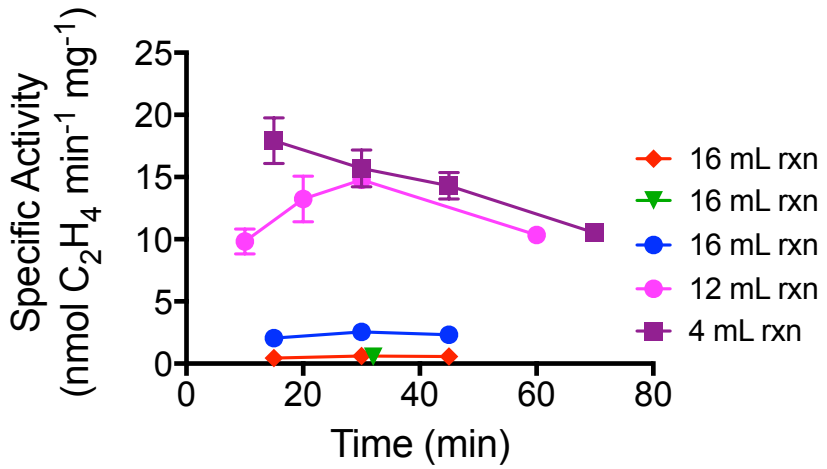

Figure 5.21 Smaller reaction volumes lead to high specific activities for photoreduction.

Furthermore, it was also established that increasing the concentration of Ru-MoFe much above 0.1 mg/mL leads to a decrease in the overall observed specific activity, and this observation was attributed to the inability of light to reach the entire sample as the concentration of light-absorbing catalyst increased. Figure 5.22

highlights the trend of decreasing specific activity for photoproduction of C_2H_4 as the concentration of Ru-MoFe is increased. Typical reactions thus contained no more than 0.1 mg/mL Ru-MoFe protein.

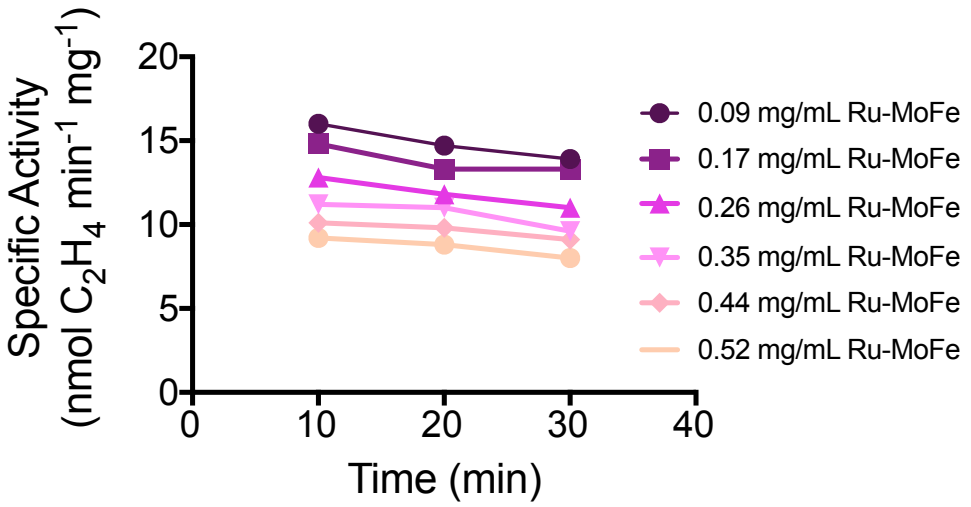

Figure 5.22 The specific activity for photoreduction increases as the concentration of Ru-MoFe protein decreases.

5.4 Conclusions

Nitrogenase is an O_2-sensitive, large multi-component enzyme, which contains multiple metal cofactors and is capable of catalyzing a variety of different reductions in an ATP-dependent manner. It is no surprise that there are many experimental obstacles to studying such a complex biological system. This chapter was concerned with efforts to optimize measurements of nitrogenase specific activities, in order to lead future researchers to measure meaningful results quickly.

C_2H_4 produced by nitrogenase is best quantified by GC-FID, and by changing the stationary phase of the packed column used for hydrocarbon separation, the time and cost devoted to maintaining and fixing the GC have decreased. Additionally, the time of experimentation has also decreased, since the new stationary phase achieves baseline separation of C_2H_2 and C_2H_4 in less time than the old alumina column. The

reproducibility of both C_2H_4 and H_2 measurements has been greatly improved by implementation of external calibrations using a known weight of purse gases.

Multiple methods for the determination of ATP hydrolysis and NH_3 formation by nitrogenase were tested throughout this work. New procedures were developed to measure ATP hydrolysis as true P_i released colorimetrically and NH_3 formation by fluorescence after derivitization with sulfite and OPA. Methods described here for measuring C_2H_4, H_2, NH_3, and ATP hydrolysis are all compatible with the ATP-regeneration system of creatine kinase and phosphocreatine. It is now possible to routinely measure the three products of biological nitrogen fixation, H_2, P_i, and NH_3, from the same reaction vial under conditions in which nitrogenase proteins are not susceptible to inhibition by ADP, as shown in Figure 5.23.

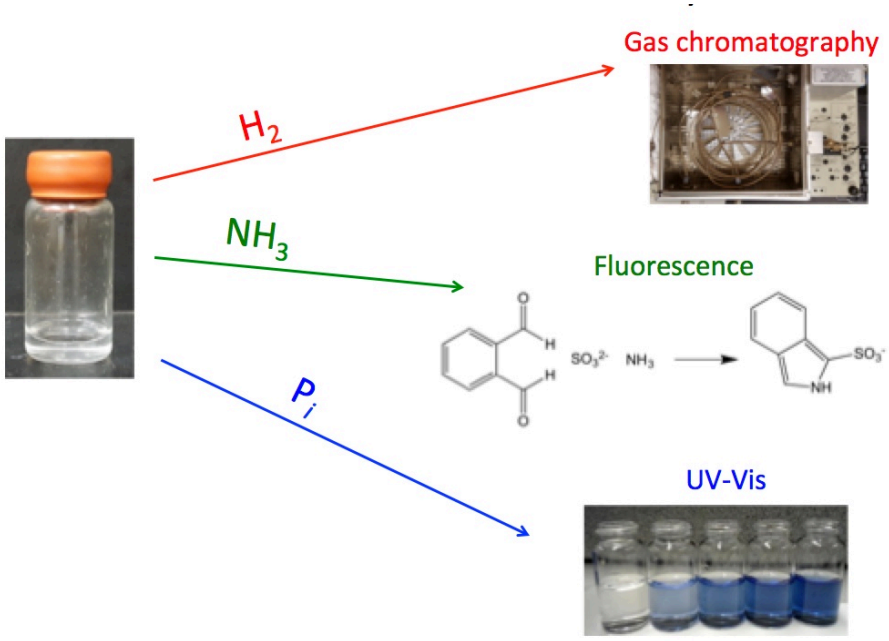

Figure 5.23 H_2 produced, NH_3 produced, and ATP hydrolyzed by nitrogenase determined from the same reaction vial using GC, fluorescence, and UV-Vis spectroscopy.

The size and complexity of nitrogenase also make it difficult to determine the concentration of protein in a solution of purified Fe or MoFe protein. This makes it

extremely challenging to determine specific activities, which measure the amount of product formed per unit of time per protein catalyst. Three techniques for evaluating the amount of active protein in a sample have been discussed. Finally, detailed explanations of troubleshooting and improvements to studying the photoreduction abilities of Ru-MoFe protein are provided for any reader interested in continuing this work.

5.5 Future Directions

Currently, the least precise measurement in nitrogenase analytical biochemistry is the measurement of H_2 produced. It is standard procedure to measure H_2 using GC-TCD, but the sensitivity of this technique for H_2 is low, preventing the determination of the NH_3:H_2 product formation ratio of nitrogenase at conditions of low flux (low Fe:MoFe protein ratios), as well as the evaluation of the specific activity of Ru-MoFe protein for photoproduction of H_2. Future work should focus on finding or creating a more sensitive method for H_2 quantification.

5.6 Acknowledgements

This work was made possible by assistance from Dr. Xinying Shi and Professor Simpson Joseph of the University of California, San Diego, who provided assistance with the purification of EF-G and 70S ribosomes and experiments with radioactive nucleotides. Additional assistance came from Dr. Richard Cochran through conversations about and assistance with GC and George Anderson in conversations about phosphate and ammonia detection methodologies.

Chapter 5 was reproduced in part, with permission, from Katz, F. E. H.; Shi, X.; Owens, C. P.; Joseph, S.; Tezcan, F. A. “Determination of nucleoside triphosphatase activities from measurement of true inorganic phosphate in the

presence of labile phosphate compounds." *Anal. Biochem.* **2017**, *520*, 62–67.

6 Conclusions

Nitrogenase is one of the most complex and most important enzymes known. Until just a century ago, all life relied upon diazotrophs harboring nitrogenase to fix atmospheric nitrogen into an accessible form. Even today, over 100 years after the development of the Haber-Bosch process to fix N_2 industrially, nitrogenase is still responsible for nearly 50% of all fixed nitrogen on earth.

No other enzyme is capable of breaking the N-N triple bond, and few synthetic systems can achieve N_2 reduction with any real efficiency. Instead, the majority of catalysts designed to reduce N_2 simply evolve H_2. Nitrogenase is remarkable in its ability to utilize up to 75% of its electrons for N_2 reduction. Clearly, part of this unique ability lies in the absolute requirement of Fe protein as the obligate electron donor to MoFe protein. The precise mechanistic rationale for how and why Fe protein couples electron transfer to ATP hydrolysis has eluded biochemists for decades.

The aim of this dissertation was to explore the specific requirement of the ATPase Fe protein through the dual lenses of PPI and protein conformational changes. First, an Fe – MoFe protein interaction observed crystallographically was probed for its mechanistic importance. Residue βK400 lies on the surface of MoFe protein within hydrogen bonding distance to multiple negatively charged residues on the surface of Fe protein in the nucleotide-free nitrogenase co-crystal structure. Residue βK400 was mutated to Glu and the resulting MoFe protein was found to be impaired in its ability to reduce both C_2H_2 and H^+.

Attempts were made to fluorescently label the nitrogenase proteins, in order to use FRET to assess the ability of βK400E MoFe protein to bind Fe protein, and evaluate whether this ability was weakened relative to wild-type MoFe protein. When these efforts proved unsuccessful, because the fluorescent probe was attached to Fe

protein in such a way as to perturb the native PPI, the dilution experiment was used instead. This experiment assessed changes in the rate of Fe – MoFe protein association resulting from mutation of βK400 to a negatively charged Glu. Compared to wild-type MoFe protein, βK400E MoFe protein required a higher concentration of Fe protein for the relationship between activity and [MoFe] to reach linearity, suggesting βK400E is impaired in its ability to bind Fe protein in a catalytically relevant way. Though the results of turnover assays were simulated by the T-L model when k_1, the rate of component protein association, was lowered 5-fold for βK400E relative to wild-type MoFe protein, the T-L cycle has been expanded to include the formation of an ensemble of encounter complexes prior to the formation of the activated, *DG2*-like complex, which is capable of electron transfer and ATP hydrolysis, and these experiments highlight that residues far away from the metal cofactors and ATP binding sites can actually play significant roles in catalysis.

Subsequently, the rate of NH_3 production by βK400E MoFe protein was evaluated. Interestingly, when the biologically relevant reaction was finally assayed, the initial explanation as to the effect of the charge reversal mutation βK400→E was not longer sufficient. βK400E MoFe protein displays a lower total activity but a slight increase in efficiency, as measured by the NH_3:H_2 product formation ratio. The logic embedded in the T-L model is that the faster the electron transfer cycles, the greater the flux, and the less H_2 evolution relative to NH_3 production. However, the increase in product formation ratio for βK400E relative to wild-type MoFe protein suggests that to engineer a more efficient nitrogenase, in terms of the amount of NH_3 produced per ATP consumed, efforts should be made to lower the electron flux, slowing the rate of electron accumulation at FeMoco rather than speeding it up.

In light of the N_2 reduction efficiency data, an explanation as to why K400 might not be fully conserved among nitrogenases emerges. One of the ways *A. vinelandii* protects nitrogenase component proteins from oxygen damage is by temporal resolution of respiration and nitrogen fixation. *A. vinelandii* must be able to fix N_2 quickly, so it can return to respiration. Nitrogenase is also found in a variety of other organisms, though, including anaerobes. For many of these organisms, O_2 protection is not a consideration, but ATP is a much more precious commodity than it is for *A. vinelandii*. Thus, they may have evolved a slower nitrogen fixing system that utilizes fewer ATP's per NH_3 and wastes fewer electrons to H_2 evolution. So then, PPI in *DG1* and the specific requirement of Fe protein as the electron donor to nitrogen fixation may be about fine-tuning the rate of NH_3 production versus efficient use of ATP in NH_3 production.

Next, the relationship between conformational changes at the P-cluster and conformational gating of electron transfer through nitrogenase was probed. It was discovered that an organism lacking βS188, *G. diazotrophicus*, instead contains a Tyr residue that is able to ligate the oxidized P-cluster. Further sequence analysis confirmed that all Group 1 nitrogenases contain either a Ser at *A. vinelandii* position β188 or a Tyr at *G. diazotrophicus* position β98. A link from both βS188 and βY98 to the surface of Fe protein can be envisioned as part of the conformational gate and awaits further investigation.

Efforts were then undertaken to apply this information to the photocatalytic Ru-MoFe protein. The low efficiency of the photocatalytic Ru-MoFe protein was previously taken as indirect evidence of conformational gating of electron transfer in nitrogenase. βS188→C was proposed as a mutation that could lower the reduction potential of the P-cluster and, in doing so, bypass the conformational gating mechanism, which should substantially increase the photocatalytic ability of Ru-MoFe

protein. Difficulties in mutagenesis prevented testing of this hypothesis with a Ru-MoFe protein containing an altered P-cluster.

The results presented in this dissertation highlight that PPI in nitrogenase are extremely dynamic in nature. Fe – MoFe protein binding is not governed by a simple on/off mechanism. It may be more apt to think of Fe protein movement along the surface of MoFe protein as two cogs of a gear, reminiscent of motor proteins that share significant sequence homology with Fe protein. The results here also serve as a reminder that residues, which are not strictly conserved, may co-vary and still play important, unrealized roles in enzyme structure and function. Furthermore, analysis of the partitioning of electrons to N_2 and H^+ reduction by wild-type and mutant nitrogenases suggests that the T-L model is not quantitative and is, at best, qualitative. Thus, mechanistic hypotheses that T&L neglected, such as the cooperativity model initially put forth by Bergensen and Turner, may have merit.[111] Though nitrogenase is an extremely challenging biochemical system to study due to its O_2 sensitivity, its large gene requirement, the difficulties associated with mutagenesis in the polychromosomal *A. vinelandii*, and the inherent challenges in measuring the biologically relevant reaction products, NH_3, H_2, and P_i, investigation of nitrogenase surely is one of the most captivating and consequential scientific endeavors.

7 Appendix

When I first joined Team Nitro of the Tezcan Lab, we had the *green book*. The *green book* was a hardcover, hunter green lab notebook with a beautifully detailed table of contents and upwards of 50 pages of nitrogenase-related protocols printed out and glued to pages of the notebook. The *green book* was my savior. When I had forgotten what volume of NH_4Cl to add to a media preparation or at what temperature to anneal during PCR, I could turn to the *green book*. But the green book was also my downfall. On many occasions, I spent weeks and even months trying, unsuccessfully, to get an experiment from the *green book* to work, only to find out months later that a former Team member had improved, shortened, or abandoned that experiment entirely, but the *green book* had not been updated to reflect that change.

The author of the *green book*, Lauren Roth, deserves enormous credit for everything that follows. Most of my original research builds off of the stellar foundation she laid as a founding member of the Tezcan Lab's Team Nitro, and I would never have been able to create anything like this if she had not gone before me and kept meticulous notes along the way.

What follows is a compilation of formal procedures and informal tips that I have adopted, modified, inherited, and invented. My hope is that here you will be able to find, not just procedures, but explanations, that you will leave this text with a better understanding of not just what I did but why I chose to do it in that way, and you will be empowered to make more informed decisions about your own experimental procedures.

7.1 Fermenter growth of *A. vinelandii* for expression of nitrogenase proteins

1 L Burk's media
20 g sucrose
2 mL "FeMoCa" (18 mM Fe, 2 mM Mo)
19 g citric acid monohydrade + 5 g $FeSO_4 * 7H_2O$ + 0.25 g $Na_2MoO_4 * 2H_2O$ in 1 L
1 mL 0.9 M $CaCl_2$
66.2 g CaCl2 * $2H_2O$ in 500 mL
1 mL 1.67 M $MgSO_4$
205.8 g $MgSO_4 * 7H_2O$ in 500 mL

*filter and store separately *
5 mL 2.0 M P_i buffer, pH 7.5
3.5 mL 3.0 M NH_4Cl

To make Burk's media, autoclave a solution of sucrose, "FeMoCa", $CaCl_2$, and $MgSO_4$ in an Erlenmeyer flask that holds approximately 5x the volume of the media. (25 mL in 125-mL flasks, 100 mL in 500-mL flasks, 1 L in 2.8-L flasks) Autoclave small aliquots of 2.0 M P_i buffer and 3.0 M NH_4Cl in separate 100-mL glass bottles. After all solutions have been autoclaved and cooled to room temperature, sterilely transfer 5 mL 2.0 M P_i buffer for every 1 L Burk's media and 1.67 mL 3.0 M NH_4Cl for every 1 L Burk's media. This will lead to final concentrations of 10 mM P_i buffer and 5 mM NH_4Cl.

Fe-Free Burk's media
Create a "MoCa" solution as described above for "FeMoCa" but omit the $FeSO_4$. Add 2 mL of "MoCa" for every 1 L media in place of "FeMoCa".

low-Ca Burk's media
Add 10% of the amount of $CaCl_2$ that would normally be added for Burk's media.

N^- Burk's media
Omit the addition of NH_4Cl.

Rifampicin$^+$ Burk's media
Create a 10 mg/mL stock of rifampicin in MeOH and store in the -20°C when not in use. Add 1 mL of this 10 mg/mL stock for every 1 L of media, for a final concentration of 10 µg/mL.

Burk's Agar plates
Add 20 g agar for every 1 L of Burk's media

In preparation for a fermenter growth, autoclave the following:
1 x 100 mL Burk's media in a 500-mL Erlenmeyer flask
1 x 1 L Burk's media in a 2.8-L Erlenmeyer flask
1 x 20 mL 2 M P_i buffer, pH 7.5 in a 125-mL Erlenmeyer flask
1 x 20 mL 3 M NH_4Cl in a 125-mL Erlenmeyer flask
1 x 1 L empty plastic container handle
1 x 250 mL 2 M P_i buffer, pH 7.5 in a 500-mL glass bottle
1 x 50 mL 3 M NH_4Cl in a 250-mL glass bottle

7.1.1 Fermenter growth: Day 1

Remove a wild-type *A. vinelandii* freezer stock from the –80°C freezer. Inoculate 100 mL N^- Burk's media (in a 500-mL flask) with the entire 1.7 mL Eppendorf tube of cells. Shake overnight at 30°C, 200rpm.

7.1.2 Fermenter growth: Day 2

In the afternoon inoculate 1 L Burk's media (in a 2.8-L flask) with 2-4 mL of cells from the 100 mL culture, depending on the $O.D._{600}$ of the inoculation culture. The doubling time of *A. vinelandii* is between 2-3 hours. Aim for a 1 L culture with an $O.D._{600}$ of 2.0 to use as the fermenter starter culture. Shake overnight at 30°C, 200rpm.

7.1.3 Fermenter growth: Day 3

Preparation of starter culture
In the morning, remove the 1 L culture from the shaker. Check that the $O.D._{600}$ is between 1.0-2.0. Sterilely pour 400 mL of this culture into an empty, autoclaved 1-L container and place in the cold room. Smell the remainder of cells to ensure they are *A. vinelandii* and have not been contaminated with *E. coli*. If the cells do not smell like sour milk, do not add them to the fermenter.

Preparation of the fermenter
Open all water valves. Turn on the fermenter. Open valve to house steam. Insert the pH meter into the fermenter, and standardize the pH meter. Rinse fermenter with water by filling 20-40 L and draining. Do this two times. Fill the fermenter with 50 L H_2O, 1 kg sucrose, 100 mL FeMoCa, 50 mL $MgSO_4$, and 50 mL $CaCl_2$. Seal and begin the sterilization procedure. It will take approximately 2 hours for the fermenter to perform the sterilization procedure and then return to 30°C.

Inoculation of fermenter culture
Immediately before leaving for the evening, and 16-20 h before intended harvest time, inoculate the fermenter culture as follows: Through the sterile funnel, add 250 mL 2 M P_i buffer, pH 7.5, then 50 mL 3 M NH_4Cl, for a final concentration of 3.0 mM NH_4Cl, which will lead to derepression of nitrogenase approximately 16 h after inoculation. Finally, add pre-measured 400 mL *A. vinelandii* cells from the 1 L culture. Seal fermenter and ensure all settings are correct. Fermenter should be set to 30°C, 200 rpm, 2.0 psi, with gas flow and exhaust heater on.

7.1.4 Fermenter growth: Day 4

$O.D._{600}$ of fermenter culture
Approximately 16 hours after fermenter inoculation, sterilely remove a 20-mL aliquot of *A. vinelandii* cells from the fermenter. Let the first 20 mL flow through and collect the second 20-mL fraction. Measure the $O.D._{600}$, which should steadily increase to about 1.5-2.0 over the course of the morning. If the $O.D._{600}$ stabilizes or drops somewhere between 1.5-2.5, the cells are likely entering derepression and beginning

to express nitrogenase. Collect a 20 mL aliquot of *A. vinelandii* cells from the fermenter and repeat the above steps each 30-60 min.

Nitrogenase activity of the fermenter culture
Add 1 mL cells to a 14-mL glass vial, seal, and add 1 mL of 1 atm C_2H_2. Incubate at 30°C in a circulating water bath for 10 min, then inject 200 µL headspace into the GC to measure C_2H_4. Cells should be harvested at peak nitrogenase activity.

pH and DO trends of fermenter culture
The fermenter monitors the pH and DO (dissolved oxygen) of the culture, both of which will slowly decline. The pH will stabilize around 6-6.5 and the DO will hit a minimum and start to increase again at the start of derepression of nitrogen fixation (nif) genes. Cells should be harvested 4-6 h after the DO hits a minimum value and begins to increase.

Cell collection and concentration
Collect the fermenter culture in a large, clean trashcan or other plastic container. Use the Millipore membrane filter to reduce the volume from 50 to 5 L. Take the 5 L culture upstairs and centrifuge in 6 1-L bottles of equal weight for 10 min at 5,000 rpm. Transfer cell pellets to a pre-weighed 250-mL plastic bottle and centrifuge for an additional 10 min at 5,000 rpm. Decant supernatant, weigh cell pellet, and freeze in –80°C.

7.2 Purification of nitrogenase Fe protein and MoFe protein from *Azotobacter vinelandii*

7.2.1 Protein purification: Day 0

Buffers
Start by making 1 L of a 1.0 M solution of Tris buffer, pH 7.75. Then, make the following buffers in order of increasing salt concentration. Filter each buffer, pour into a round bottom flask, and secure straw with grease.

a. Buffer A: 50 mM Tris, pH 7.75 (2.8 L in a 3-L round bottom with straw)
b. Buffer B: 50 mM Tris, pH 7.75, 500 mM NaCl (2.8 L in a 3-L round bottom with straw)
c. Buffer E: 50 mM Tris, pH 7.75, 100 mM NaCl (4.8 L total, 2.8 L in a 3-L round bottom with straw, and 1 L in a 1-L round bottom without a straw)
d. Buffer C: 50 mM Tris, pH 8.0, 500 mM NaCl (2.8 L in a 3-L round bottom with straw)

Remove DT from anaerobic tent
Transfer into clean, dry glass vials according to the following table, seal with septa.

Buffer	DT (g)
A	2.44
B	2.44
E (2.8L)	2.44
E (1L)	0.87
C	2.44

De-gas on Schlenk line
De-gas buffers 8 x 8 min. De-gas DT 8 x 4 min or on the auto suck.

7.2.2 Protein purification: Day 1

Equilibration of the DEAE column
Transfer 2.44 g DT to buffer E (2.8L) via cannula and de-gas buffer E for an additional 2 x 8 min. Hook up buffer E to pump A of the FPLC and run through DEAE column at 2.0-3.0 mL/min. The total volume of the DEAE column is about 200 mL, and approximately 5 column volumes of buffer E should flow through the DEAE column before cell lysate is loaded.

Preparation for cell lysis with Microfluidizer
Thaw cell pellet. Remove buffer E (1L) from Schlenk line, add 0.87 g DT and 10 mg DNase1, shake, re-seal, and set on ice. Hook up N_2 tank to Microfluidizer. Turn on Microfluidizer and prime chamber by removing EtOH and adding reducing buffer E. Do this at least 4 times. Check for leaks, and if no leaks are identified, fill the chamber with ice to prevent overheating of cells. When cells are thawed, resuspend no more than 150 g cell pellet in about 200 mL reducing buffer E. Resuspended cells should resemble the cells in Figure 7.1. Make sure there are no chunks remaining, as these can easily clog the Microfluidizer chamber. It is better for cells to be too dilute than too concentrated. Transfer cells to Microfluidizer container. Cover with foil and place an open needle from Schlenk line over cells to create a bed of Ar.

Cell lysis with Microfluidizer
Lyse anaerobically at 16,000 psi. Collection vessel should be covered in foil and an open needle of Ar from the Schlenk line should flow over the collection vessel. Lysed *A. vinelandii* cells will change color from light brown to dark brown/black due to the high content of proteins with Fe:S clusters (i.e., nitrogenase), as shown in Figure 7.2. Quickly pour lysed cells into the Microfluidizer container for a second pass through the Microfluidizer. Repeat for a third time, and collect the third pass in an anaerobic centrifuge container. Add an additional 100 mL reducing buffer E to the Microfluidizer container and collect in a second anaerobic centrifuge container. De-gas both containers 15 x 1 min. Keep containers on ice while de-gassing. Centrifuge at 12,500 rpm for 75 minutes to pellet cell debris. Nitrogenase proteins will remain in the supernatant.

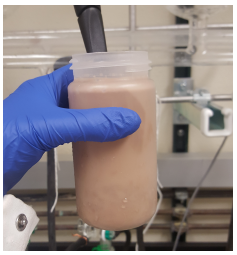

Figure 7.1 *A. vinelandii* cell pellet resuspended in Buffer E prior to cell lysis.

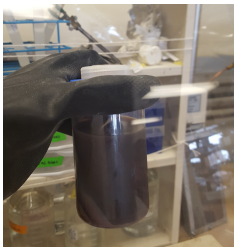

Figure 7.2 *A. vinelandii* cell lysate after lysis with Microfluidizer.

Loading crude cell lysate onto the DEAE column
Immediately transfer centrifuge bottles to the anaerobic tent (along with a 500-mL pear shaped flask and red septa). Once inside the tent, open containers and immediately decant supernatant fraction into a pear shaped flask. *A. vinelandii* pellets poorly; if the liquid is not decanted immediately, separation of the supernatant and precipitate fractions will not be achieved. Add ~2 but not more than 5 mM DT to the crude protein solution. Seal flask, bring out of tent, and load onto DEAE column at 1.5 mL/min. Wash DEAE column overnight with buffer E at a flow rate that achieves approximately a 1.5-L wash.

7.2.3 Protein purification: Day 2

Eluting DEAE column
In the morning, flow-through from DEAE column should be clear. Do not begin eluting from the DEAE column if the flow-through is not clear. Transfer 2.44 g DT to both buffers A and B via cannula. De-gas each buffer for an additional 2 x 8 min. Hook both buffers A and B up to FPLC to their respective pumps. Start an FPLC run that monitors both 280 and 410 nm, flowing at 3.0 mL/min and increasing from 20-100% B over the course of 1500 mL. An example DEAE chromatograph is shown in Figure 7.3, and Figure 7.4 shows the color changes to the DEAE resin as nitrogenase proteins elute. De-gas 20 collection vials (from 24-70 mL) on the auto-suck.

Analyzing fractions from DEAE column
Bring all fractions from DEAE column into the anaerobic tent. The fractions should resemble the fractions in Figure 7.5. When the O_2 has dropped adequately, add 2 µL of each fraction to 18 µL water or buffer in 0.7 mL tubes. Remove tubes from tent, add 10 µL SDS reducing loading dye, and heat samples in the thermocycler for 3 min at 98°C. Load 12 µL of each solution onto 10% SDS PAGE gels. Let run for 60 min at 200 V, or until the dye runs off of the gels. Let gels soak in staining solution for at least 30 min before places in destain solution.

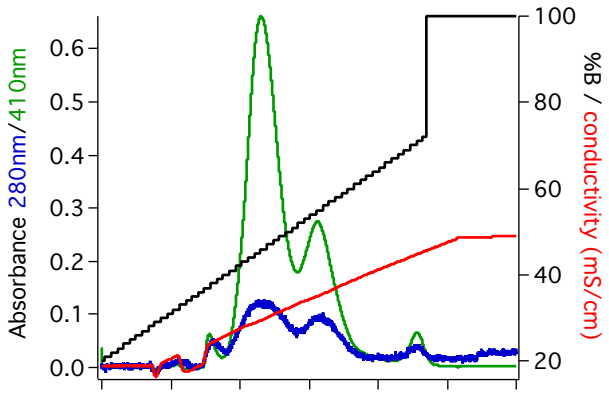

Figure 7.3 Example chromatogram from large DEAE column highlighting separation of MoFe protein from Fe protein.

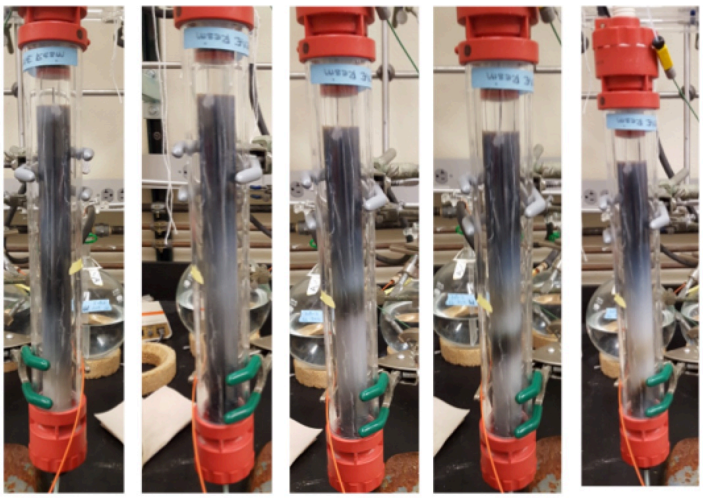

Figure 7.4 Elution of MoFe and Fe proteins from large DEAE column.

Figure 7.5 Protein fractions arranged from left to right in order of elution from DEAE column.

7.2.4 Protein purification: Day 3

Pool and concentrate Fe and MoFe protein fractions with small DEAE
Combine the MoFe protein fractions of sufficient purity in a 250-mL pear-shaped flask and add an equal amount of Buffer A (50 mM Tris, pH 7.75, NO NaCl) to the pooled proteins to lower the NaCl concentration. Load this entire solution onto the small DEAE column, as shown in Figure 7.6, which has been equilibrated with reducing buffer E. The volume of the small DEAE column is about 20 mL, and about 5 column volumes are required to make the column reducing. Do not run the small DEAE column above 2.0 mL/min, or else there is a risk of the column leaking. After the entire fraction is loaded, elute with buffer B (50 mM Tris, pH 7.75, 500 mM NaCl). Collect no more than 30 mL concentrated MoFe protein. Wash the DEAE column with 5 column volumes of buffer B, followed by 5 column volumes of buffer E, and repeat the process for Fe protein.

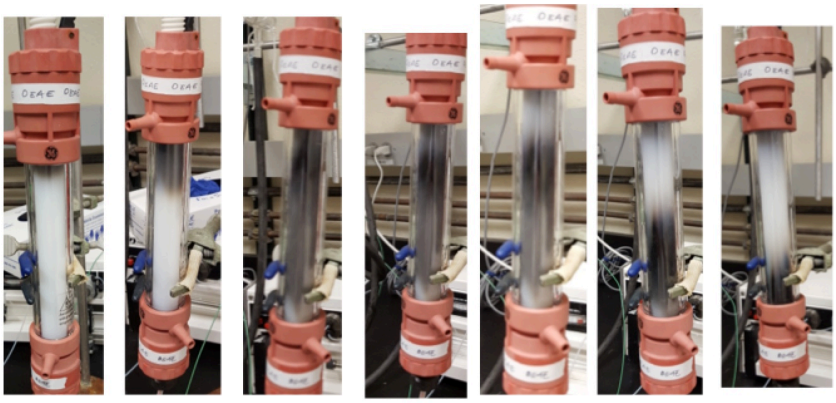

Figure 7.6 Concentration of MoFe protein on small DEAE column.

Preparation for Day 4
Make sure there are 100 clean, dry glass vials (10-27 mL) for collection on Day 4. Prepare columns for size exclusion chromatography on Day 4. Using a cannula add DT to both buffer C containers, de-gas for an additional 2 x 8 min, and hook up to respective FPLC's and columns. Run about 800 mL buffer through each column overnight. Label 24 orange-capped conical vials for LN_2 dewar and bring into tent to equilibrate before freezing protein on Day 5.

7.2.5 Protein purification: Day 4

Size-exclusion chromatography
Before 8:00 am on Day 4, load 4 mLs concentrated Fe protein onto one SEC column and load 4 mLs concentrated MoFe protein onto the other SEC column. De-gas 40 collection vials. Collect from both columns and load a second run BEFORE group meeting at 11:30. Load the third run for each column right after group meeting, and load the fourth (if necessary) run around 3-4pm.

7.2.6 Protein purification: Day 5

10% SDS-PAGE analysis
Add 2 µL of each fraction to 18 µL water or buffer in 0.7 mL tubes. Remove tubes from tent, add 10 µL SDS reducing loading dye, and heat samples in the thermocycler for 3 min at 98°C. Load 12 µL of each solution onto 10% SDS PAGE gels. Let run for 60 min at 200 V, or until the dye runs off of the gels. Let gels soak in staining solution for at least 30 min before places in destain solution.

Pool, concentrate, and freeze Fe and MoFe proteins
Assemble 2 Amicons (one with a 10 kDa membrane filter and one with a 100 kDa membrane filter) and bring into tent. Run anaerobic buffer through the Amicon equivalent to 50% of the Amicon total volume. Repeat this a second time. While Amicons are equilibrating, finish destaining gels and determine which fractions to pool for Fe and MoFe proteins. Concentrate proteins separately to ~30 mg/mL Fe protein and ~20 mg/mL MoFe protein. Take 6 aliquots of 20 µL of Fe protein and MoFe protein and remove from tent to do both Bradford and chelation assays to determine protein concentrations.

7.3 Measurement of all nitrogenase reaction components from a single reaction vial

7.3.1 SOP for the SRI 8610C GC

1. Turn on the GC box (back left) and then immediately open the Peak Simple software on the computer (Vista OS).
2. If you are measuring H_2…
    a. Turn the temperature to 80°C.
        i. Go to “Edit,” select “Channels,” and click on the box labeled “Temperature” for Channel 1. Change the temperature from 30°C to 80°C.
    b. Open the red lid of the GC box and turn the TCD switch from the “OFF” (upright) position to the “LOW” (forward position).
    c. Verify that the N_2 or Ar gas is on and the tank is not empty.
3. If you are measuring C_2H_4…
    a. VERIFY THAT THE TCD DETECTOR IS IN THE “OFF” (UPRIGHT) POSITION BEFORE PROCEEDING.
    b. Turn the temperature to 110°C.
        i. Go to “Edit,” select “Channels,” and click on the box labeled “Temperature” for Channel 1. Change the temperature from 30°C to 110°C.
    c. Verify that the He, air, and H_2 tanks are on and none are empty.
    d. Light the flame by holding the switch in the upward position until you hear a “pop.”
4. Press the space bar to run a blank measurement and do not begin analysis until the noise level is satisfactory, typically 10-15 min after the detector has been turned on.
5. Go to “Edit,” select “Channels,” and click on the box labeled “Postrun” to edit the file names for your analysis.

6. Shut down procedure when analysis is finished: set the temperature back to 30°C, close the program, save results, close H_2 and air tanks if using FID, and let GC box cool to 30°C on the digital readout before turning off the GC box. Refer to Table 9.1 for standard settings.

Table 7.1 Best practices for use of an SRI 8610C GC in studies of nitrogenase

	Quantify H_2	Quantify C_2H_4
Column	10' x 1/8" packed, washed molecular sieve (5A 80/100)	6' x 1/8" HayeSep N packed column
Column supplier	Ohio Valley Specialty Company	SRI Instruments
Oven temp	80 °C	110 °C
Detector	TCD	FID
Carrier gas and flow rate	N_2 or Ar – 8 psi Set the regulator at the gas tank 10-15 psi above 8 psi	He – 8 psi Set the regulator at the gas tank 10-15 psi above 8 psi
Additional gases and flow rates		Air – 8 psi H_2 – 18 psi Set the regulator at the gas tank 10-15 psi above 8 psi
Typical standard curve	y = 0.5x with N_2 carrier gas y = 1.5x with Ar carrier gas y = peak area x = nmol H_2	y = 150x y = peak area x = nmol C_2H_4
Headspace injection volume	500 µL	200 µL

7.3.2 Troubleshooting the GC

Problem: No peak

- Is the TCD detector in the "LOW" position if measuring H_2?
- Is the flame lit if measuring C_2H_4?
- Is the injection needle clogged?
- Is the carrier gas leaking?
- Are any of the required gas tanks empty?

7.3.3 Reagents required for standard activity assays

1. Buffer A: 50 mM Tris, pH 8.0, 5 mM $MgCl_2$
    a. The $MgCl_2*6H_2O$ is extremely hydroscopic. Thus, weighing out old $MgCl_2*6H_2O$ may not be effective for creating a solution that is truly 5 mM Mg^{2+}. There is nothing wrong with making the solution up to 10 mM $MgCl_2$, but if even at this concentration, proteins are not active (due to not enough Mg^{2+} to bind ATP), purchase a fresh container of $MgCl_2*6H_2O$.
2. Buffer B: 1.0 M Tris base, not pHed
    a. It is imperative that this buffer is created using tris base and not tris acid, and also that it is filtered but not pHed, as it will be used to neutralize the DT.

3. Buffer C: 50 mM Tris, pH 8.0, 500 mM NaCl
    a. Buffer A, B, and C must be filtered prior to use and should not be used much more than 1 month after filtration.
4. Dithionite powder
5. ATP
6. Phosphocreatine
7. Creatine kinase

7.3.4 Materials required for standard activity assays

1. clean, oven-dried 14 mL vials
2. clean, oven-dried 7 mL vials
3. clean, oven-dried 2 mL conical glass vials
4. 1 clean, oven-dried 1 L round-bottom flask (only if performing C_2H_2 reduction assay)
5. small red septa
6. large red septa
7. Hamilton syringes

*** For C_2H_2 reduction or H^+ only assays, Schlenk line must be under Ar. To assay for NH_3, Schlenk line must be purged and switched to N_2. ***

7.3.5 Procedure required for standard activity assays

1. Protein preparation
    a. Get proteins out of liquid N_2 dewar and bring into tent, along with 2 mL conical glass vials and red septa.
    b. Spin down protein in 1.7 mL Eppendorf tubes.
    c. De-salt on 10DG if needed (i.e. to remove trace DT, change salt concentration, change from Tris to Hepes, etc.).
    d. If protein concentration is unknown, remove aliquots for Fe-chelation assay.
2. Vials
    a. Mix 0.061 g Na_2ATP, 0.20 g phosphocreatine, and 0.0125 g creatine kinase with 20 mL buffer A. Add 1 mL of this solution to each of 18 14-mL reaction vials.
    b. Add the appropriate amount of buffer C to each vial, refer to Tables 9.2 and 9.3.

Table 7.2 Example set-up for Fe protein specific activity assay vials.

	MoFe:Fe molar ratio	µL MoFe protein	µL Fe protein	µL buffer C
A	0	0	23	117
B	0.25	5.6	23	111
C	0.5	11.2	23	106
D	0.75	16.8	23	100
E	1	22.4	23	94
F	1.5	33.6	23	83
G	2	44.9	23	72
H	3	67.3	23	50
I	4	89.7	23	27

Table 7.3 Example set-up for MoFe protein specific activity assay vials.

	Fe:MoFe molar ratio	µL MoFe protein	µL Fe protein	µL buffer C
A	0	20	0	120
B	5	20	11.6	109
C	10	20	23.1	97
D	12	20	27.7	92
E	15	20	34.7	85
F	20	20	46.2	74
G	25	20	57.8	62
H	30	20	69.3	51
I	40	20	92.4	28

3. Materials to de-gas
    a. De-gas Hamilton syringes in 50 mL sidearm flask(s) (6 x 5 min).
    b. De-gas 18 reaction vials on auto suck.
    c. De-gas 2-mL aliquot of buffer B on auto suck.
    d. De-gas 0.348 g DT (2 mmol) on auto suck.
    e. Vacuum 1 L round bottom for C_2H_2 assay (30 min).
    f. Vacuum 250 mL round bottom for C_2H_2 assay and 500 mL round bottom for H_2 assay.
4. Assay
    a. Add 2 mLs buffer B to 0.348 g DT. Then add 15 µL of this solution to each activity assay.
    b. Shake at 30°C for 10 min.
    c. If assaying for C_2H_4, add 1 mL C_2H_2 gas to each activity assay. Shake 30°C for an additional 10 min.
    d. Add the protein that varies among vials (for MoFe protein assays, add Fe protein, while for Fe protein assays, add MoFe protein first). Shake 30°C for an additional 10 min.
    e. Add the other component protein to each vial in 30 sec intervals.
    f. After 10 min, quench assays with 400 µL 4 M NaCl, seal well with grease, and set upside down.

7.3.6 C_2H_4 evolution assay

1. Preparation of the standard curve:
    a. The pressure of the He, oxygen, or H_2 tanks connected to the GC should never drop below 500 psi – DO NOT wait until the tank is empty to change; change this tank whenever the total pressure hits 500 psi. The purity rating on these tanks is not guaranteed at very low gas levels, and running the GC with a low gas tank can damage both the column and the detector.
    b. Degas a 250-mL round-bottom flask for 10 min on the Schlenk line. Weigh the empty flask. Fill it with pure C_2H_4. Weigh filled flask. Aliquot 10-50 µL of gas from the 250-mL round-bottom flask into 14, 24, or 27 mL vials (depending on the range of standard curve needed). Quickly cover the rubber septum of the 14 mL vial with grease.
    c. Make 15 injections: three each of 10, 20, 30, 40, and 50 µL injections. Plot peak area v. nmol C_2H_4 injected and generate a best-fit line. The slope of this line should be around 150. If the slope does not fall $120 < m < 180$, something is wrong with the standardization.

7.3.7 H_2 evolution assay

1. Preparation of the standard curve:
    a. The GC should be turned on to 80°C with Ar as the carrier gas and the TCD turned to LOW. The TCD should always be in the off position when the GC is heated above 80°C (i.e. for a C_2H_2 reduction assay), so make sure this is turned back to OFF at the end of each use.
    b. The pressure of the Ar tank connected to the GC should never drop below 500 psi – DO NOT wait until the tank is empty to change; change this tank whenever the total pressure hits 500 psi. The purity rating on these tanks is not guaranteed at very low gas levels, and running the GC with a low gas tank can damage both the column and the detector.
    c. Ideally the GC should run for ~ 1hr with the TCD on LOW before any standards or samples are injected.
    d. Degas a 500 mL-round-bottom flask for 15 min on the Schlenk line. Weigh the empty flask. Fill it with pure H_2 (in the hood). Let H_2 gas flow for ~ 30 sec (as you would for C_2H_2 or C_2H_4) before injecting gas into the round-bottom flask. Weigh filled flask. Aliquot 1 mL of gas from the 500 mL round-bottom flask into a 14 mL vial. Quickly cover the rubber septum of the 14 mL vial with grease.
    e. Make 15 injections: three each of 10, 20, 30, 40, and 50 µL injections. Plot GC peak area (H_2 peak should be between 2-2.3 min) v. nmol H_2 injected and generate a best-fit line. The slope of this line should be around 0.5. If the slope does not fall $0.25 < m < 0.75$, something is wrong with the standardization.
    f. Each injection will take a minimum of 7 minutes. There are 3 peaks that elute in both the standards and the samples, at approximately 2.2, 4.2, and 7.0 minutes.

7.3.8 ATP hydrolysis assay reagents

1. 100.0 mM P_i standard solution
    a. Calculate the amount of Na_2HPO_4 and NaH_2PO_4 needed to make 1L of an ~pH 7.0 solution of 100.0 mM phosphate. Weigh >1.000 g of Na_2HPO_4 and >1.000 g NaH_2PO_4 on the analytical balance. Add pre-weighed powders to >1000.0 g distilled H_2O to a pre-weighed 1L glass container. Add a stir bar to dissolve as needed. Aliquot ~10 mL volumes into plastic 15 mL conical vials. Calculate concentration in ppm and convert to M assuming the density of water is 1.00000 kg/L at lab temperature.
2. $(NH_4)_6Mo_7O_{24}$ solution
    a. Dissolve 1.5 g $(NH_4)_6Mo_7O_{24}$*$4H_2O$ in 50 mL distilled water. This solution is stable for at least 6 months when stored in the fridge in a plastic 50 mL conical vial.
3. H_2SO_4 solution
    a. To 90 mL distilled water, add 14 mL H_2SO_4. This solution in stable indefinitely when stored in the hood in a glass container. Do not add this solution to the mixed reagent until it has cooled to room temperature.
4. ascorbic acid solution
    a. Dissolve 2.7 g ascorbic acid in 50 mL distilled water. This solution is stable for no more than 6 months when stored in the fridge in a plastic 50 mL conical vial.
5. potassium antimonyl-tartrate solution
    a. Dissolve 0.068 g potassium antimonyl-tartrate in 50 mL distilled water. This solution is stable for at least 6 months when stored in the fridge in a plastic 50 mL conical vial.
6. 400 mM $CaCl_2$ solution in 100 mM Tris, pH 8.0
7. 0.25 M HCl solution

7.3.9 ATP hydrolysis assay procedure

1. About 2 but no more than 3 hours before phosphate analysis, make the mixed reagent and store on the benchtop. To make the mixed reagent, to 10 parts reagent #2, add 10 parts reagent #4, then 5 parts reagent #5, and finally 25 parts reagent #4. If H_2SO_4 solution has been made fresh on the same day, wait until it has cooled to room temperature before making the mixed reagent.
2. Add 10.0 mL distilled water to 30-40 glass vials (number of assays and standards to analyze) and set aside.
3. The linear range of the phosphomolybdate assay is ~0-20 uM Pi. Determine the amount of dilution necessary for activity assay solutions to fall in this range.
    a. Example: If a day's assays are predicted to produce 0-5 mM Pi, samples will need to be diluted ~250x prior to analysis.
4. In a 1.7 mL Eppendorft tube, add 500 uL NaCl-quenched activity assay to 500 uL H_2O and 300 uL 400 mM $CaCl_2$ in 100 mM Tris, pH 8.0.
5. Centrifuge for 5 min at 10,000 rpm.

6. Remove 1.2 mL (in 2 x 600 µL aliquots) supernatant from each tube. Do not touch or disturb the soft, white pellet with the pipet. If this occurs, re-centrifuge for 5 min at 10,000 rpm, and only then remove the 1.2 mL.
7. Add 1.0 mL distilled water, and centrifuge a 2nd time for 5 min at 10,000 rpm.
8. Remove 1.0 mL supernatant from each tube. Do not touch or disturb the soft, white pellet with the pipet. If this occurs, re-centrifuge for 5 min at 10,000 rpm, and only then remove the 1.0 mL supernatant.
9. Add 1.0 mL distilled water, and centrifuge a 3rd time for 5 min at 10,000 rpm.
10. Remove 1.0 mL supernatant from each tube. Do not touch or disturb the soft, white pellet with the pipet. If this occurs, re-centrifuge for 5 min at 10,000 rpm, and only then remove the 1.0 mL supernatant.
11. Add 1.0 mL distilled water, and centrifuge a 4th time for 5 min at 10,000 rpm.
12. Remove 1.0 mL supernatant from each tube. Do not touch or disturb the soft, white pellet with the pipet. If this occurs, re-centrifuge for 5 min at 10,000 rpm, and only then remove the 1.0 mL supernatant.
13. Re-suspend the pellet by adding 900 µL 0.25 M HCl and gently mixing with a pipet. (total of 2x dilution of original sample so far)
14. Add 50 µL of each re-suspended sample to 10.0 mL distilled water (should already be aliquoted out in 20 mL glass vials).
15. Add 1 mL mixed reagent to each glass vial.
16. Let color develop for at least 1 hour but not more than 2, and measure absorbance at 885 nm.

7.3.10 Measuring NH_3 produced by nitrogenase

When measuring NH3 production by nitrogenase in the presence of a high concentration of additional amines, i.e., the regeneration solution, the following fluorescence assay must be used. However, when measuring NH3 production by nitrogenase without the regeneration system, i.e., for photoreduction assays, the absorbance method may be used.

7.3.11 Reagents for NH_3 fluorescence assay (OPA method)

1. 10.00 mM NH_4Cl standard solution
    a. Calculate the amount of NH_4Cl needed to make 1L of 10.00 mM NH_4Cl. Weigh >1.000 g NH_4Cl on the analytical balance. Add pre-weighed powder to >1000.0 g distilled H_2O in a pre-weighed 1L glass container. Add a stir bar to dissolve as needed. Aliquot ~10 mL volumes into plastic 15 mL conical vials. Calculate concentration in ppm and convert to M assuming the density of water is 1.00000 kg/L at lab temperature.
2. 100 mM P_i, pH 11.0
    a. Calculate the amount of Na_2HPO_4 and NaH_2PO_4 needed to make 1L of an ~pH 11.0 solution of 100 mM P_i in order to minimize the amount of additional salts added.
3. 20 mM *o*-phthalaldehyde (OPA) solution
    a. In the dark, add 0.536 g OPA to 50 mL methanol. Then, after OPA has dissolved add 150 mL distilled water. Store in a plastic, foil-covered container.

    b. This solution must be made fresh the day of analysis; do not make more than 2 hours in advance.
4. 6 mM Na_2SO_3 in 100 mM P_i, pH 11.0
    a. This solution must be made fresh the day of analysis; do not make more than 2 hours in advance.
5. Mixed reagent
    a. Mix 1 part reagent #3 and 1 part reagent #4 immediately before analysis.

7.3.12 Procedure for NH_3 fluorescence assay (OPA method

1. Both OPA (reagent #3) and Na_2SO_3 (reagent #4) must be made fresh each day and stored separately until immediately before use.
2. The linear range of the fluorescent OPA assay is ~0-6 µM NH_3. Determine the amount of dilution necessary for activity assay solutions to fall in this range.
    a. Example: If a day's assays are predicted to produce 0-500 µM NH_3, samples will need to be diluted ~100x prior to analysis.
    b. When the final concentrations of all standards and samples are in the range 0-6 µM NH_3, the following fluorimeter parameters should work: excite at 365 with 2 nm slits, observe emission from 400-450 with 1 nm slits. Total fluorescence counts measured should fall in the range of ½ to 5 million to be considered reliable. If samples contain more or less NH_3, slit widths may need to be adjusted accordingly.
    c. The background fluorescence of the OPA solution and the mixed fluorescence reagent both increase with time, even if kept in the dark. Thus, standards and samples should be made up at the same time.
3. Prepare 10-12 NH_3 standard solutions in DI water that fall in the range 0-1000 µM NH_3.
4. Add 400 µL of each standard and NaCl-quenched activity assay solution to a fresh microcon. Centrifuge at 10,000 rpm for 6 min. Do not exceed 10,000 rpm, as the microcons may leak protein above this speed.
5. Remove 100 µL of the microcon flow-through and add to 900 µL distilled water in a fresh 1.7 mL Eppendorf tube. Mix well. (This is a 10x dilution of the initial assay sample.)
6. Add 200 µL of this diluted sample to a fresh 2.0 mL tube. Make sure the standards have been prepared in the same way, and 200 µL of diluted standards are also in fresh 2.0 mL tubes.
7. Immediately before analysis, add 1 part reagent #3 to 1 part reagent #4. Then, aliquot 1.8 mL of this mixed reagent into each 2.0 mL tube, which already contains 200 µL of the sample or standard to be analyzed.
8. Let solutions develop in the dark for at least 120 but no more than 180 minutes. (This is now a 100x dilution of the initial assay sample.)
9. Measure fluorescence at 422 nm after excitation at 365 nm.

7.3.13 Reagents for NH_3 absorbance assay (Indophenol method)

1. Phenol solution: 20 g phenol in200 mL 95% v/v EtOH
2. Sodium nitroprusside solution: 0.50 g sodium nitroprusside ($Na_2Fe(CN)_5NO*2H_2O$) in 100 mL H_2O. Store covered away from light.

3. Alkaline sodium citrate: 100 g sodium citrate and 5 g NaOH in 500 mL H_2O. Store in a sealed plastic bottle.
4. Sodium hypochlorite solution: reagent grade from Sigma, with 10-15% available chlorine
5. Oxidizing solution: mix 100 mL reagent 3 with 25 mL reagent 4. Keep solution sealed when not in use and prepare fresh before each analysis.

Note: Samples should contain 0-50 μM NH_3 in a final volume of 1 mL when mixed with color reagents. Samples should not contain ANY TRIS buffer or any other amine-containing buffer. HEPES and DT both inhibit color development at concentrations greater than 10 mM.

7.3.14 Procedure for NH_3 absorbance assay (Indophenol method)

1. Add 400 μL of each standard and NaCl-quenched activity assay solution to a fresh microcon. Centrifuge at 10,000 rpm for 6 min. Do not exceed 10,000 rpm, as the microcons may leak protein above this speed.
2. Remove 200 μL of the microcon flow-through and add to 800 μL distilled water in a fresh 1.7 mL Eppendorf tube. Mix well. (This is a 5x dilution of the initial assay sample.)
3. To the 1.0 mL solution in a 1.7 mL Eppendorf tube, add 40 μL phenol solution. Next, add 40 μL of the sodium nitroprusside solution, followed by 100 μL of the oxidizing solution. After adding all 3 reagents to a single sample, proceed to the next sample. Allow all standards and samples to develop at RT in the dark for about 1 h before measuring the absorbance at 640 nm.

7.4 Assessing the purity, activity, and integrity of purified nitrogenase component proteins

7.4.1 Bradford Assay

The Bradford assay measures the absorbance of dye bound to the surface of the protein. The λ_{max} = 595 nm, but the ε varies greatly based on the reaction time, temperature, etc., so standard curves must be run each time the analysis is conducted.

BSA standards

Make 500 μL 1.0 mg/mL BSA in H_2O. From this sub-stock, make 40 μL solutions of 0-1.0 mg/mL BSA. Dilute nitrogenase protein samples to be between 0-1.0 mg/mL protein. Take 20 μL of each standard and protein sample and add to 1.0 mL room temperature Bradford dye. Invert and let sit for no more than 10 min. Measure the absorbance at 595 nm and plot Abs v. [mg/mL].

7.4.2 Fe-chelation

The Fe-chelation assay measures the absorbance of $Fe(bpy)_3$. The ε_{522} = 8650 $M^{-1}cm^{-1}$ and does not vary much so a standard curve does not need to be created each day. To a 20 μL aliquot of protein from the tent (at least 10 mg/mL FeP

and at least 5 mg/mL MoFeP), add 380 µL 8 M GdHCl and 100 µL bpy solution (100 mM 2,2-bipyridine in 50% v/v acetic acid). Invert and let samples sit at room temperature for 5 min and no more than 1 h. ε_{522} = 8650 $M^{-1}cm^{-1}$.

7.4.3 ICP-MS

ICP-MS is used to measure the Fe and Mo content of nitrogenase proteins. Additionally, the Ru content can be measured if needed. ICP-MS is an extremely sensitive technique. Standard solutions and samples must be made in an identical matrix containing at least 1.5 but not more than 2.0% ICP-MS grade HCl. Samples may contain no more than 100 ppm protein and must contain a smaller concentration of NaCl than Fe and Mo to be measured. First, using microcons in the tent, buffer exchange protein into water to remove all NaCl and buffer salts. When the protein sample contains > 20 mg/mL protein and < 0.01 µM NaCl, remove from tent and dilute sample in aqueous HCl (1.5 – 2.0%) such that the Fe content is between 0 – 1500 ppb and the Mo content is between 0 – 150 ppb. Prepare standard solutions by weight in the same acid, placing Mo and Fe in the same standards, using the 1000 ppm ICP-MS standard solutions as a concentrated stock.

7.5 Creating permanent mutations in the *Azotobacter vinelandii* genome for generation of nitrogenase protein variants

Site-directed mutagenesis in *A. vinelandii* is a two-step process. To summarize, an appropriate deletion strain of *A. vinelandii* that is impaired in its ability to fix nitrogen (N^- phenotype) is selected from Table 9.4. Then, exogenous plasmid DNA, which contains the mutation of interest, is incorporated onto the genome of *A. vinelandii* during cell replication through double homologous recombination, restoring the organism's ability to fix nitrogen. Successful transformants can be screened on media lacking a source of fixed nitrogen. When creating a site-directed mutant that cannot fix nitrogen (i.e., ΔLeu127-Fe protein), the deleted region must be replaced with some antibiotic resistance cassette, typically kanamycin resistance. Then, successful incorporation of exogenous plasmid DNA into the *A. vinelandii* genome during cell replication can be screened by loss of kanamycin resistance. Here, we will discuss step 2 of the mutagenesis, assuming that an intact, appropriate deletion strain is available.

Table 7.4 Deletion strains provided by the Dean lab

	Other names	Amino acids deleted	Antibiotic resistance
DJ11	CA12; ΔnifHDK	nifH aa67 – nifK aa 309	
DJ13	CA11; ΔnifK	Pst1 deletion: nifK aa136 – nifK aa293	
DJ33	ΔnifDK	KpnI deletion: nifD aa102 - nifK309	
DJ34	ΔnifHDKTY	SalI deletion: ORF12 aa194 – nifE aa389	
DJ98	ΔnifM	StuI site of the nifM coding region.	Kanamycin
DJ200	ΔnifDK	PstI deletion: nifD aa47 - nifK aa293	Kanamycin
DJ1764	ΔnifH	Unknown	
DJ1049		Kanamycin resistance cartridge inserted into nifM at aa71, his-tag on Fe protein.	Kanamycin
DJ1192	ΔnifD	KpnI deletion: nifD aa103 - nifD aa377	Kanamycin
DJ1255		tungsten tolerance, nifDK deletion, vnfK deletion	Rifampicin Kanamycin Gentomycin
DJ1258		tungsten tolerance, nifDK deletion, his-tag on vnfK	Rifampicin Gentomycin

7.5.1 Generating plasmids using the Polymerase Chain Reaction

Below are the plasmids currently available in the lab:
PMY001 – contains all of nifHD
PMY002 – contains all of nifK
pWAX001 – contains all of nifHDK

All plasmids contain nif genes in a p-GEM T Easy vector from Promega. Follow the recipe below for PCR.

PCR Recipe
5 µL 10x Pfu reaction buffer
50-100 ng dsDNA template
1 µL FORWARD primer
1µL REVERSE primer
1 µL dNTPs mix
1 µL Pfu Turbo
H_2O to a final volume of 50 µL

Table 7.5 Themocycler protocol for PCR using Pfu Turbo

	Temperature	Time	Purpose
1	95°C	5 min	Denature
2	95°C	1 min	Denature
3	5°C below the Tm of primers	1 min	Anneal
4	72°C	15 min	Extend
5	Repeat steps 2-4 12-15x		
6	4°C	HOLD	

7.5.2 Transformation into E. coli

Add 1 µL DpN1 digest to each 50 µL PCR reaction. Mix thoroughly. Let incubate at 37°C in the warm room for a minimum of 1 hour; it is okay for the reaction to proceed overnight. Remove XL-1 blue *E. coli* cells from –80°C and place immediately on ice. Sterilely add 50 µL XL-1 blue *E. coli* cells to 5 µL digested PCR product in a sterile test tube. Let sit on ice for 30 min. Turn on the water bath to 42°C. After 30 min, transfer test tubes from ice to 42°C water bath for exactly 45 seconds and immediately place test tubes to ice. Sterilely add 2 mL LB media (no ampicillin) to each transformation, and shake in warm room at 37°C for exactly 1 h. Remove LB agar plates containing 100 µg/mL ampicillin from cold room and let come to room temperature (either on the bench or in the warm room). After 1 h, plate 200 µL of 2 mL cultures onto LB-Amp plates. Incubate plates overnight in the warm room.

7.5.3 Mini Prep to obtain pure plasmid DNA

Use single colonies from LB Amp plates to inoculate 5-mL solutions of LB media containing 100 µg/mL ampicillin. Shake overnight in the warm room at 37°C. Lyse the cells and purify the plasmid DNA according to the mini prep kit instructions. Elute plasmid DNA with H_2O and not the Elution buffer. Measure DNA concentration using the absorbance at 260 nm, and send for sequencing to verify successful plasmid construction.

7.5.4 Transformation of plasmid DNA into A. vinelandii deletion strain

Reagents

Fe-free/low Ca Burk's media
Fe-free Burk's agar plates
Buffer – 20 mM MOPS, pH 7.2, 20 mM $MgSO_4$
Low Ca/N^- Burk's media
N^-/rif^+ Burk's agar plates

Whereas *E. coli* cells (XL-1 blue) become competent after a brief heat shock, *A. vinelandii* cells must be starved of Fe in order to become competent to uptake plasmid DNA. At least 5 days before transforming, streak an Fe-free Burk's plate with the *A. vinelandii* deletion strain to be utilized. After 2 or 3 days, cells should turn bright green. This indicates the release of a fluorescent siderophore of *A. vinelandii* and is a

sign of low Fe. Restreak the cells on a fresh Fe-free Burk's plate for a second round of Fe-free growth.

About 20 h before transforming, scoop a few colonies off this Fe-free Burk's plate and use to inoculate 50 mL Fe-free/low Ca Burk's media in a 125-mL flask. Shake at 150 rpm, 30°C. The large volume and slow shaking will both promote low-O_2 conditions, which will further stress the *A. vinelandii* cells. About 2 h before the transformation, begin monitoring the $O.D._{600}$ of the cells. Cells should be bright green and reach an $O.D._{600}$ of 0.25-0.50 before the transformation begins. If the cells are more or less dense than this, the transformation will most likely not work. Since the doubling time of *A. vinelandii* is about 2 h, if the cells have an $O.D._{600} < 0.1$, do not bother with the transformation that day. Instead, use those cells to inoculate fresh Fe-free Burk's cultures that contain varying amounts of NH_4^+. Shake these cultures at 150 rpm, 30°C overnight and attempt the transformation the following day.

When the cells have reached an appropriate $O.D._{600}$ and green color, sterilely mix 50 µL cells with 50 µL sterile MOPS buffer (pH 7.2, 20 mM Mg_2^+). Add 2-4 µg pure plasmid DNA to this mixture. As a negative control, create one mixture that contains no plasmid DNA. Incubate at 30°C for 30 min. Do not shake. After 30 min, dilute by adding 0.4 mL low-Ca/N^- Burk's media to the mixture. Plate two dilutions of this solution (50 µL and 200 µL) onto two separate N^- Burk's plates. As a positive control, plate 50 µL of each transformation onto an N^+ Burk's plate. Incubate all plates at 30°C. Colonies should appear after 3-5 days. As single colonies appear, restreak each single colony onto a fresh N^- Burk's plate.

7.5.5 Confirming mutation by sequencing

Sterilely remove a few colonies from the 2nd N^- Burk's plate and resuspend in 40 µL H_2O. This should be a visibly murky solution; if not, add more cells. Heat the above solution to 95°C for 15 min. Cool quickly on ice. Add 2 µL of heated cells to the PCR reaction.

PCR recipe

1. 0.75 µL Phusion polymerase
2. 10 µL 5x HF Phusion buffer
3. 1 µL (20 µM) FORWARD primer
4. 1 µL (20 µM) REVERSE primer
5. 2 µL heated *A. vinelandii* cells
6. 1 µL DMSO
7. 1.2 µL 10 mM dNTPs mixture
8. H_2O to a final volume of 50 µL

Table 7.6 Thermocylcer protocol for PCR using Phusion polymerase

	Temperature	Time	Purpose
1	98°C	30 s	Denature
2	98°C	10 s	Denature
3	Tm of primer with lower Tm	30 s	Anneal
4	72°C	30 s per kilobase	Extend
5	Repeat steps 2-4 35x		
6	4°C	HOLD	

Aragose gel to confirm successful colony PCR

While stirring, heat 160 mL 1x TAE buffer and 1.6 g agarose (white powder). Let the solution come to a boil. Remove from heat; add 16 µL 10,000x dye, mix thoroughly, pour into gel holder. Let sit for 30 min before use. Load 6-10 µL DNA ladder and 6 µL of each PCR sample (5 µL PCR sample + 1 µL 6x loading dye). Run at 100 V for 45 min. Examine under a UV lamp to detect successful PCR reactions. Send 20 µL of PCR products that contain only 1 band by gel for sequencing, along with appropriate primers in a separate tube.

7.6 Working with MoFe protein variants capable of photoreduction

7.6.1 Synthesis of Ru-phenIA

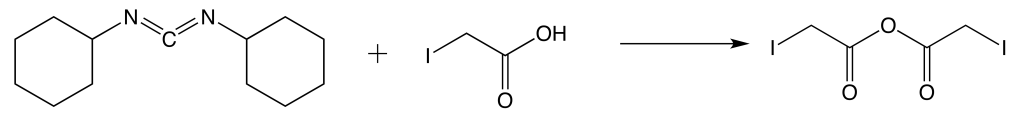

Figure 7.7 Synthesis of iodoacetic acid anhydride

As a precursor, prepare iodoacetic acid anhydride by adding 2.64 g (12.8 mmol) of DCC to a stirred solution of 5.0 g (26.8 mmol) of iodoacetic acid in 75 mL of ethyl acetate. Dicyclohexylurea precipitates immediately, but the mixture was allowed to stir for 2 h in the dark. Dicyclohexylurea was removed by filtration, and the resulting solution was evaporated to dryness and used immediately. The melting temperature of this product is ~40-50°C, so if after rotovapping for >1 h, there is still a liquid in the round bottom, it may be product.

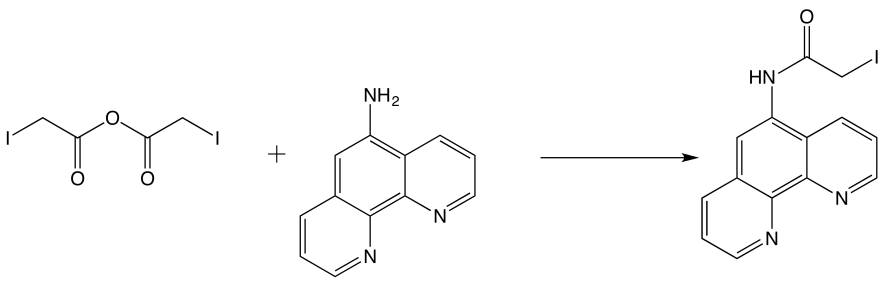

Figure 7.8 Synthesis of 5-Iodoaceamido-1,10-phenanthroline (PhenIA)

A total of 0.5 g (2.56 mmol) of 5-amino-1,10-phenanthroline was dissolved in 90 mL of acetonitrile with slight heating. To this stirred solution, the freshly prepared iodoacetic acid anhydride dissolved in 10 mL of acetonitrile was added. The mixture was allowed to react in the dark overnight. The precipitated product was isolated by filtration and washed with cold 5% sodium bicarbonate, followed by water and dried in vacuo.

Synthesis of Ru-PhenIA

Crude PhenIA should be reacted with $Ru(bpy)_2Cl_2$ in approximately a 10:1 molar ratio. I use about 80 mg crude PhenIA with 40 mg $Ru(bpy)_2Cl_2$ in 20 mL MeOH. Reflux the mixture at 75°C overnight and under an inert atmosphere. Do not use the dry condensers; use the real condensers. This reaction is slow and will not take place without a lot of heat and time.

Covalent attachment of Ru-phenIA to MoFe protein to create Ru-MoFe protein

Dried, crude Ru-PhenIA should be dissolved in a minimal amount of DMSO and flash frozen in small aliquots. Use approximately a 100-fold excess of crude Ru-PhenIA product over MoFe protein, since there are 2 reactive Cys residues per MoFe protein on αC45A/L158C MoFe protein. If using a MoFe protein that does not contain the αC45A mutation, and there are 4 reactive Cys residues per MoFe protein, double the concentration of crude Ru-PhenIA product in the reaction.

First, buffer-exchange MoFe protein on an equilibrated 10-DG containing P_i buffer, pH 7.5, 100 mM NaCl to remove all DT. Then mix 100:1 Ru-PhenIA:MoFe in P_i buffer, pH 7.5, 100 mM NaCl anaerobically and in the dark. Let reaction proceed for 2 hours. Stop the labeling reaction by running the solution over an equilibrated 10-DG containing P_i buffer, pH 7.5, 100 mM NaCl. Concentrate the labeled protein to at least 50 μM, remove 20 μL for a Bradford assay, and immediately freeze the labeled protein in the LN_2 dewar.

8 References

(1) Howard, J. B.; Rees, D. C. *Chem. Rev.* **1996**, *96*, 2965.

(2) Anderson, J. S.; Rittle, J.; Peters, J. C. *Nature* **2013**, *501*, 84.

(3) Yandulov, D. V.; Schrock, R. R. *Science* **2003**, *301*, 76.

(4) Rodriguez, M. M.; Bill, E.; Brennessel, W. W.; Holland, P. L. *Science* **2011**, *334*, 780.

(5) Pool, J. A.; Lobkovsky, E.; Chirik, P. J. *Nature* **2004**, *427*, 527.

(6) Smil, V. *Enriching the earth: Fritz Haber, Carl Bosch, and the transformation of world food production*; MIT press, 2004.

(7) Rees, D. C.; Tezcan, F. A.; Haynes, C. A.; Walton, M. Y.; Andrade, S.; Einsle, O.; Howard, J. B. *Philos. T. R. Soc. A.* **2005**, *363*, 971.

(8) Burgess, B. K.; Lowe, D. J. *Chem. Rev.* **1996**, *96*, 2983.

(9) Igarashi, R. Y.; Seefeldt, L. C. *Crit. Rev. Biochem. Mol.* **2003**, *38*, 351.

(10) Tezcan, F. A.; Kaiser, J. T.; Mustafi, D.; Walton, M. Y.; Howard, J. B.; Rees, D. C. *Science* **2005**, *309*, 1377.

(11) Peters, J. W.; Fisher, K.; Newton, W. E.; Dean, D. R. *J. Biol. Chem.* **1995**, *270*, 27007.

(12) Lowe, D.; Thorneley, R. *Biochem. J.* **1984**, *224*, 877.

(13) Owens, C. P.; Katz, F. E. H.; Carter, C. H.; Luca, M. A.; Tezcan, F. A. *J. Am. Chem. Soc.* **2015**, *137*, 12704.

(14) Bishop, P. E.; Jarlenski, D. M. L.; Hetherington, D. R. *Proc. Natl. Acad. Sci. U.S.A.* **1980**, *77*, 7342.

(15) Bishop, P. E.; Premakumar, R.; Dean, D. R.; Jacobson, M. R.; Chisnell, J. R.; Rizzo, T. M.; Kopczynski, J. *Science* **1986**, *232*, 92.

(16) Chisnell, J. R.; Premakumar, R.; Bishop, P. E. *J. Bacteriol.* **1988**, *170*, 27.

(17) Sippel, D.; Einsle, O. *Nature Chem. Biol.* **2017**, *13*, 956.

(18) Rees, J. A.; Bjornsson, R.; Schlesier, J.; Sippel, D.; Einsle, O.; DeBeer, S. *Angew. Chem. Int. Ed.* **2015**, *54*, 13249.

(19) Kennedy, C.; Toukdarian, A. *Annu. Rev. Microbiol.* **1987**, *41*, 227.

(20) Mayer, S. M.; Lawson, D. M.; Gormal, C. A.; Roe, S. M.; Smith, B. E. *J. Mol. Biol.* **1999**, *292*, 871.

(21) Zhang, L.-M.; Morrison, C. N.; Kaiser, J. T.; Rees, D. C. *Acta Crystallogr. D* **2015**, *71*, 274.

(22) Howard, J. B.; Kechris, K. J.; Rees, D. C.; Glazer, A. N. *PloS one* **2013**, *8*, e72751.

(23) Simpson, F. B.; Burris, R. H. *Science* **1984**, *224*, 1095.

(24) Lindahl, P.; Papaefthymiou, V.; Orme-Johnson, W.; Münck, E. *J. Biol. Chem.* **1988**, *263*, 19412.

(25) Katz, F. E.; Owens, C. P.; Tezcan, F. *Isr. J. Chem.* **2016**, *56*, 682.

(26) Duval, S.; Danyal, K.; Shaw, S.; Lytle, A. K.; Dean, D. R.; Hoffman, B. M.; Antony, E.; Seefeldt, L. C. *Proc. Natl. Acad. Sci. U.S.A.* **2013**, *110*, 16414.

(27) Lanzilotta, W. N.; Fisher, K.; Seefeldt, L. C. *Biochemistry* **1996**, *35*, 7188.

(28) Danyal, K.; Mayweather, D.; Dean, D. R.; Seefeldt, L. C.; Hoffman, B. M. *J. Am. Chem. Soc.* **2010**, *132*, 6894.

(29) Danyal, K.; Dean, D. R.; Hoffman, B. M.; Seefeldt, L. C. *Biochemistry* **2011**, *50*, 9255.

(30) Hageman, R. V.; Burris, R. *Proc. Natl. Acad. Sci. U.S.A.* **1978**, *75*, 2699.

(31) Willing, A. H.; Georgiadis, M. M.; Rees, D. C.; Howard, J. B. *J. Biol. Chem.* **1989**, *264*, 8499.

(32) Willing, A.; Howard, J. B. *J. Biol. Chem.* **1990**, *265*, 6596.

(33) Chan, M. K.; Kim, J. S.; Rees, D. C. *Science* **1993**, *260*, 792.

(34) Kim, J.; Woo, D.; Rees, D. *Biochemistry* **1993**, *32*, 7104.

(35) Georgiadis, M.; Komiya, H.; Chakrabarti, P.; Woo, D.; Kornuc, J.; Rees, D. *Science* **1992**, *257*, 1653.

(36) Schindelin, H.; Kisker, C.; Schlessman, J. L.; Howard, J. B.; Rees, D. C. *Nature* **1997**, *387*, 370.

(37) Thorneley, R. N.; Lowe, D. *Biochem. J.* **1983**, *215*, 393.

(38) Lowe, D.; Thorneley, R. N. *Biochem. J.* **1984**, *224*, 895.

(39) Thorneley, R. N.; Lowe, D. *Biochem. J.* **1984**, *224*, 903.

(40) Thorneley, R. N.; Lowe, D. *Biochem. J.* **1984**, *224*, 887.

(41) Wilson, P. E.; Nyborg, A. C.; Watt, G. D. *Biophys. Chem.* **2001**, *91*, 281.

(42) Chiu, H.-J.; Peters, J. W.; Lanzilotta, W. N.; Ryle, M. J.; Seefeldt, L. C.; Howard, J. B.; Rees, D. C. *Biochemistry* **2001**, *40*, 641.

(43) Tezcan, F. A.; Kaiser, J. T.; Howard, J. B.; Rees, D. C. *J. Am. Chem. Soc.* **2014**, *137*, 146.

(44) Spatzal, T.; Perez, K. A.; Einsle, O.; Howard, J. B.; Rees, D. C. *Science* **2014**, *345*, 1620.

(45) Spatzal, T.; Perez, K. A.; Howard, J. B.; Rees, D. C. *Elife* **2015**, *4*.

(46) Sippel, D.; Rohde, M.; Netzer, J.; Trncik, C.; Gies, J.; Grunau, K.; Djurdjevic, I.; Decamps, L.; Andrade, S. L.; Einsle, O. *Science* **2018**, *359*, 1484.

(47) Deits, T. L.; Howard, J. *J. Biol. Chem.* **1990**, *265*, 3859.

(48) Deits, T. L.; Howard, J. B. *J. Biol. Chem.* **1989**, *264*, 6619.

(49) Christiansen, J.; Chan, J. M.; Seefeldt, L. C.; Dean, D. R. *J. Inorg. Biochem.* **2000**, *80*, 195.

(50) Seefeldt, L. C. *Protein Sci.* **1994**, *3*, 2073.

(51) Watt, G. D.; Bulen, W. A.; Burns, A.; Lamonthadfield, K. *Biochemistry* **1975**, *14*, 4266.

(52) Stocchi, V.; Cucchiarini, L.; Magnani, M.; Chiarantini, L.; Palma, P.; Crescentini, G. *Anal. Biochem.* **1985**, *146*, 118.

(53) Yates, M.; Thorneley, R.; Lowe, D. *FEBS Lett.* **1975**, *60*, 89.

(54) Katz, F. E.; Shi, X.; Owens, C. P.; Joseph, S.; Tezcan, F. A. *Anal. Biochem.* **2017**, *520*, 62.

(55) Christiansen, J.; Goodwin, P. J.; Lanzilotta, W. N.; Seefeldt, L. C.; Dean, D. R. *Biochemistry* **1998**, *37*, 12611.

(56) Wiig, J. A.; Lee, C.-C.; Fay, A. W.; Hu, Y.; Ribbe, M. W. In *Nitrogen Fixation*; Springer: 2011, p 93.

(57) Hageman, R. V.; Burris, R. H. *Biochemistry* **1978**, *17*, 4117.

(58) Hauser, C. T.; Tsien, R. Y. *Proc. Natl. Acad. Sci. U.S.A.* **2007**, *104*, 3693.

(59) Ubbink, M. *FEBS Lett.* **2009**, *583*, 1060.

(60) Burgess, B. K.; Wherland, S.; Newton, W. E.; Stiefel, E. I. *Biochemistry* **1981**, *20*, 5140.

(61) Wilson, P. *Proc. R. Soc. Lond. B* **1969**, *172*, 319.

(62) Wyss, O.; Lind, C.; Wilson, J.; Wilson, P. *Biochem. J.* **1941**, *35*, 845.

(63) Wyss, O.; Wilson, P. *Proc. Natl. Acad. Sci. U.S.A.* **1941**, *27*, 162.

(64) Jacobs, D.; Mitchell, D.; Watt, G. *Arch. Biochem. Biophys.* **1995**, *324*, 317.

(65) Bolleter, W.; Bushman, C.; Tidwell, P. W. *Anal. Chem.* **1961**, *33*, 592.

(66) Dilworth, M. J.; Eldridge, M. E.; Eady, R. R. *Anal. Biochem.* **1992**, *207*, 6.

(67) Goyal, S. S.; Rains, D. W.; Huffaker, R. C. *Anal. Chem.* **1988**, *60*, 175.

(68) Lindroth, P.; Mopper, K. *Anal. Chem.* **1979**, *51*, 1667.

(69) Corbin, J. L. *Appl. Environ. Microb.* **1984**, *47*, 1027.

(70) Genfa, Z.; Dasgupta, P. K. *Anal. Chem.* **1989**, *61*, 408.

(71) Strickland, J. D. H.; Parsons, T. R.; Strickland, J. D. H. *A practical handbook of seawater analysis*; Fisheries Research Board of Canada: Ottawa, 1972.

(72) Peters, J. W.; Stowell, M. H.; Soltis, S. M.; Finnegan, M. G.; Johnson, M. K.; Rees, D. C. *Biochemistry* **1997**, *36*, 1181.

(73) Surerus, K. K.; Hendrich, M. P.; Christie, P. D.; Rottgardt, D.; Ormejohnson, W. H.; Munck, E. *J. Am. Chem. Soc.* **1992**, *114*, 8579.

(74) Owens, C. P.; Katz, F. E.; Carter, C. H.; Oswald, V. F.; Tezcan, F. A. *J. Am. Chem. Soc.* **2016**, *138*, 10124.

(75) Zimmermann, R.; Münck, E.; Brill, W. J.; Shah, V. K.; Henzl, M. T.; Rawlings, J.; Orme-Johnson, W. H. *Biochim. Biophys. Acta* **1978**, *537*, 185.

(76) Rawlings, J.; Shah, V.; Chisnell, J.; Brill, W.; Zimmermann, R.; Münck, E.; Orme-Johnson, W. *J. Biol. Chem.* **1978**, *253*, 1001.

(77) Tittsworth, R. C.; Hales, B. J. *J. Am. Chem. Soc.* **1993**, *115*, 9763.

(78) Pierik, A. J.; Wassink, H.; Haaker, H.; Hagen, W. R. *Eur. J. Biochem.* **1993**, *212*, 51.

(79) Roth, L. E.; Nguyen, J. C.; Tezcan, F. A. *J. Am. Chem. Soc.* **2010**, *132*, 13672.

(80) Roth, L. E.; Tezcan, F. A. *J. Am. Chem. Soc.* **2012**, *134*, 8416.

(81) Radford, R. J.; Nguyen, P. C.; Tezcan, F. A. *Inorg. Chem.* **2010**, *49*, 7106.

(82) Castellano, F. N.; Dattelbaum, J. D.; Lakowicz, J. R. *Anal. Biochem.* **1998**, *255*, 165.

(83) Nagpal, P.; Jafri, S.; Reddy, M.; Das, H. *J. Bacteriol.* **1989**, *171*, 3133.

(84) Cavalcante, V. A.; Dobereiner, J. *Plant and soil* **1988**, *108*, 23.

(85) Fisher, K.; Newton, W. E. *Biochim. Biophys. Acta* **2005**, *1750*, 154.

(86) Page, W.; Sadoff, H. *J. Bacteriol.* **1976**, *125*, 1080.

(87) Maldonado, R.; Jimenez, J.; Casadesús, J. *J. Bacteriol.* **1994**, *176*, 3911.

(88) Brigle, K. E.; Setterquist, R. A.; Dean, D. R.; Cantwell, J. S.; Weiss, M. C.; Newton, W. E. *Proc. Natl. Acad. Sci. U.S.A.* **1987**, *84*, 7066.

(89) Robinson, A.; Burgess, B.; Dean, D. *J. Bacteriol.* **1986**, *166*, 180.

(90) Jacobson, M. R.; Cash, V. L.; Weiss, M. C.; Laird, N. F.; Newton, W. E.; Dean, D. R. *Mol. Gen. Genet.* **1989**, *219*, 49.

(91) Page, W.; Von Tigerstrom, M. *J. Bacteriol.* **1979**, *139*, 1058.

(92) Hardy, R.; Knight Jr, E. *Biochim. Biophys. Acta* **1966**, *122*, 520.

(93) Hadfield, K. L.; Bulen, W. A. *Biochemistry* **1969**, *8*, 5103.

(94) Hallenbeck, P. C. *Arch. Biochem. Biophys.* **1983**, *220*, 657.

(95) Watt, G. D.; Reddy, K. *J. Inorg. Biochem.* **1994**, *53*, 281.

(96) Erickson, J. A. N., A. C.; Johnson, J. L.; Truscott, S. M.; Gunn, A.; Nordmeyer, F. A.; Watt, G. D. *Biochemistry* **1999**, *38*, 14279.

(97) Peters, J. W.; Fisher, K.; Newton, W. E.; Dean, D. R. *J. Biol. Chem.* **1995**, *270*, 27007.

(98) Cashel, M.; Lazzarini, R. A.; Kalbacher, B. *J. Chromatogr. A* **1969**, *40*, 103.

(99) Baginski, E. S.; Epstein, E.; Zak, B. *Ann. Clin. Lab. Sci.* **1975**, *5*, 399.

(100) Fiske, C. H.; Subbarow, Y. *J. Biol. Chem.* **1925**, *66*, 375.

(101) Fiske, C. H.; Subbarow, Y. *J. Biol. Chem.* **1929**, *81*, 629.

(102) Kim, C.-H.; Newton, W. E.; Dean, D. R. *Biochemistry* **1995**, *34*, 2798.

(103) Seefeldt, L. C.; Mortenson, L. E. *Protein Sci.* **1993**, *2*, 93.

(104) Li, J. B., B. K.; Corbin, J. L. *Biochemistry* **1982**, *21*, 4393.

(105) Wintermeyer, W.; Rodnina, M. V. *Essays Biochem.* **2000**, *35*, 117.

(106) García-Ortega, L. Á.-G., E.; Gavilanes, J. G.; Martinez-del-Pozo, Á.; Joseph, S. *Nucleic Acids Res.* **2010**, *38*, 4108.

(107) Sander, G.; Parlato, G.; Crechet, J. B.; Nagel, K.; Parmeggiani, A. *Eur. J. Biochem.* **1978**, *86*, 555.

(108) Seo, H.-S.; Abedin, S.; Kamp, D.; Wilson, D. N.; Nierhaus, K. H.; Cooperman, B. S. *Biochemistry* **2006**, *45*, 2504.

(109) Parmeggiani, A.; Sander, G. *Mol. Cell. Biochem.* **1981**, *35*, 129.

(110) Taylor, S.; Ninjoor, V.; Dowd, D.; Tappel, A. L. *Anal. Biochem.* **1974**, *60*, 153.

(111) Bergersen, F.; Turner, G. *Biochem. J.* **1973**, *131*, 61.